SMIP89

SEMINAR ON SEISMOLOGICAL AND ENGINEERING IMPLICATIONS OF RECENT STRONG-MOTION DATA

Sacramento, California
May 9, 1989

PREPRINTS

Sponsored by

Strong Motion Instrumentation Program
Division of Mines and Geology
California Department of Conservation

Supported in Part by

National Science Foundation
California Seismic Safety Commission
Applied Technology Council

STEERING COMMITTEE

Chris D. Poland
James H. Gates
Stephen A. Mahin
Anthony F. Shakal
J. Carl Stepp
Brian E. Tucker

The Strong Motion Instrumentation Program (SMIP) is administered by the Division of Mines and Geology, California Department of Conservation. It is advised by the Strong Motion Instrumentation Advisory Committee (SMIAC), a committee of the California Seismic Safety Commission. SMIP is funded by an assessment on building permits issued in cities and counties in California.

SMIP gratefully acknowledges the assistance of the Applied Technology Council and Chris Rojahn in planning and coordinating the SMIP89 Seminar.

DISCLAIMER

TABLE OF CONTENTS

* Manuscript not available at the time of printing.

OVERVIEW OF THE STRONG MOTION INSTRUMENTATION PROGRAM MAY 1989

A.F. Shakal and M.J. Huang
California Department of Conservation
Division of Mines and Geology

ABSTRACT

The purpose of the Strong Motion Instrumentation Program (SMIP) is to improve methods to protect California citizens and property from earthquake-induced structural hazards. Toward this end, the program records strong earthquake shaking in structures and at ground response sites to obtain the data necessary for the improvement of seismic design codes. SMIP also promotes and facilitates the improvement of seismic codes through data utilization projects. The SMIP89 Seminar is a component of that effort.

INTRODUCTION

SMIP was established after the 1971 San Fernando earthquake caused unexpectedly severe damage to buildings that had been designed according to contemporary code standards. To acquire the data necessary to improve the prediction of strong motion and the detection of structural problems, many more strong-motion stations were needed than were provided by the existing federal program. SMIP was created to fill that need.

The program installs and maintains strong-motion instruments in representative structures and geological environments throughout California. Since its inception, over 450 installations of various types have been completed. Sites are selected for instrumentation on the basis of the recommendations of a committee of the California Seismic Safety Commission. This advisory committee is made of leading engineers and seismologists from California universities, government, and private industry.

Strong-motion data recovered from the instruments in the SMIP network are processed and made available to engineers and seismologists engaged in predicting or designing for earthquake shaking. A large number of earthquake records have been recorded and analyzed, including many from the 1987 Whittier Narrows earthquake, and the very important records from the Imperial County Services Building damaged during the 1979 Imperial Valley earthquake.

Obtaining adequate recordings during the next major earthquake is essential for improving earthquake resistant design. Given the rarity of great earthquakes and the rapid growth in California, if the next event occurs without being adequately recorded another opportunity to gain the data necessary may not occur for many years and thousands of new structures will be built without that knowledge. This realization led to an acceleration in the program's instrumentation rate in 1988 through increased funding.

INSTRUMENTATION OBJECTIVES AND NETWORK STATUS

SMIP currently has a total of 450 stations installed at selected locations through the state of California, as shown on the map in Fig. 1. Table 1 summarizes the present status and target numbers of installations in each of three categories: ground-response, buildings, and lifeline structures.

Table 1. SMIP Network Status and Goals

Installation Type	Total Network Plan	Installed To Date	Remaining High Priority	Remaining To Complete Network
Ground-Response				
Isolated Sites	500	328	120	172
Dense Arrays	20	2	8	18
Buildings				
All Types	400	91	170	309
Lifelines				
Dams	30	21	9	9
Transportation	40	8	15	32
Water & Power	25	1	14	24
Total	1015	451	336	564

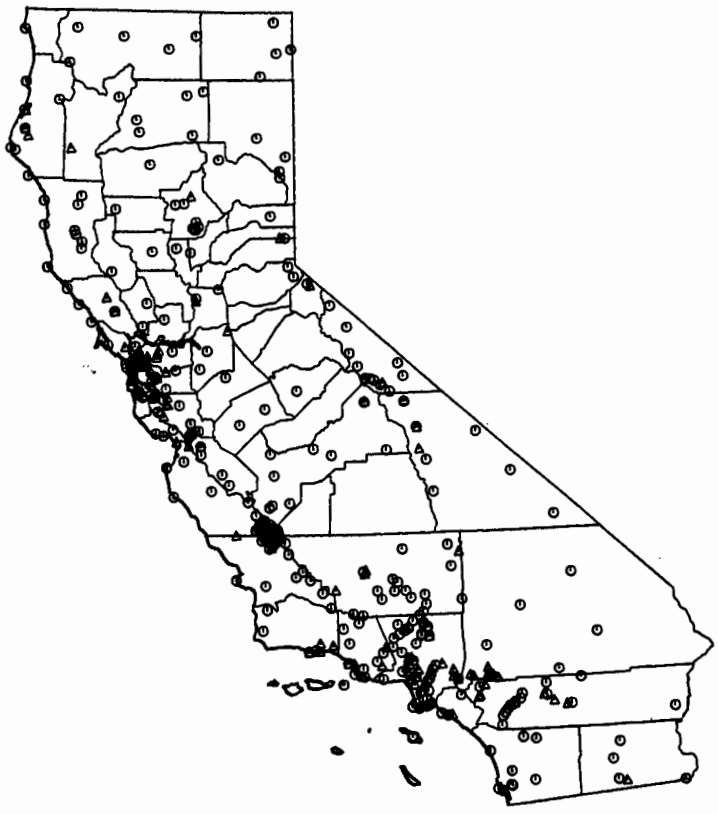

Fig. 1 Stations of the Strong Motion Instrumentation Program as of January 1989.

Ground-Response Instrumentation

The objectives of ground-response instrumentation are to measure earthquake shaking in a range of geologic conditions including rock, deep and shallow alluvium, and liquefiable deposits. Recording the motion at specific locations with respect to the earthquake fault is also important to allow study of the details of the rupture process and the attenuation of seismic waves radiated from the source region.

A total of 328 ground-response stations have been installed. Many are in small 1-story buildings like schools and fire stations, but most have been installed in small, light fiberglass instrument enclosures approximately 1 meter high. The goal of the installation design is to minimally affect incoming seismic motion while providing adequate coupling to the ground and protection for the instrument. The instrumentation objectives for the installation of ground-response stations over the next 15 years include adding an additional 120 isolated sites and 8 specialized dense arrays.

Building Instrumentation

The objectives for the instrumentation of buildings are to effectively record selected modes of the response of specific building types during strong shaking. For each type of building, certain modes of response and deformation are most important, and these determine where the sensors are located. Since the motion at the base of the building may not accurately represent the input motion, an additional recording site may be located on the ground at some distance from the building.

Building instrumentation systems have sensors located at key points in a structure and connected to a centrally-located recorder. At the time of the 1971 San Fernando earthquake, instrumented buildings usually had only three separate accelerographs -- one located on the top floor, one at mid-height, and one on the ground floor -- as called for by the Uniform Building Code. The San Fernando data indicated that the records would be more useful if the sensors were interconnected and recordings were obtained from more than just three points in the building. With a modern central-recording system sensors can be located almost anywhere within a building and be connected, via shielded cabling, to a central recording unit that records all of the signals simultaneously.

As indicated in Table 1, 91 buildings have been instrumented by SMIP. Building instrumentation objectives over the next 15 years include the instrumentation of an additional 170 buildings. Typically, 12 to 15 sensors are located in a building. The sensors are positioned in the structure so that specific measurement objectives will be achieved. An example showing part of the sensor layout for a structure is given in Fig. 2. The building (the Law and Justice Center of San Bernardino County) is base-isolated, with rubber isolators placed between the foundation and the 5-story super-structure. Sensors were placed to record the relative motion across the isolators, as well as the motion of the super-structure itself. Several records have been obtained in the building, but no base motion stronger than 0.05 g has been recorded. The records are interesting nonetheless (Fig. 2), since they show a reduction in high frequency motion across the isolators.

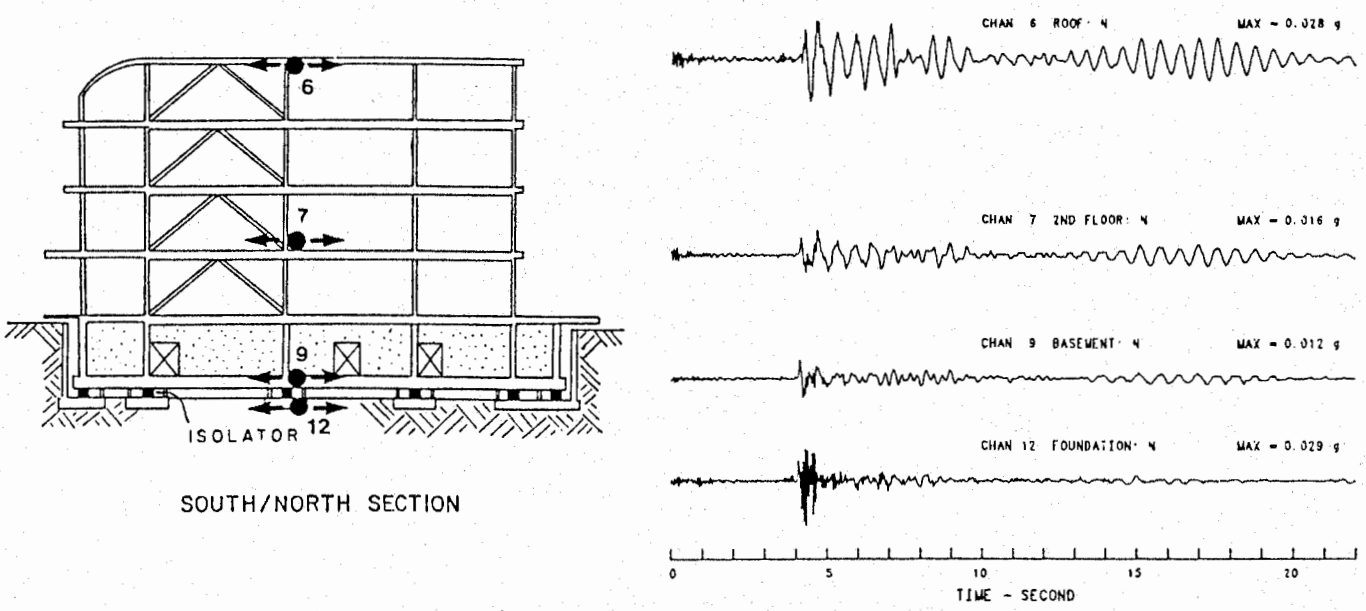

Fig. 2 Cross-section of the base-isolated San Bernardino County Law and Justice building (left) and accelerograms obtained from sensors at the roof, the 2nd floor, and above and below the isolators during the Redlands earthquake of October 2, 1985.

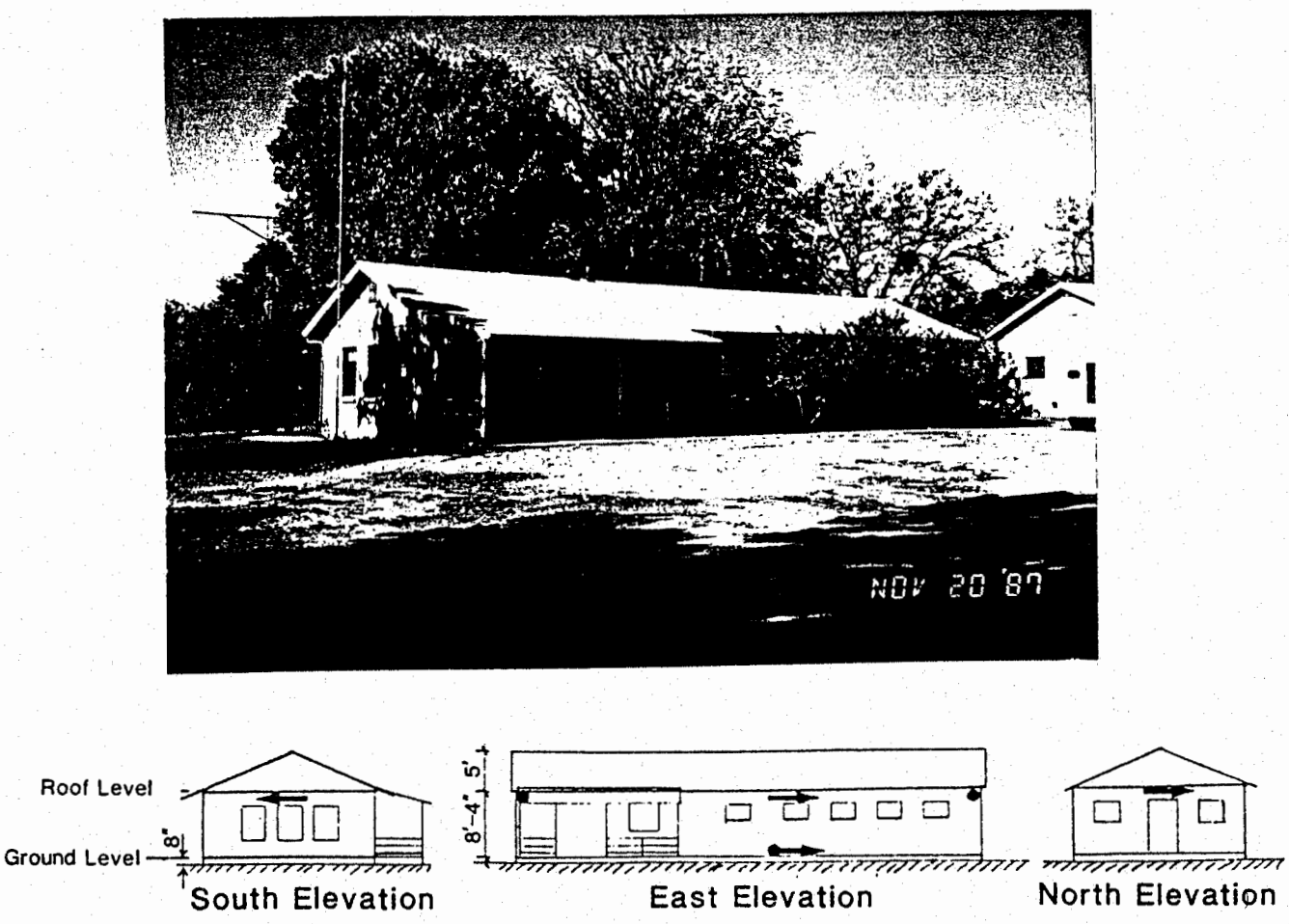

Fig. 3 The one-story masonry CDF dormitory building near Parkfield and the locations of the six sensors installed in the building.

The motions have so far been too small to excite the non-linear response of the isolation system.

The most important building records recorded by SMIP are those from the Imperial County Services Building. These records from the 16 sensors installed in the building document the strong shaking and the resulting structural failure of a modern multi-story building during the 1979 Imperial Valley earthquake. Several studies have analyzed these data to study the details of the failure process [1].

The instrumentation of smaller structures typically involves fewer sensors. As an example, Fig. 3 shows a 1-story masonry structure instrumented in Parkfield, in the vicinity of an earthquake predicted by the USGS. Six sensors have been installed to record the motions of this structure; no data have yet been recorded at this site.

Records obtained from buildings can be used to estimate the earthquake forces in a building. For example, the lateral force at each level can be estimated by multiplying the weight of each floor by the acceleration. These values are listed in Table 2 for a 10-story building in San Jose for the motion recorded during the 1984 Morgan Hill earthquake. For comparison, the original design forces reported in the ATC-2 report at each level and the total base shear in each direction are also listed. The dynamic earthquake forces are between 25 and 160 percent greater than the static design forces. The base shear is about 1.5 times the design shear in the longitudinal direction and 2 times in the transverse direction. This example illustrates the value of strong motion data in comparing actual earthquake forces to those used in design.

Lifeline Instrumentation

Lifeline structures instrumented by SMIP include bridges, dams, and power plants. Table 1 lists the number instrumented in several categories and the number remaining in the highest priority categories. The most important record from a lifeline obtained to date is from the Vincent Thomas suspension bridge, discussed in detail below.

NETWORK OPERATION AND MAINTENANCE

Maintenance techniques for strong-motion instruments have been developing since the early 1930's. Thorough training of personnel and regular, careful servicing are the key elements of an effective maintenance program. For a program like SMIP, which is continually installing new instruments as well as maintaining previously installed instruments, the budget balance between installation and maintenance is important. An instrument installed one year increases the maintenance costs for subsequent years. Component parts of the total budget for SMIP, including installation and maintenance, are shown in Fig. 4 projected for the next 15 years.

In addition to instrument maintenance, a maintenance aspect not readily apparent is station maintenance. Stations must occasionally be moved and reinstalled at the request of the property owner. Experience indicates that 1-2% of SMIP stations have to be abandoned and re-installed each year due to change of property ownership or changing physical conditions at the site.

Table 2. Maximum lateral forces estimated for a 10-story concrete building in San Jose during the 1984 Morgan Hill earthquake.

Floor Level	Weight (kips)	Longitudinal(NS) Direction (at t-19.36 sec. in the record) Acceleration (g)	Earthquake Force (kips)	Design Force (kips)	Transverse(EW) Direction (at t-17.82 sec.) Acceleration (g)	Earthquake Force (kips)	Design Force (kips)
Roof	2700	0.18 *	486	384	0.20 *	540	332
10	2400	0.17	408	311	0.19	456	269
9	2400	0.16	384	282	0.18	432	244
8	2400	0.15	360	253	0.17	408	219
7	2400	0.13	312	224	0.16	384	194
6	2400	0.12	288	195	0.14	336	169
5	2400	0.11 *	264	166	0.13 *	312	144
4	2400	0.10	240	137	0.12	288	119
3	2400	0.09	216	109	0.10	240	94
2	2400	0.07 *	168	85	0.08	240	73
Total Base Shear			3126	2146		3588	1857
Percent of Total Weight			13%	9%		15%	8%

Footnotes: Design forces are from ATC-2 report (1974).
* -- Maximum acceleration values from the record; the maximum accelerations for other levels are estimated by linear interpolation between the values at the levels recorded.

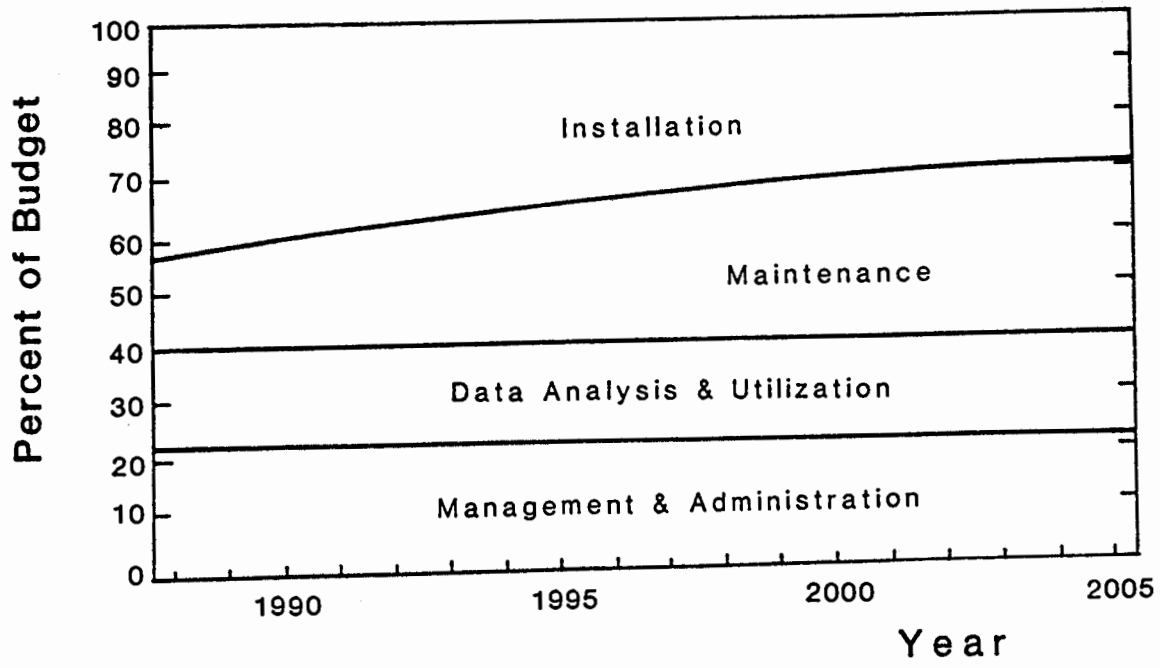

Fig. 4 Component parts of the SMIP budget projected for the next 15 years.

Accelerogram Processing

SMIP developed an in-house digitization capability in 1981 which is patterned after that developed by Trifunac and Lee in 1979 [2]. In this system, the film accelerogram is scanned, while mounted on a rotating drum, by a traveling photodensitometer. The processing procedure is described in reports produced by the program. Analyses of the system noise are used to develop signal-to-noise ratios to guide record filtering during processing.

Data Utilization

An effort to increase the application of the data collected by SMIP to the improvement of building codes was recently initiated. Studies have been funded for analysis of strong-motion data by researchers, working with graduate students (as a part of their professional training) and with the engineers who initially designed the structure being studied. These projects are aimed at answering specific questions regarding the response of the structures or the ground through utilization of existing strong-motion data. The results of these studies will be presented in annual seminars such as SMIP89 and published in technical journals.

IMPORTANT DATA FROM THE 1987 WHITTIER NARROWS EARTHQUAKE

The Whittier Narrows earthquake of October 1, 1987 was a moderate magnitude (5.9 M_L) event recorded by many strong-motion stations. Over 100 stations of the SMIP network, including 63 ground-response stations, 27 buildings, eight dams, and one suspension bridge recorded the event.

On average, the recorded peak accelerations are higher than predicted by the Joyner-Boore model [3] for a magnitude 6 event. The data of the SMIP network [4] and the U.S. Geological Survey stations [5] are plotted against epicentral distance in Fig. 5. The mean and +/- 1 standard deviation curves of Joyner and Boore have been included for comparison. The distribution of the Whittier data is biased high compared to the Joyner-Boore curves. The ability to more accurately predict peak ground motion will be increased by the study and understanding of this difference.

An interesting record was recovered at the Tarzana station, 44 km from the epicenter. A peak acceleration of 0.62 g was recorded although many stations even in the epicentral area recorded smaller peak values. In addition, stations in the vicinity of the Tarzana station recorded values of about 0.15 g. The site is located in a region of low rolling hills between the alluvial San Fernando Valley and the Santa Monica Mountains. The site is underlain by shallow soil over siltstone; soil depth has been estimated to be less than 10 m. The cause of the unusual record is not yet known but is important to understanding earthquake strong motion.

The record obtained at the Administration Building of the California State University at Los Angeles (CSULA), a 9-story reinforced concrete structure about 9 km from the epicenter is particularly interesting. The structure has a "soft first story" design very similar to the 6-story Imperial County Services Building in El Centro which suffered column failure in the 1979 Imperial Valley earthquake. The locations of the sensors in the

CSULA building and the accelerogram recorded in the Whittier Narrows earthquake are shown in Fig. 6. The maximum acceleration was about 0.40 g at the base and 0.50 g at the roof. For comparison, the 1979 Imperial County Services record had a peak value of 0.35 g at the base, and 0.60 g at the roof, and was longer in duration. The CSULA administration building suffered some damage in the earthquake. A cast-in-concrete steel column and two shear walls had some cracks which were repaired with epoxy.

The Vincent Thomas suspension bridge near Long Beach, south of Los Angeles and 40 km southwest of the epicenter, was instrumented with 26 sensors in 1981, with cost sharing from the federal government. Fig. 8 shows the locations of the sensors on the bridge structure. The record is the first significant strong-motion record ever obtained from a long-span suspension bridge. The maximum acceleration at the base of the towers was 0.08 g, while the acceleration of the suspended deck in the side-span reached 0.28 g. At the center of the side span the deck edges moved about 10 cm vertically as the deck oscillated in torsion with a period of about 1 second. The longer central span underwent little torsional oscillation in the first 20 seconds of the motion, after which it began oscillating in torsion with a period of approximately 1 second. Analysis of these data will allow theoretical models of the bridge response during strong shaking to be improved.

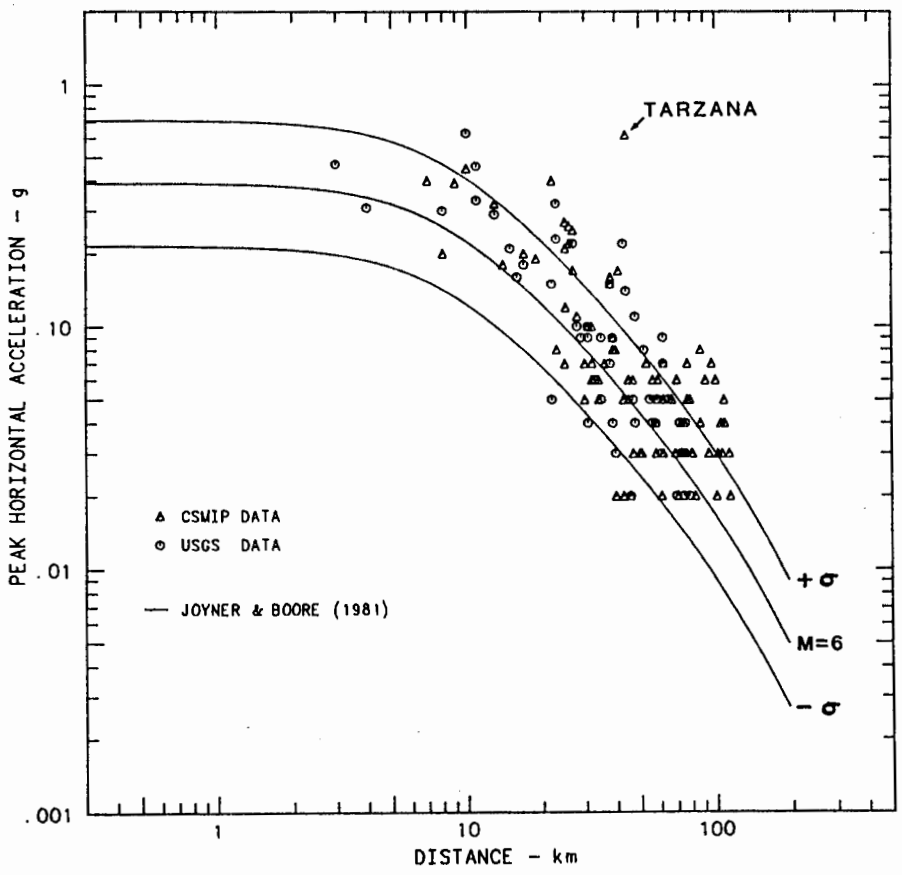

Fig. 5 Peak acceleration data for the Whittier Narrows earthquake plotted against epicentral distance.

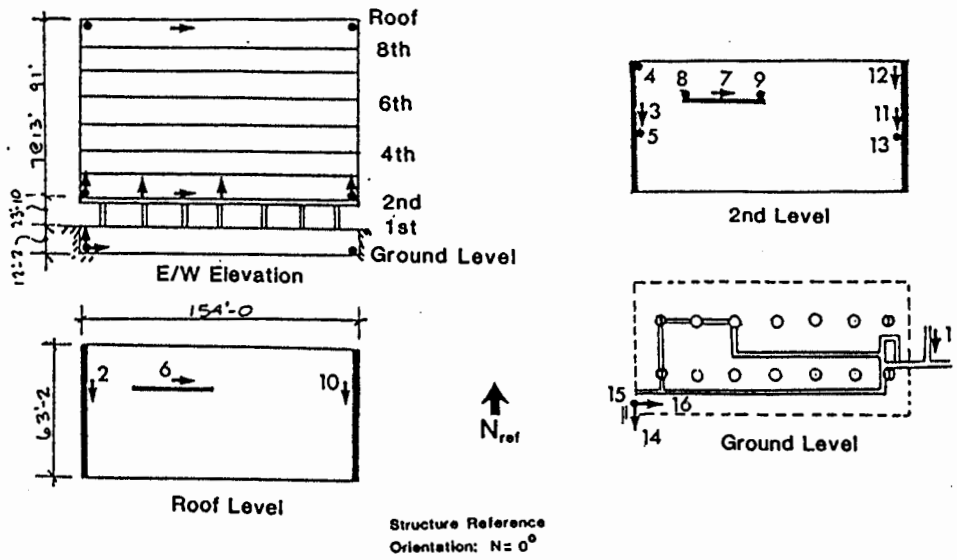

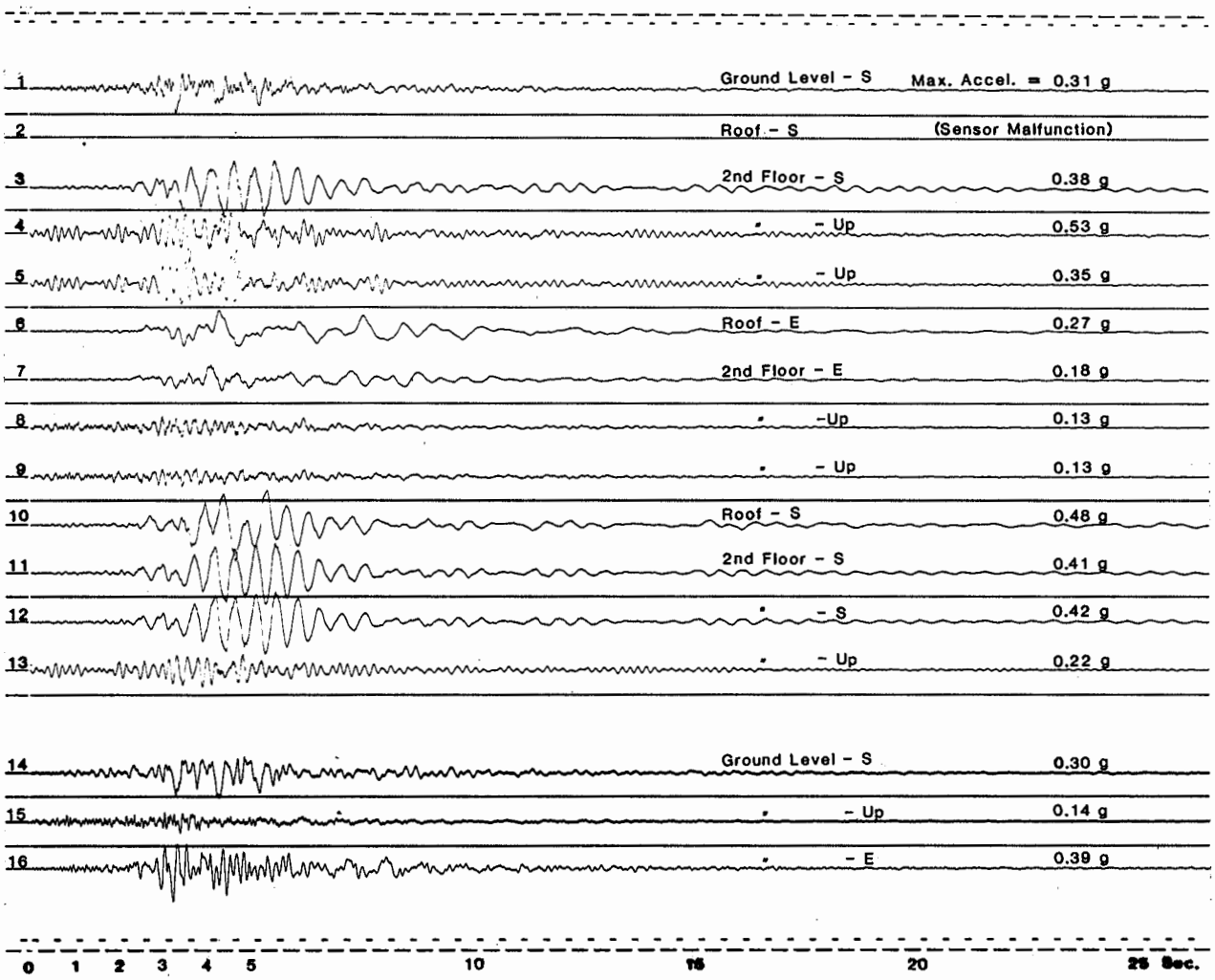

Fig. 6 Sensor locations and accelerogram recorded at the CSULA Administration building during the Whittier Narrows earthquake.

CONCLUSION

In its 16-year history, SMIP has made important contributions to our understanding of strong motion, in particular regarding the response of soft-story structures and the attenuation of seismic waves in California crustal geology. Since the number of SMIP installations will double in the next 15 years, and with the implementation of a data interpretation and utilization component to SMIP, the program's contributions will grow. A crucial cause of the success of SMIP is the extensive advice given by California engineers, seismologists and public officials.

REFERENCES

1. Zeris, C., S. Mahin and V. Bertero (1986) "Analysis of the Seismic Performance of the Imperial County Services Building", Proc. 3rd U.S. National Conference on Earthquake Engineering, Charleston, Vol. 2, pp. 847-858.
2. Trifunac, M.D. and V.W. Lee (1979) "Automatic Digitization and Processing of Strong Motion Accelerograms", Report 79-15, University of Southern California, Los Angeles, California.
3. Joyner, W.B. and D.M. Boore (1981) "Peak horizontal acceleration and velocity from strong-motion records including records from the 1979 Imperial Valley, California, earthquake", Bull. Seismological Society America, vol. 71, 2011-2038.
4. Shakal, A.F., M.J. Huang, C.E. Ventura, D.L. Parke, T.Q. Cao, R.W. Sherburne, and R. Blazquez (1987) "CSMIP Strong-Motion Records from the Whittier, California Earthquake of 1 October 1987", Div. Mines and Geology Report No. OSMS 87-05.
5. Etheredge, E. and R. Porcella (1987). "Strong-Motion Data from the October 1, 1987 Whittier Narrows Earthquake", U.S. Geological Survey Open-File Report 87-616.

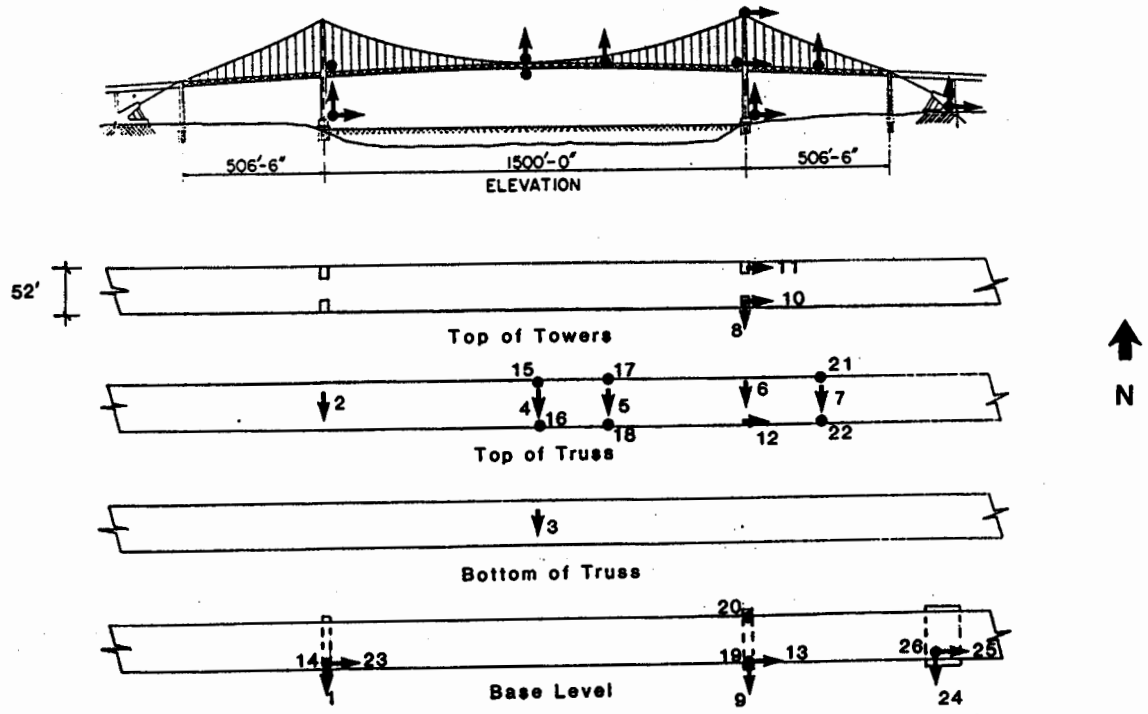

Fig. 7 Locations of sensors on the Vincent Thomas suspension bridge.

Influence of focal mechanism on peak accelerations of strong motions of the Whittier Narrows, California earthquake and an aftershock

John E. Vidale

University of California at Santa Cruz

Abstract

Focal mechanisms affect the pattern of the peak accelerations of the October 1, 1987 Whittier Narrows earthquake and its October 4 aftershock. The peak accelerations observed on 21 Strong Motion Instrumentation Program and 22 United States Geological Survey accelerograms correlates well with the ratio of shear wave amplitude computed from the thrust mechanism of the mainshock and the strike-slip mechanism of the aftershock. This correlation means that seismic energy is radiated from the fault with close to the standard double-couple radiation pattern at the frequencies 3 to 6 Hz corresponding to the peak accelerations.

Introduction

The double-couple nature of earthquakes is well-known, as is the resulting pattern of radiated seismic waves (see Sykes, 1967, and Stauder, 1968, for example). The body of literature documenting the effect of radiation pattern on seismic waves with periods of 1 to 500 seconds is large. For the periods that typically control peak accelerations of strong motions, 0.1 to 1.0 seconds, however, such radiation patterns have not been observed. Liu and Helmberger (1985, figure 14) find that the radiation of an aftershock of the 1979 Imperial Valley earthquake shows a double-couple pattern at a frequency of 1 Hz but not at 2 Hz. These shorter periods, which are of most interest to earthquake engineers, might fail to show a clear radiation pattern for several reasons. Sufficient scattering in the crust, which would affect the short-period energy more than the long-period energy because it has traveled more wavelengths between the earthquake and the seismometers, would tend to blur the radiation pattern into a more uniform distribution. The fault plane itself might not be equally smooth on all scales, and so perhaps short-period seismic radiation is more complex than a double couple. The data in this paper show, however, that at frequencies of 3 to 6 Hz, the radiation pattern is observable. This result supports the conclusion that these two earthquakes have radiation patterns at high frequencies that are similar to the patterns at longer-periods and scattering does not significantly diminish the radiation pattern of the earthquake source.

The dataset of peak accelerations

The M_L 5.9 Whittier Narrows earthquake occurred on October 1, 1987. The hypocenter was located at 14.6 km depth, and the mechanism is a gently dipping thrust (Haukkson and Jones, 1989). Numerous aftershocks filled the volume from 8 to 17 km depth extending about 4 km in all directions

horizontally. Bent and Helmberger (1989) analyze the teleseismic body waves and propose a double source; their second source is 11 km deep and 5 times larger than the first with a slightly different mechanism. It is important to consider the location and mechanism of the largest patch of moment release to understand the peak accelerations. The double source they propose is best studied with teleseismic body-waves since the strong ground motions are more complicated by the Los Angeles basin near-surface structure. I use the depth and mechanism of their second and largest source to represent the mainshock in this paper. The M_L 5.3 aftershock that occurred on October 4, 1987 was located 2 km northwest of the mainshock at a depth of 13.3 km, with a strike-slip mechanism on a vertical plane (Haukkson and Jones, 1989).

Shakal et al. (1987) collected the data from 22 strong-motion stations that recorded both the mainshock and the aftershock. Etheredge and Porcella (1987, 1988) published records from an additional 30 stations that recorded both events. The locations of these 52 stations are shown in Figure 1. The University of Southern California also retrieved data for these two earthquakes from about 80 strong motion stations; however, these data are not yet available. Soon, digitized mainshock records from the USC network will be available, but the aftershock records are not available in unprocessed form nor is there a schedule for digitizing them. The USC data would fill a large gap in our coverage to the east of the hypocenters, so the conclusions of this paper can be tested against the USC data when it is processed and released. From the USC data, Trifunac (1988) has noted that the pattern of peak amplitudes of the mainshock differs from the pattern for the aftershock, and hypothesizes that this difference is due to the radiation pattern.

The peak horizontal accelerations for both the mainshock and the October 4 aftershock for each station are given in table 1 of Vidale (1989). The peak is estimated by computing the square root of the sum of the squares of the peaks from the published copies of the film records for the two horizontal components. This measure differs from Campbell (1981), who used the mean of the two horizontal components, and Joyner and Boore (1981), who used the larger of the two. The differences between these measures do not affect the conclusions of this paper. A more accurate measure of the peak accelerations would require digitized records, and is not yet possible since no aftershock records have yet been digitized. These stations are a mixture of free-field, basement, and ground floor installations. Although basement records have been reported to show smaller peak accelerations than free-field records (Campbell, 1981), the difference is small and will not affect the conclusions of this paper, which are drawn only from the ratios of the two events, not the absolute levels.

The peak accelerations from the mainshock and the aftershock are plotted in Figures 2 and 3. The waveforms are all displayed in Etheredge and Porcella (1987, 1988) and Shakal et al. (1987). Large changes in peak amplitude occur over short distances. Such changes are not likely to result from radiation pattern, which varies smoothly over the focal sphere, but instead may be the variations in near-receiver focusing, reverberations, and receiver shear impedance that has been amply documented (see Vidale and Helmberger, 1988, for example). These near-receiver effects should be minimized by the use of ratios.

Since the mainshock and the aftershock have different focal mechanisms and occur in nearly the same place, as seen in Figure 1, the near-receiver effects

may be mostly canceled by considering only the ratio between the peak accelerations of the two events. The cancellation will not be perfect because the polarization of the seismic waves incident on each station differs between the two events, and the site response can depend on polarization. Cancellation of station effects by taking the ratio of a pair of events has been a standard tool in studying teleseismic body-waves and long-period surface waves.

Figure 4 shows the ratio of peak accelerations from the mainshock to those of the aftershock. Most of the horizontal peak accelerations have a peak frequency in the range 3 to 6 Hz, estimated visually. The ratio averages 2, so the mainshock produced about twice the peak acceleration in the 3 to 6 Hz range as the aftershock, although from standard M_L-moment relations (see Chavez and Priestly, 1985, for example), the mainshock produced 4 to 8 times more moment release than the aftershock.

Not all stations allow the recovery of a reliable estimate for the ratio of the mainshock peak acceleration to that of the aftershock in a consistent frequency range. Stations 141, 262, 289, 436, 634, 969, 5239, 5030, and 5031 are omitted from Figures 4, 6, and 7. Stations 141, 436, 634, and 5239 are dominated by motions whose frequencies are less than 3 Hz for the mainshock, but not the aftershock. Apparently, the mainshock produced much more than twice the 1 to 3 Hz energy of the aftershock. Only stations with similar frequency content for both events will be included in subsequent analysis. Bandpass filtering would allow the use of these records, but fewer than a quarter of the records we use have been digitized. Stations 262, 5030, and 5031 are too weak (less than 0.02 g) to reliably measure the peak acceleration for the aftershock. Station 289 is located on the crest of a dam and shows a strong linear polarization in the same direction for both events, suggesting strong polarization-dependent receiver effects. All the stations were judged with uniform criterion for frequency content and sufficient strength. Station 289 was rejected after its disagreement with the predictions from radiation pattern were noted, but its site on the crest of a dam should have excluded it from consideration at the outset, and no other stations is such questionable locations are included. The reason for omitting Station 969 will be given below.

The peak amplitude ratios shown in Figure 4 vary much more smoothly than the peak amplitudes shown in Figures 2 and 3. Amplitude ratios less than 1.6 cluster in two pockets located just north and west-southwest of the epicentral region. The ratios above 2.0 cluster in three areas to the west-northwest, south, and southeast of the epicentral region. The smoothness of the variations suggest that most of the near-receiver structure has been canceled out.

In a whole space, the radiation pattern of S waves, rather than the weaker P-waves, determines the strength of body waves as a function of direction from the source. The magnitude of the total S wave vector is computed by taking the square root of the sum of the squares of the SH and SV magnitudes, see Aki and Richards (1980), for example. The total S wave pattern has six nodal points evenly spaced around the focal sphere, and four lobes evenly spaced on the great circle that passes through the pressure and tension axes. Figures 5a and 5b show the total S-wave radiation pattern for the mainshock and aftershock focal mechanisms, respectively. The nodal points lie in different places on the focal sphere for the two mechanisms. Figure 5c shows the ratio of the two patterns, which may be considered as a prediction of the ratio of the S-

wave amplitudes of the mainshock to those of the aftershock.

Figure 6 projects the predicted ratio on the surface of the earth. A small correction to the pattern seen in Figure 5c is required since the two events occurred in slightly different locations. Thus the rays to nearby receivers depart from the focal sphere at different take-off angles and azimuths. This projection requires the assumption of a source depth and a velocity structure to convert take-off angle into epicentral distance. A smooth, laterally-invariant basin shear-wave velocity structure is assumed. It is similar to the basin structure given in Vidale and Helmberger (1988). The range that corresponds to each take-off angle is determined with the travel time scheme of Vidale (1988). An 11 km depth has been assumed for both sources, following Bent and Helmberger's (1989) 11 km depth estimate for the dominant source in the M_L mainshock and in the absence of any centroid depth estimate for the M_L 5.3 event, for which the aftershocks ranged in depth from 10 to 14 km (Haukkson and Jones, 1989). I do not doubt the deeper epicentral depths, but the 11 km depth I used probably corresponds to the peak moment release and the source of the peak accelerations. The change in pattern resulting from placing the sources at 14 km depth in accord with their hypocentral locations is discussed below.

Comparison between Figure 4 and Figure 6 shows that the predicted and observed patterns are very similar. The high and low ratio lobes that appear are all predicted, and all predicted lobes appear, if there are stations located to sample them. The stations nearest the epicenter show a systematic overestimation in the predicted shear wave ratios compared with the observations. Adjusting the locations and the mechanisms of the earthquakes would probably improve the fit. However, I think the results are more unbiased when the initial model is used than if additional free parameters corresponding to variations in mechanisms and locations are introduced after inspecting the misfit. The assumptions of point sources and one-dimensional velocity structure are likely to be the largest sources of errors. If both sources are placed at 14 rather than 11 km depth, the areas of high and low relative amplitude predicted from the mechanism move farther from the source. Station 969 is not included in Figure 4. The mechanism coefficient for the aftershock is 0.03 and that for the mainshock is 0.25, giving a predicted ratio of 8.3, far to the right of the rest of the points in Figure 4. The model predicts that the peak for the mainshock would be one fourth of that at a lobe, and the peak for the aftershock would be one thirtieth of that at a lobe. The observed ratio of 2.2 indicates that, as one might expect, the node for the aftershock is not clean enough to drop the amplitude to only 0.03 of maximum value, therefore this ratio is considered unstable.

Figure 7 compares the observed and predicted ratios directly. Despite considerable scatter, a correlation of 0.63 exists between the observed ratio and the ratio of peak accelerations predicted by the focal mechanisms.

Discussion

The influence of focal mechanism on the observed peak acceleration is demonstrated in Figure 7. The ratios of the observed peak accelerations correlate well with the ratios predicted by the focal mechanisms. The scatter seen in Figure 7 may be due to numerous causes. The polarization of the shear waves incident on a station will differ between the two events, and to the extent that the

receiver amplification and path effects are functions of polarization, the observations will differ from the predictions. The source locations are assumed to be known, to be small, and to be at the same depth, but the mainshock and aftershock are not point sources compared to the shear wavelength at 3 to 6 Hz, directivity has been shown to affect accelerations (Boatwright and Boore, 1982), and the depth of the source of the peak accelerations is not precisely known. Scatter also arises from variation in the dominant frequency of the peak acceleration. Since the source spectra of the mainshock and the aftershock probably differ, the variation in frequency will cause deviations from the predicted pattern. Above, I discarded the 4 worst cases where the mainshock peak accelerations have frequencies markedly lower than the aftershock peak accelerations, but such frequency differences probably remain to some extent.

If the peak acceleration is modulated by the focal mechanism, i.e. nodes show very small accelerations, the points in Figure 7 should cluster about a straight line through the origin like line A. If the pattern from the focal mechanism were completely obscured, the points would cluster about the horizontal line B. Line A fits much better than line B. The tendency is that at locations where a node in the radiation pattern is expected, the observed peak acceleration is less and conversely, in a lobe, the peak acceleration is higher.

Line C, with a non-zero intercept but nearly constant slope where the predictions range from 0.5 to 1.5, is the shape of curve I would expect to observe. The non-zero intercept would reflect that some energy is observed where shear wave nodes are predicted, either from scattering of body waves by the geological structures over a solid angle wide enough to partially fill in the nodes or surface waves or P waves may fill in where S body waves are weak. Small-scale variation in the orientation of the fault plane or slip direction would also tend to obscure the nodes. The data do not require a significantly non-zero intercept.

The strength of the correlation means that these node-filling mechanisms are weak. The correlation between S wave strength and peak accelerations means that surface waves are either generated near the receiver or do not influence peak accelerations. In the longer-period range 1 to 10 sec, Vidale and Helmberger (1988) show that each basin generates new surface waves, so conversion of shear body waves to surface waves is probably common.

The S body waves are not scattered enough to obscure the nodes. Previous studies have not had the advantage of two events with different focal mechanisms in the same place, consequently have failed to resolve the radiation pattern at the frequencies of the peak accelerations where receiver effects are also strong. Boatwright and Boore (1982) compare two events with a similar focal mechanism, which minimizes differences in motions due to distinct mechanisms, leaving differences that they attributed to directivity. Liu and Helmberger (1985) looked for the 4-lobed SH radiation pattern from an impulsive strike-slip event on the transverse component. They fail to see the pattern at the 4 to 6 Hz frequency characteristic of the peak accelerations, but they see the pattern emerge when the records are low-passed at 1 Hz. My observations here may disagree with those of Liu and Helmberger (1985) for several reasons. Two events with different mechanisms are compared here, while Liu and Helmberger (1985) attempted to see the radiation pattern from a single event. The observation of Liu and Helmberger (1985) is from the Imperial Valley, which shows

extended coda duration, implying that the basin sediments produce more scattering and surface wave generation than most areas. Finally, total S strength is used here, allowing SH and SV mixing, whereas Liu and Helmberger (1985) assume no contamination of the transverse component by SV energy.

Since the radiation pattern has a measurable effect on the peak accelerations in this case, I address briefly the question of generic patterns that arise from strike-slip and thrust mechanisms. Joyner and Boore (1981) and Campbell (1981) empirically determined the attenuation of peak acceleration with distance, such empirical formulae could be improved by incorporating focal mechanisms. Campbell (1981) examined peak accelerations statistically and notes that reverse faults generate 28 per cent stronger peak accelerations than strike-slip events. A possible explanation of this is obtained by considering that the total shear wave radiation pattern has 6 nodal points that are located at the pressure, tension, and the neutral axes of the focal sphere. There are also 4 lobes that are placed along the great circle connecting the pressure and tension axes, each placed midway between a pressure and a tension axis. By considering the S-wave radiation patterns in Figures 5a and 5b, for sources placed at 10 km depth in a basin structure, the thrust case is seen to have 4 nodes for rays that leave the source horizontally, which surface at a distance of 15 km. The two lobes in the lower hemisphere contain rays that surface hundreds of km from the source, outside the regions of strong motions. The two lobes in the upper hemisphere send rays that appear within 10 km of the epicenter.

The strike-slip event also has 4 nodes for rays that leave the source almost horizontally. The lobes, however, are located such that they concentrate strong motions in the distance range 10 to 40 km. Depending on the range over which that strong motions are recorded, the thrust pattern could appear to be two patches of very strong shaking surrounded by an area of lesser shaking. The strike-slip case would show a more even distribution of strong and weak shaking. Within 10 km, the thrust event would produce stronger shaking. In the range 10 to 40 km, the strike-slip event would produce stronger shaking. A similar conclusion may be drawn from the average body-wave radiation coefficients listed in table 5 of Boore and Boatwright (1984).

Conclusions

The focal mechanism modulates the level of peak accelerations in the 1987 Whittier Narrows earthquake and its October 4, 1987 aftershock. This observation precludes great variations in mechanism in the 3 to 6 Hz range, which corresponds to a 300 to 1000 m scale length on the fault plane. This also suggests that the energy contributing to the peaks in acceleration left the source region as direct S body waves. Scattering does not obscure the influence of earthquake focal mechanism at 3 to 6 Hz.

References

Aki and Richards, 1980. *Quantitative Seismology*, W.H. Freeman and company, San Francisco, 932 p.

Bent, A.L., and D.V. Helmberger, (1989). Source complexity of the 1 October 1987 Whittier Narrows Earthquake, *J. Geophys. Res.*, this issue.

Boatwright, J., D.M. Boore, (1982). Analysis of the ground accelerations radiated by the 1980

Livermore Valley Earthquake for directivity and dynamic source characteristics, *Bull. Seism. Soc. Am.*, **72**, p. 1843-1865.

Boore, D.M., and J. Boatwright, (1984). Average body-wave radiation coefficients, *Bull. Seism. Soc. Am.*, **74**, p. 1615-1621.

Campbell, K.W., (1981). Near-source attenuation of peak horizontal acceleration, *Bull. Seism. Soc. Am.*, **71**, p. 2039-2070.

Chavez, D.E., and K.F. Priestly, (1985). M_L observations in the Great Basin and M_0 versus M_L relationships for the 1980 Mammoth Lakes, California, earthquake sequence, *Bull. Seism. Soc. Am.*, **75**, p. 1583-1598.

Etheredge, E., and R. Porcella, (1987). Strong-motion data from the October 1, 1987 Whittier Narrows earthquake, U.S. Geological Survey open-file report 87-616.

Etheredge, E., and R. Porcella, (1988). Strong-motion data from the Whittier Narrows aftershock of October 4, 1987, U.S. Geological Survey open-file report 88-38.

Haukkson, E., L. Jones, (1989). The 1987 Whittier Narrows Earthquake sequence in Los Angeles, southern California, seismological and tectonic analysis, *J. Geophys. Res.*, this issue.

Joyner, W.B., and D.M. Boore, (1981). Peak horizontal acceleration and velocity from strong motion records including records from the 1979 Imperial Valley, California, earthquake, *Bull. Seism. Soc. Am.*, **71**, p. 2011-2038.

Liu, H.L., and D.V. Helmberger, (1985). The 23:19 aftershock of the 15 October 1979 Imperial Valley Earthquake; more evidence for an asperity, *Bull. Seism. Soc. Am.*, **75**, p. 689-709.

Shakal, A.F., M.J. Huang, C.E. Ventura, D.L. Parke, T.Q. Cao, R.W. Sherburne, and R. Blazquez, (1987). CSMIP strong-motion records from the Whittier, California earthquake of October 1, 1987, Report No. OSMS 87-05, California Strong Motion Instrumentation Program.

Stauder, W., (1968). Mechanism of the Rat Island earthquake sequence of February 4, 1965, with relation to island arcs and sea-floor spreading, *J. Geophys. Res.*, **73**, p. 3847-3858.

Sykes, L.R., (1967). Mechanism of earthquakes and the mechanics of faulting on the mid-ocean ridges, *J. Geophys. Res.*, **72**, p. 2131-2153.

Trifunac, M.D., (1988). The Whittier Narrows, California earthquake of October1, 1987- Note on peak accelerations during the 1 and 4 October earthquakes, *Earthquake Spectra*, **4**, p. 101-113.

Vidale, J.E., (1989). Influence of focal mechanism on peak accelerations of strong motions of the Whittier Narrows, California earthquake and an aftershock, *J. Geophys. Res.*, in press, Whittiers Narrows Special Section.

Vidale, J.E., (1988). Finite-difference travel time calculation, *Bull. Seism. Soc. Am.*, **78**, p. 2062-2076.

Vidale, J.E. and D.H. Helmberger, (1988). Elastic finite-difference modeling of the 1971 San Fernando, Ca. earthquake, *Bull. Seism. Soc. Am.*, **78**, pp. 122-142.

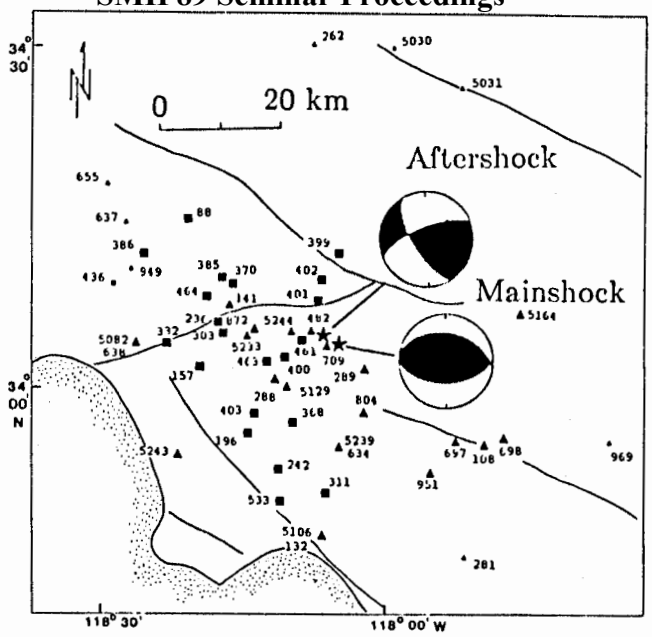

Figure 1. Map showing the locations of the 52 stations listed in Table 1, which recorded both the Oct. 1 mainshock and the Oct. 4 aftershock. Triangles indicate stations described by Shakal et al. (1987) and squares indicate stations described by Etheredge and Porcella (1987, 1988). Smaller symbols indicate stations that are disregarded in this analysis for reasons explained in the text. The epicenters given by the USGS for the mainshock and aftershock are shown as stars. The mechanism for the mainshock is taken from Bent and Helmberger (1989) and the mechanism for the aftershock is taken from Haukkson and Jones (1989). The light lines show faults and the coastline; see Haukkson and Jones (1989) for a discussion of the regional tectonics.

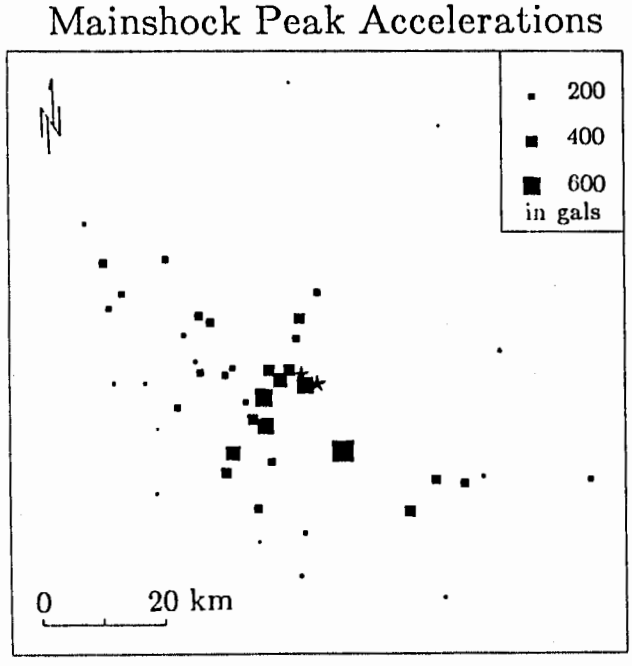

Figure 2. Map showing the peak horizontal accelerations from the Whittier Narrows mainshock for 47 of the stations listed in Table 1. The size of each symbol is proportional to the peak acceleration, which ranges from 50 to 770 gals.

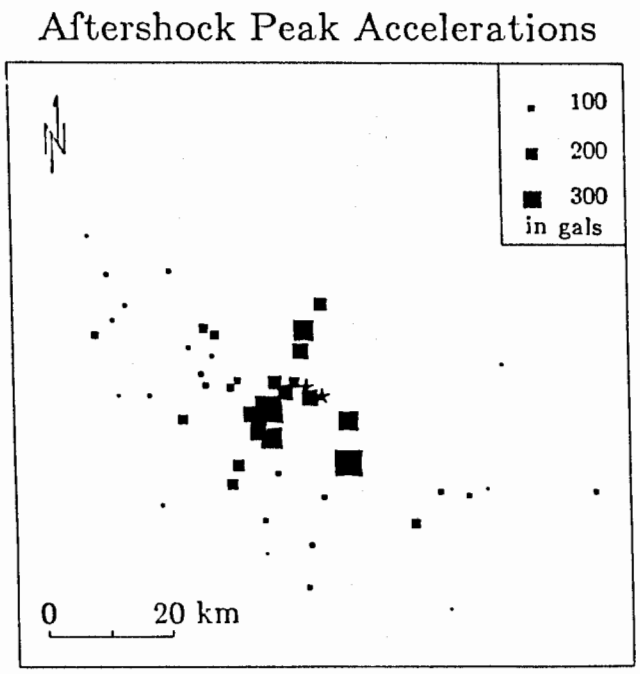

Figure 3. Map showing the peak horizontal accelerations from the Oct. 4 aftershock for 43 of the stations whose aftershock peak accelerations are listed in Table 1. The size of each symbol is proportional to the peak acceleration, which ranges from 30 to 480 gals.

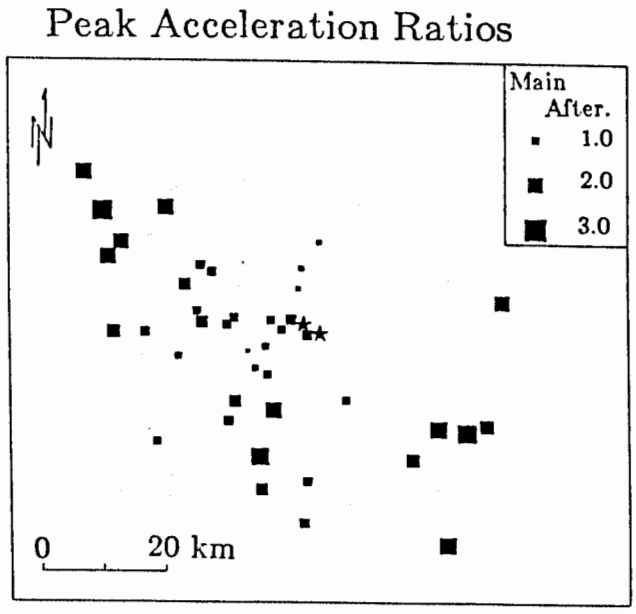

Figure 4. Map showing peak acceleration from the mainshock divided by the peak acceleration from the aftershock for the 43 stations for which a predicted ratio is given in Table 1. The size of each symbol is proportional to the ratio, and the ratios range from 0.7 to 4.0.

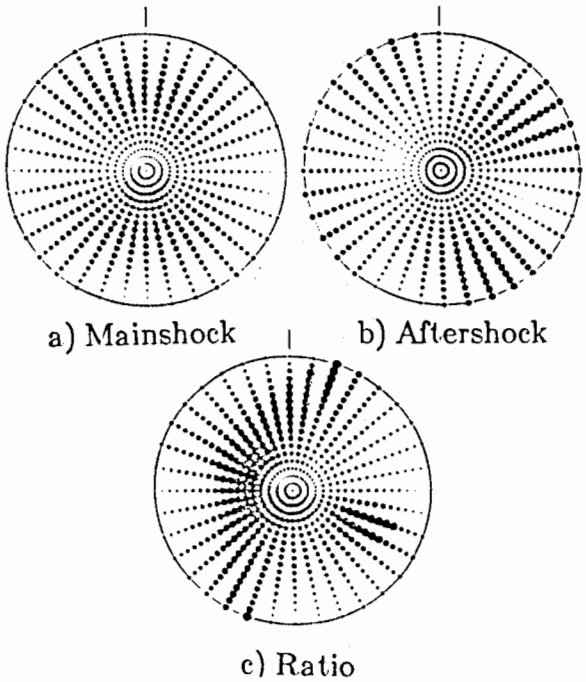

Figure 5 (a). Lower hemisphere projection of the total shear wave radiation pattern for the Whittier Narrows mainshock. The symbols are plotted every 10° in azimuth and every 5° in take-off angle. The size of the symbols is proportional to the strength of the shear waves radiated at that take-off angle and azimuth. The mainshock mechanism has ϕ = 280, δ = 40, and λ = 98. (b). The shear wave radiation pattern for the Whittier Narrows aftershock. The aftershock mechanism has ϕ = 250, δ = 70, and λ = 25. (c). The shear wave pattern from the mainshock divided by the shear wave pattern of the aftershock. This plot is not corrected for the difference in epicentral location of the two events. The plotting is clipped at a maximum ratio of two.

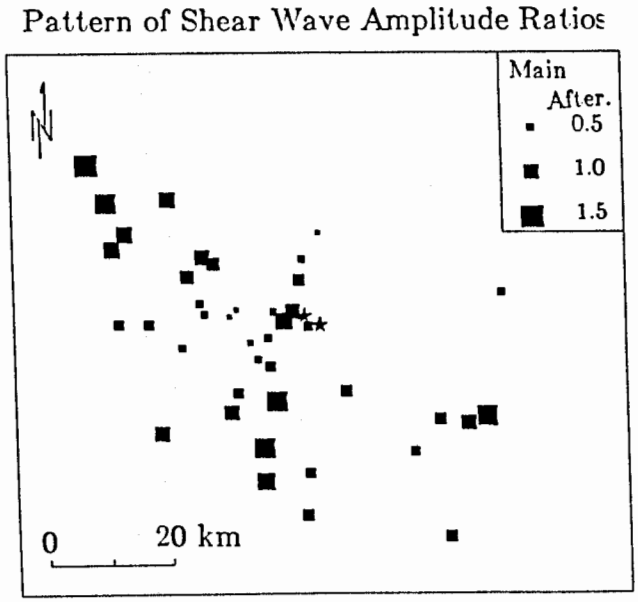

Figure 6. The ratio of motions from the mainshock to motions from the aftershock expected from the S-wave mechanism mapped to the Earth's surface. The difference in source location between the mainshock and aftershock is taken into account. The size of each symbol is proportionate to the ratio, and the ratios range from 0.3 to 1.5.

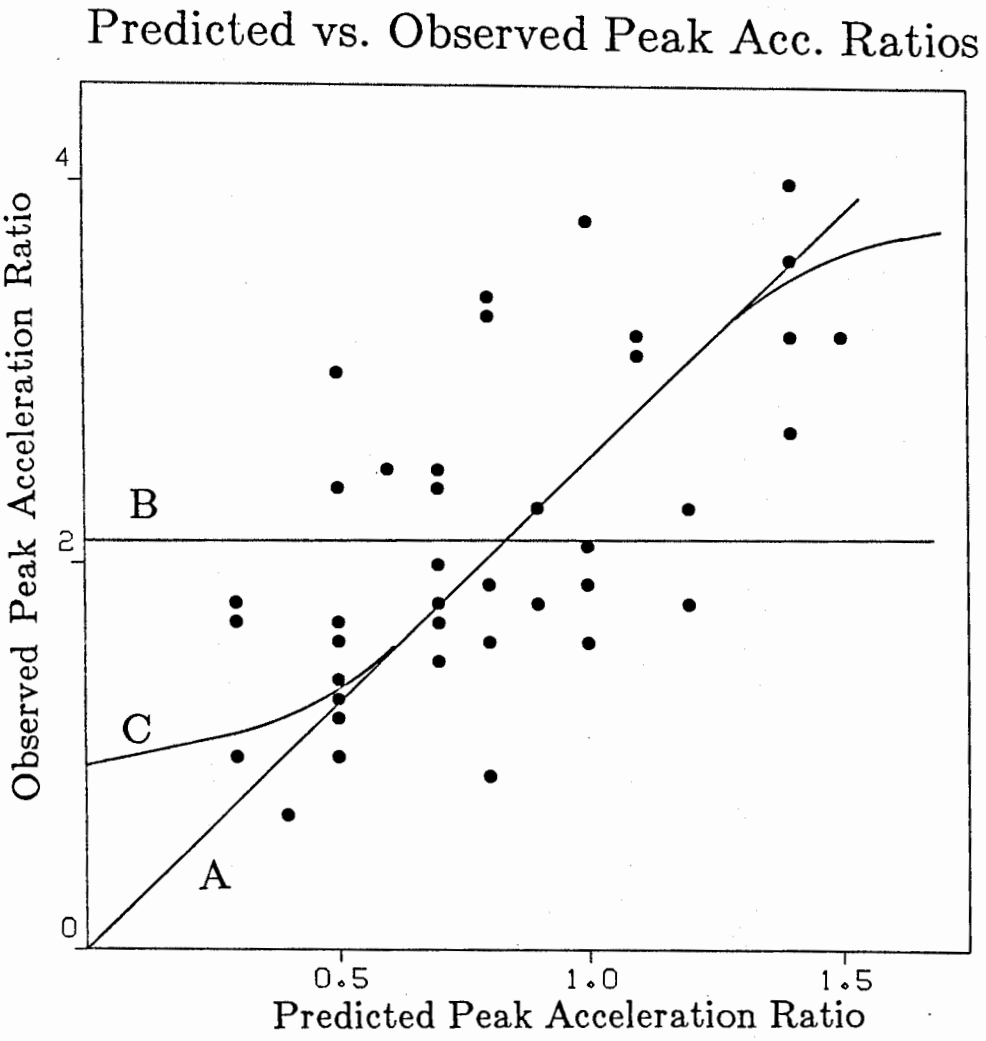

Figure 7. Predicted ratios of peak accelerations from the mainshock and aftershock compared to observed ratios for the first 43 stations listed in Table 1. If the amplitude is proportional to the radiation pattern, the points should scatter around a line that passes through the origin, such as line A. The slope need not be one since the two earthquakes were of different size. If the amplitudes did not depend on focal mechanism, the points would scatter about a horizontal line, such as line B. There is a suggestion that the nodes are not as devoid of seismic energy as predicted, since line C fits marginally better than lines A or B.

A Simple Crustal Structure Satisfying Strong Ground Motion between Whittier and North Palm Springs

Ralph J. Archuleta and Ruth A. Harris
Department of Geological Sciences
University of California, Santa Barbara

Abstract

The October 1, 1987, Whittier Narrows M_L 5.9 earthquake produced a pattern of peak acceleration and intensity that showed a marked geographical asymmetry: the west and northwest regions had larger values than those to the east. A possible cause of this asymmetry was the earth's subsurface geological structure that managed to attenuate or defocus more severely the seismic waves that travelled east of Whittier than those travelling west or northwest. To investigate the subsurface S-wave structure we chose to consider a refraction profile generated by two natural sources, the Whittier Narrows earthquake and the July 8, 1986, North Palm Springs M_L 5.9 earthquake, 135 km due east of Whittier Narrows. After analyzing strong motion data from the mainshocks, high-gain vertical seismograms of aftershocks, and synthetic seismograms we conclude that the strong motion data are consistent with a simple layered medium with a Poisson ratio of approximately 0.25.

Introduction

The Whittier Narrows M_L 5.9 earthquake of October 1, 1987, occurred on an east-west striking thrust fault at a depth of 14.6 km [Hauksson and Jones, 1988]. The focal mechanism showed a pure thrust mechanism on a 25° north dipping plane. Given this mechanism for the earthquake there is no *a priori* reason that one would expect any asymmetry in the ground motion east or west of the source region. However, the peak accelerations [Brady et al., 1988; Shakal et al., 1988; Trifunac, 1988] and the intensity [Leyendecker et al., 1988] show comparable values of these quantities extending over much larger area west of the epicenter than east (Figure 1). One possible cause of this asymmetry could be the subsurface velocity structure. To examine this possibility we examined the data as one would if there were a reversed refraction profile. Rather than using explosions as is the case with exploration seismology, we could use naturally occurring sources, namely, the Whittier Narrows earthquake, the July 8, 1986, North Palm Springs M_L 5.9 earthquake and possibly the October 1, 1985, Redlands M_L 4.9 earthquake. Each of these earthquakes occurred within 10 km of an east-west line at 34° N latitude and all at approximately the same depth. Our concern was not with the P-wave velocity structure which has been well determined and used extensively in locating earthquakes in southern California [Hadley and Kanamori, 1977], rather our interest is in the S-wave velocity structure. S waves are generally the source of the maximum accelerations and generate the type of motion most damaging to structures.

Method

The approach we considered consisted of three parts: (1) collection of seismograms from the U.S. Geological Survey network of high-gain vertical seismometers, (2) travel time analysis of the seismograms together with the strong motion records, and (3) generation of synthetic

seismograms, based on both the faulting mechanism and the velocity structure, to be compared with the recorded accelerograms. Each of these parts are discussed in detail below.

Seismogram Collection

The USGS high-gain vertical seismometers are used primarily to locate earthquakes in southern California. Consequently they invariably go offscale right after the first arriving P wave for events as large as Whittier Narrows or North Palm Springs, making the S wave unrecognizable. However, both of these mainshocks produced a large number of aftershocks, some of which would have magnitudes such that the S waves would be recognizable on these seismograms. From these seismograms we could approximate the S-wave travel time. The advantage of these stations is that they are more numerous than strong motion stations allowing for more accurate determination of the S wave. The disadvantage is that the stations generally record only the vertical component of motion which can have converted waves arriving at nearly the same time as the true S wave.

We selected those USGS stations that lay between Whittier and North Palm Springs (Figure 2). Using aftershocks of the mainshocks we plotted the seismograms on a reduced travel time plot (Figures 3 and 4). Each seismogram was scaled by the gain of the station to normalize the amplitudes to one common gain. (The gains are not always known thus limiting the use of these seismograms to travel time analysis only.) Next the amplitudes were multiplied by R, where R is the epicentral distance between the station and the source, to account for geometrical attenuation of the S wave. The seismograms are plotted versus distance. The origin time is based on a reduced travel time: the true time minus a term that is R divided by some velocity, the P-wave velocity of the medium between depths of 16 km and 32 km. The strong arrival marked by the dashed line is the presumed S wave. From the slope of the dashed line the S wave velocity can be determined, 3.64 km/s. The fact that the same velocity is determined regardless of the source being at Whittier or at North Palm Springs demonstrates that the velocity structure is basically horizontally layered. A dipping structure would have produced two different apparent velocities that could be resolved by allowing for a dipping structure. To examine the travel paths that the S wave followed from the source to the stations we analyzed the travel times.

Travel Time Analysis

The travel time analysis was based on tracing seismic rays through an assumed velocity structure (Cerveny et al., 1977). Because the S-wave velocity 3.64 km/s was 0.58 times the P-wave velocity, i.e, a Poisson solid, we initially assumed that the entire medium was a horizontally layered Poisson solid (Figure 5). With this assumption we placed a source at a depth of 14.6 km and generated a suite of rays that left the source with different takeoff angles. Figure 6 shows the ray paths and the travel time of each S wave for the distance range 0 - 100 km. This travel time is compared with the S wave on the strong motion data. (It would be circular reasoning to compare it with the data on the vertical seismograms)

In order to compare the predicted travel time with the data, the accelerogram must have absolute time, otherwise one can arbitrarily shift the accelerogram to get a perfect fit. While there are about 20 CDMG and USGS strong motion stations between Whittier and North Palm Springs near 34° North latitude, the actual number that have absolute time and have been digitized is 7 (Figure 7). Comparing the predicted travel time with the observed travel time we find that the predicted time is about 0.2 to 0.5 seconds earlier. For S waves this agreement is excellent considering that the near-surface material in the model has a high velocity compared to what is observed in this general area [Fumal and Tinsley, 1985]. Thus by allowing for a veneer of

sediment cover the travel times can be brought into better agreement. An example of the predicted and observed S wave arrival time is shown in Figure 8. Although the S waves on the high-gain vertical seismometers and match between the predicted S-wave arrival time and that observed on the strong motion horizontals provide convincing evidence for a simple crustal structure, the amplitude information must be compared with predictions that are based on the source as well as the crustal structure.

Synthetic Seismograms

As mentioned above, the focal mechanism of the Whittier Narrows earthquake does not suggest any east-west asymmetry in the ground motion. The strike is east-west and the slip direction is due south with the north side of the fault overriding the south side. If there were to be asymmetry one could expect it to be stronger motion south of the epicenter compared to north of the epicenter due to directivity and interaction of seismic waves and the free surface in the hanging wall above the fault plane. This does appear to be the case as seen in the intensity data [Leyendecker et al, 1988] and peak horizontal accelerations [Trifunac, 1988]. To see if the earthquake mechanism along with the velocity structure could have produced low amplitudes east of Whittier, we generated complete synthetic seismograms [Bouchon, 1981]. Completeness refers to the fact that the seismograms contain all possible elastic waves for the given velocity structure, i.e., body waves, head waves, surface waves, and all possible overtones (reverberations within a layer or combinations of layers). The earthquake source is represented as a point source double-couple with a seismic moment of 1.0×10^{25} dyne-cm with a 90° strike and 90° slip angle on a 25° north dipping fault plane. The synthetic particle velocity time history is computed for each strong motion station and compared with the particle velocity obtained by integrating the accelerogram. The synthetics are computed for frequencies between DC and 8.0 Hz; the data have been lowpassed with a corner at 8.0 Hz for an equal comparison. As an initial comparison we look at the transverse component which should be only SH waves (Figure 9a and 9b). Using only a point source and neglecting the finiteness of the fault, we cannot expect to match more than the first cycle of the particle velocity in the data. Although the comparison between the synthetic and data is not perfect, the fit does show that the amplitudes are in fair agreement. The amplitude depends both on the source function and on the impedances of the crustal material.

Conclusions

Considering the amplitudes and arrival times are in fair agreement supports the hypothesis that the asymmetry in the observed ground motion is due to amplification west of Whittier rather than anomalous attenuation of amplitudes east of Whittier.

References

Bouchon, M., (1981). A simple method to calculate Green's functions for an elastic layered medium, *Bull. Seism. Soc. Am.*, **71**, 959-971.

Brady, A. G., E. C. Etheredge, and R. L. Porcella (1988). The Whittier Narrows, California earthquake of October 1, 1987- preliminary assessment of strong ground motion records, *Earthquake Spectra*, **4**, 55-74.

Cerveny, V. I., A. Molotkov, and I. Psencik, (1977). *Ray Method in Seismology*, Karlova University, Prague, 231 pp.

Fumal, T. E., and J. C. Tinsley, (1985). Mapping shear-wave velocities of near-surface geologic materials, in Evaluating Earthquake Hazards in the Los Angeles Region- an earth-science

perspective, *U.S. Geological Survey Professional Paper 1360*, ed. by J. I. Ziony, 127-149.

Hadley, D., and H. Kanamori, (1977). Seismic structure of the Transverse Ranges, California, *Geol. Soc. Am. Bull.*, **88**, 1469-1478.

Jones, L., and E. Hauksson (1988). The Whittier Narrows, California earthquake of October 1, 1987 - seismology, *Earthquake Spectra*, **4**, 43-53.

Leyendecker, E. V., L. M. Highland, M. Hopper, E. P. Arnold, P. Thenhaus, and P. Powers, (1988). The Whittier Narrows, California earthquake of October 1, 1987 - early results of isoseismal studies and damage surveys, *Earthquake Spectra*, **4**, 1-10.

Shakal, A., M. J. Huang, and T. Q. Cao, (1988). The Whittier Narrows, California earthquake of October 1, 1987 - CSMIP strong motion data, *Earthquake Spectra*, **4**, 75-100.

Trifunac, M. D., (1988). The Whittier Narrows, California earthquake of October 1, 1987- note on peak accelerations during the 1 and 4 October earthquakes,*Earthquake Spectra*, **4**, 101-113.

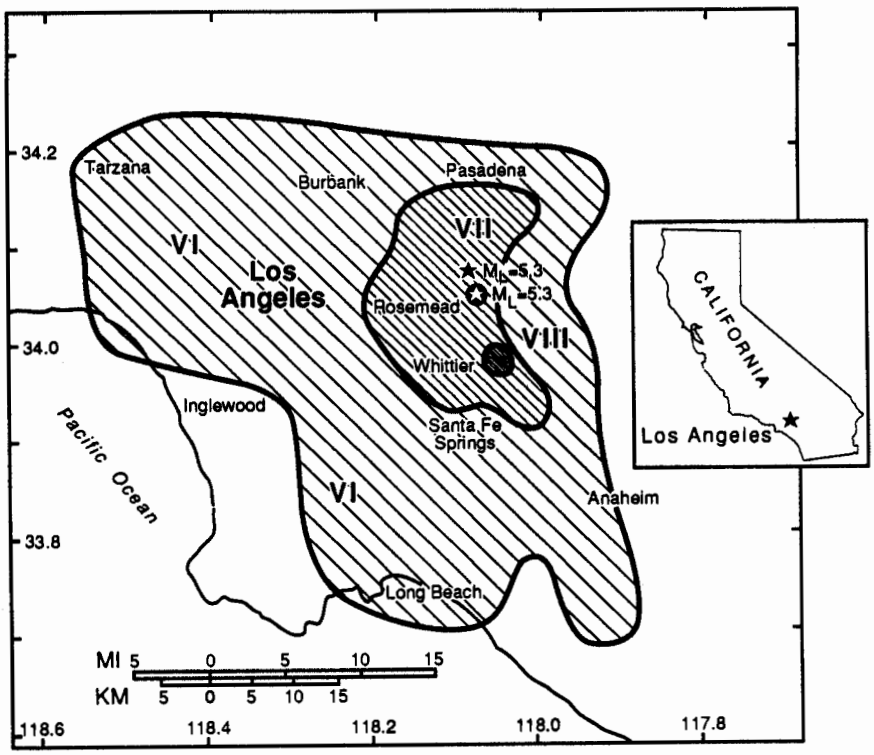

Figure 1. Modified Mercalli intensity isoseismals in the Los Angeles area for the Whittier Narrows earthquake of October 1, 1987. From Leyendecker et al., (1988).

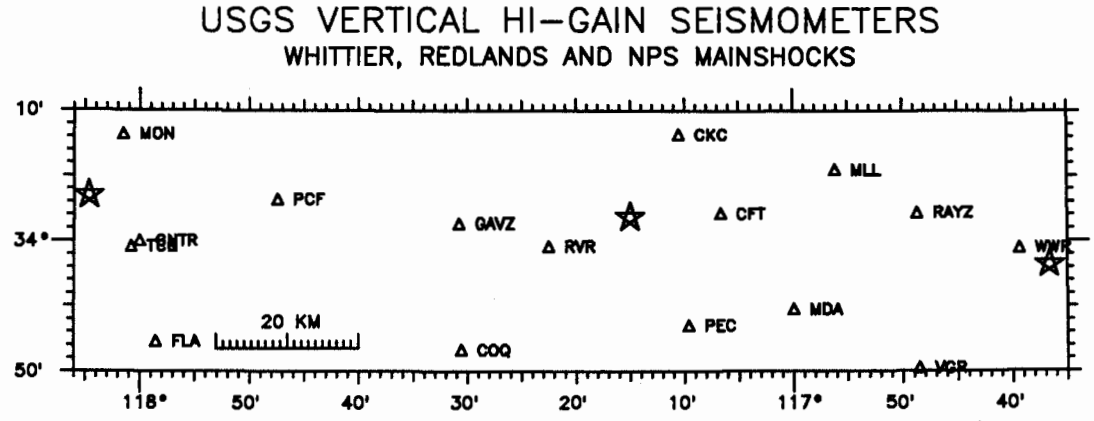

Figure 2. Plan view of U.S.G.S. high-gain vertical stations between Whittier and North Palm Springs, California. Epicenters of the Whittier Narrows, Redlands and North Palm Springs earthquakes shown by stars.

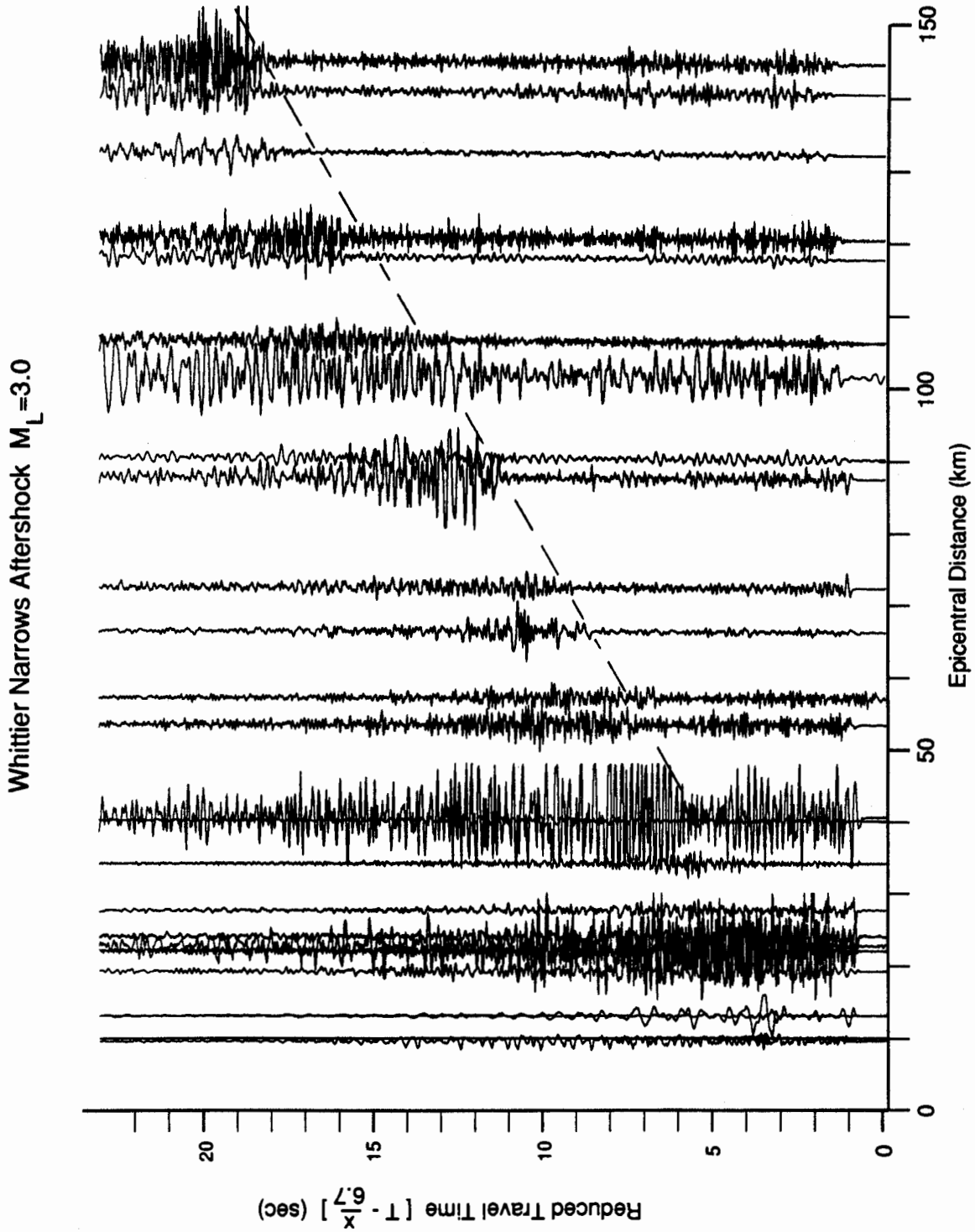

Figure 3. Reduced travel time plot for an aftershock of the Whittier earthquake (10/1/87 at 15:05, 11.5 km depth, M_L3.0) recorded by USGS high gain vertical stations. Reduction velocity is 6.7 km/sec. Seismograms have been scaled by station gain (where known) and for geometrical spreading.

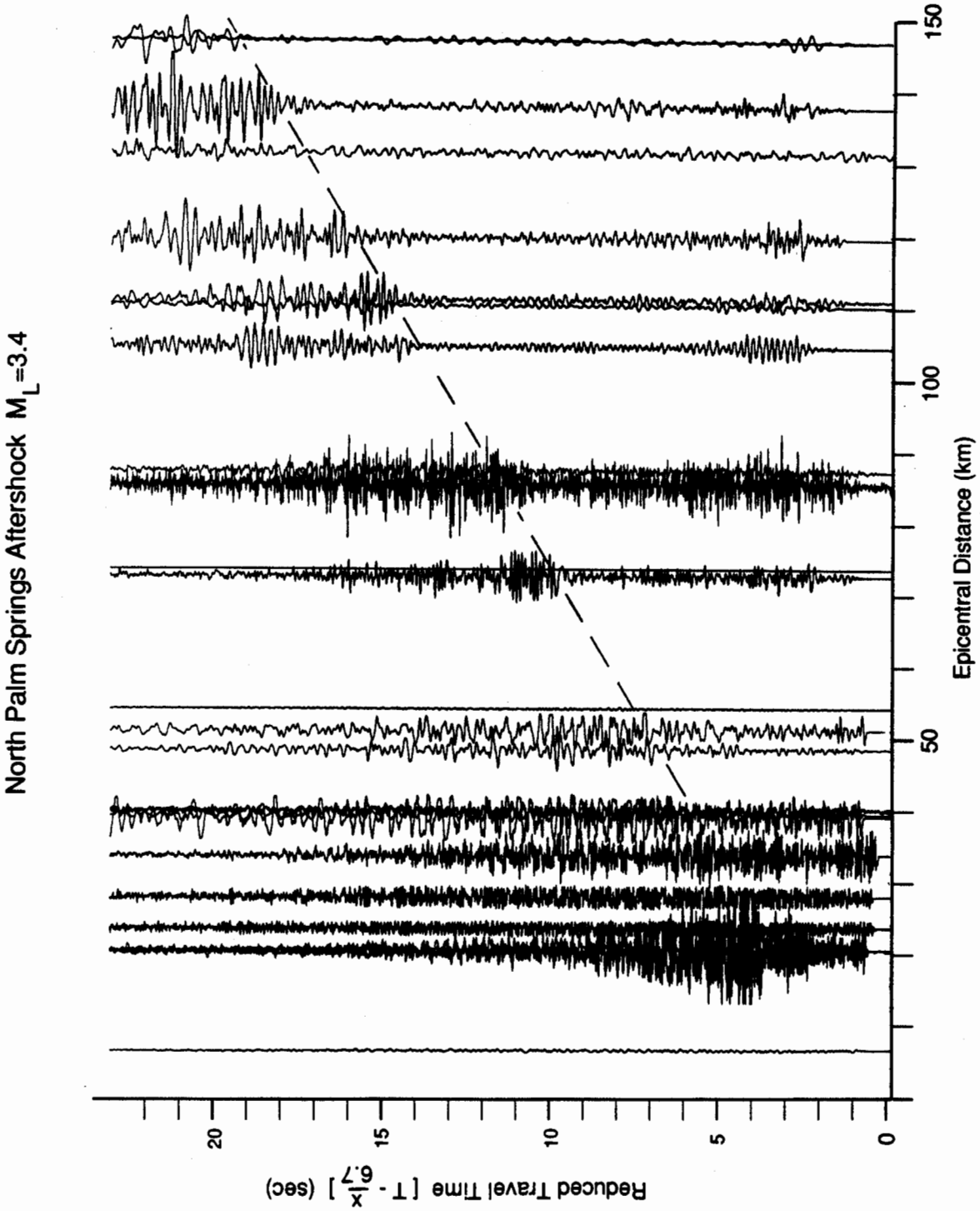

Figure 4. Reduced travel time plot for an aftershock of the North Palm Springs earthquake (7/14/86 at 01:43, 12 km depth, M_L3.4) recorded by USGS high gain vertical stations. Reduction velocity is 6.7 km/sec. Seismograms scaled for station gain (where known) and for geometrical spreading.

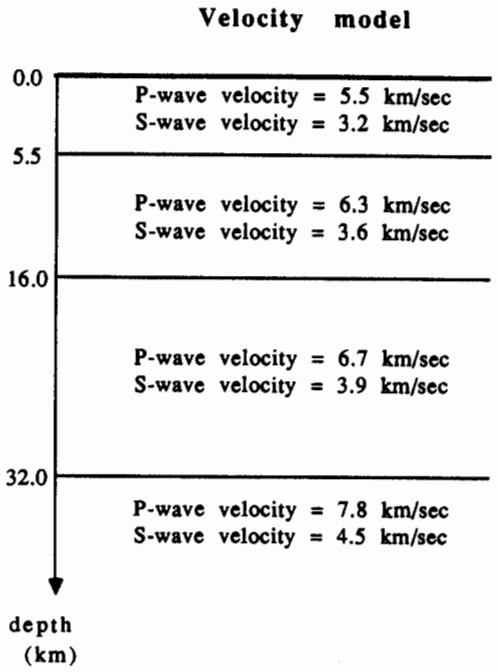

Figure 5. P and S-wave velocity structure used in our study. P-wave velocity structure is from Hadley and Kanamori (1977). S-wave velocity structure is result of analysis of high gain vertical data, which gives a P to S wave velocity ratio of 1.732.

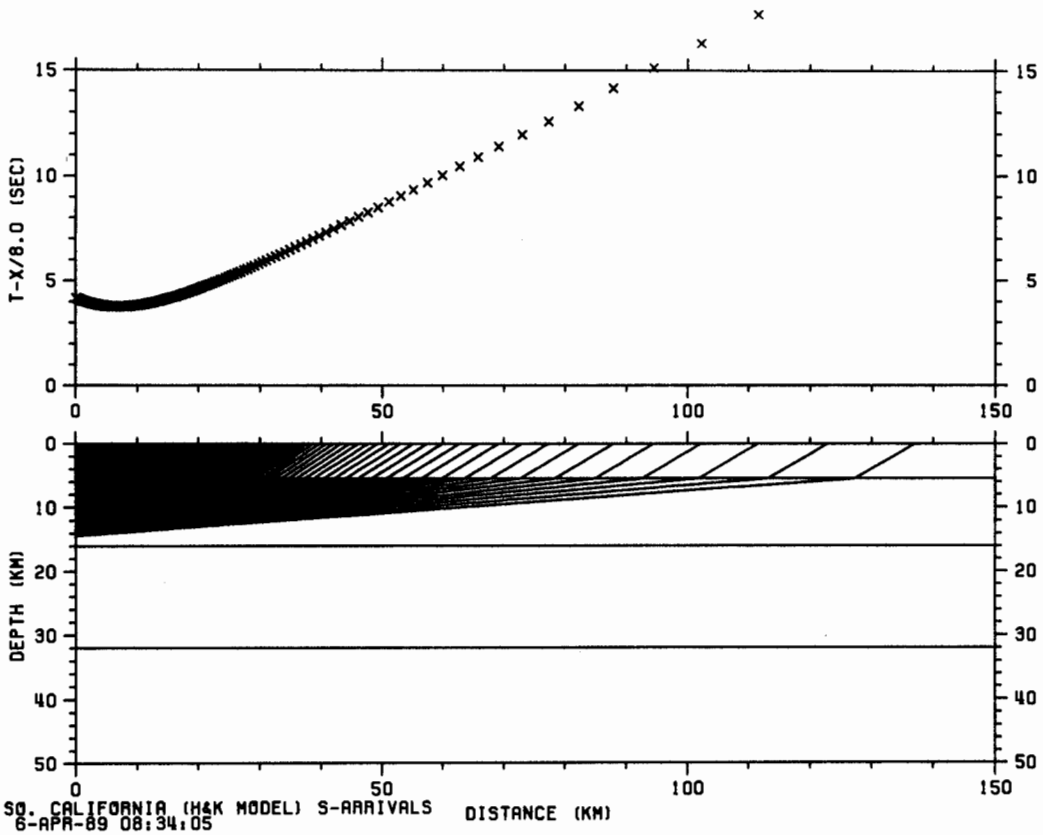

Figure 6. Plot of S-wave arrival times versus distance from the Whittier epicenter for rays traced through the S-wave velocity model shown in Figure 5.

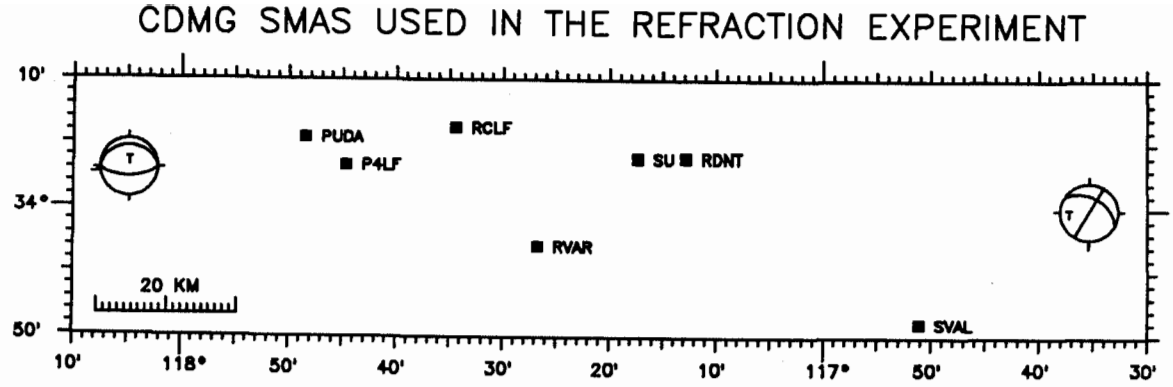

Figure 7. CDMG strong-motion stations used in our study. These stations were the only free-field or in building basements that have both absolute time and have been digitized.

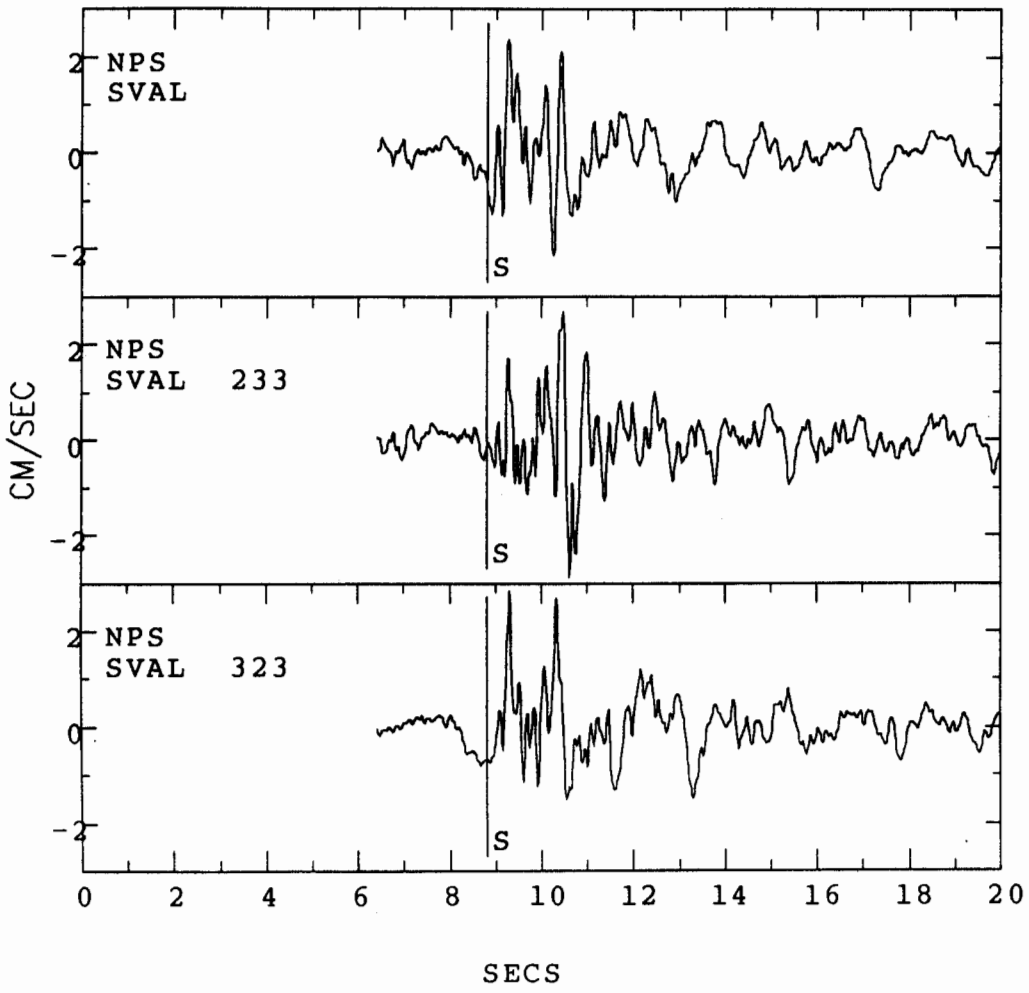

Figure 8. Actual and predicted S-wave arrival time at the Silent Valley station which recorded the North Palm Springs earthquake (epicentral distance, 28 km). Zero time is the origin time of the earthquake. Prediction of S-wave arrival is denoted by the vertical line. Components shown are vertical (down motion is positive), radial, transverse particle velocity obtained by integrating acceleration.

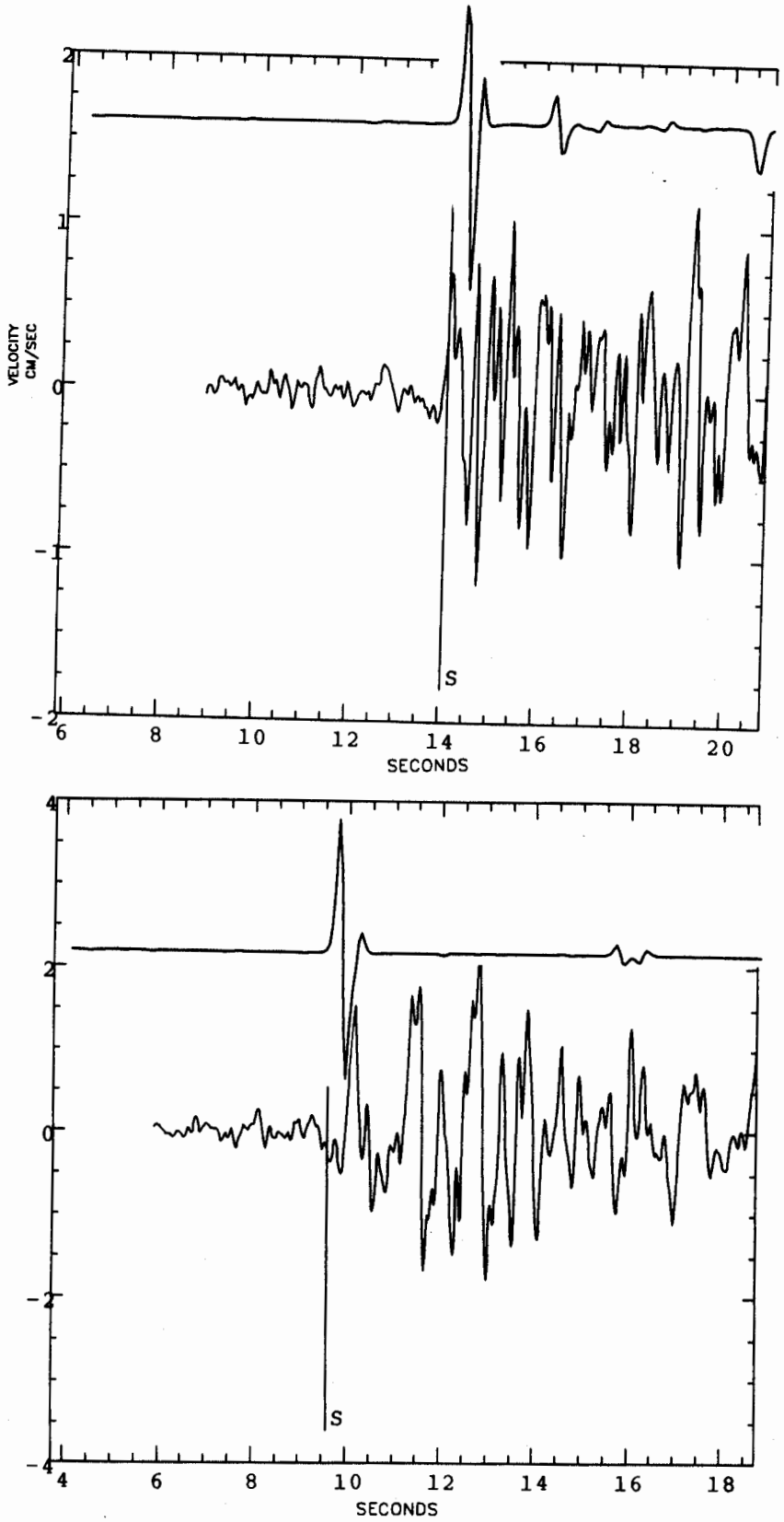

Figure 9. Predicted and observed transverse components of particle velocity. Synthetics include both the focal mechanism of the Whittier Narrows earthquake and the horizontally layered medium. Stations are (a) Rancho Cucamonga Law and Justice Center Free Field at 47 km epicentral distance and (b) Pomona 4th and Locust Free Field at 30 km epicentral distance.

DAMAGE POTENTIAL OF WHITTIER NARROWS EARTHQUAKE GROUND MOTIONS

H. Krawinkler
Professor of Civil Engineering, Stanford University

A. Nassar
Research Assistant, Stanford University

ABSTRACT

This paper summarizes parts of a project that is concerned with an assessment of the damage potential of the ground motions recorded during the October 1, 1987 Whittier Narrows earthquake. Damage potential is defined here as the seismic demand imposed on building structures with due consideration given to representative structural response characteristics. The demand parameters considered in this study include strength demand, ductility demand, and energy and cumulative damage demands. The seismic demands are predicted from ground motion recordings, utilizing simplified elastic and inelastic bilinear SDOF structural models.

INTRODUCTION

Although it was only of magnitude 5.9, the October 1, 1987 Whittier Narrows earthquake has caused considerable damage in the larger Los Angeles area. The question to be addressed is whether the ground motions generated in this earthquake justify the extent of damage and whether they are more severe than is anticipated for a magnitude 5.9 earthquake. The great number of ground motions recorded during this earthquake provide a great opportunity to address the issue of damage potential and evaluate predicted and observed performance. They also permit an assessment of attenuation of ground motion effects with distance from the epicenter.

The study summarized in part in this paper provides quantitative data on damage potential and much needed information for a correlation between predicted demands and observed performance of building structures. It addresses and provides partial answers to the following questions: How large was the seismic demand imposed by the Whittier Narrows earthquake and how did the demand attenuate with distance from the epicenter? Are presently used simplified models of demand prediction adequate for a global performance assessment? Does modern Code design provide the intended level of protection against damage and collapse? If not, what are the major lessons that can be learned for improvement of design practice?

This paper focuses on an evaluation of ground motion and seismic demand parameters and their attenuation with distance from the epicenter. Seismic demand predictions are correlated with estimates of seismic capacity of generic structures in order to assess the damage potential of the ground motions. The results presented here are based on a comprehensive evaluation of the acceleration histories recorded at CSMIP stations located between 7 and 108 km from the epicenter.

EVALUATION OF GROUND MOTION PARAMETERS

Selection of Records

The overriding consideration in the selection of records was that each record could be viewed as a "free-field" record. Thus, only records from instrument shelters or single-story buildings were considered in order to avoid records that could be considerably contaminated by structural feedback. From the three extensive collections of records that were obtained from the earthquake (CDMG, USGS, USC), only the CSMIP stations maintained by CDMG were utilized so far in this study. Very few of the USGS records qualify as "free-field" records, and the USC maintained records from the Los Angeles Strong Motion Accelerograph Network were not available in digitized form early enough to be incorporated at this time.

The locations of the 36 CSMIP stations utilized in this study are shown in Fig. 1, together with vectors indicating the directions and magnitudes of the peak values of accelerations (Fig. 1(a)) and velocities (Fig. 1(b)). These vectors were obtained by vectorially combining the two horizontal components of each record and identifying direction and magnitude of the maximum time history value. Although the main purpose of this figure is to illustrate spatial attenuation, it is interesting to note the trend towards a radial pattern of the vectors, with the epicenter as the focal point.

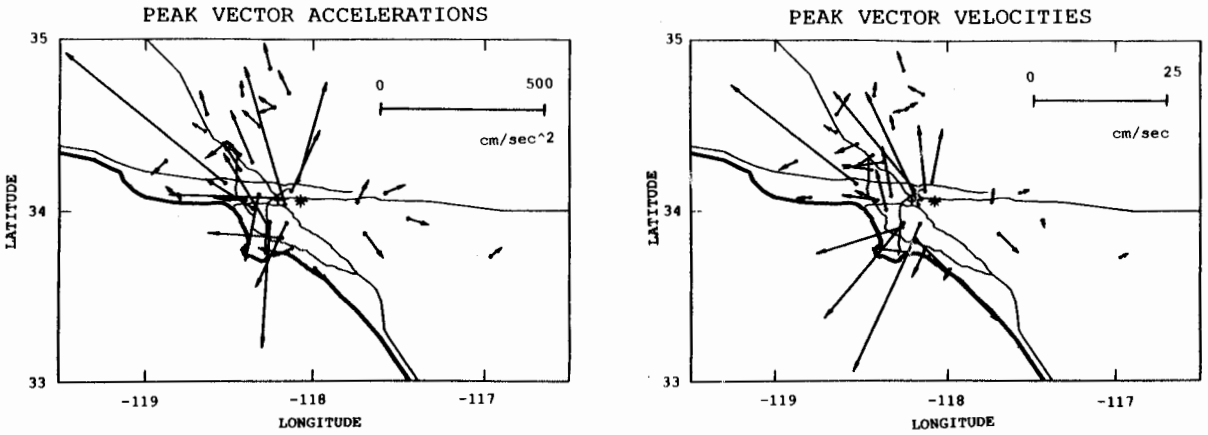

(a) Peak Vector Accelerations (b) Peak Vector Velocities

Fig. 1. Locations and Peak Values of CSMIP Records

There are three peculiar records in this set. One is the Mt. Wilson record (#24399, e = 19 km) which was eliminated from further consideration because it is the only rock site record. The other two are the Tarzana record (#24436, e = 44 km) and the Downey record (#14368, e = 17 km). Both records are unusual, the Tarzana record because of its very large PGA value (0.54g), and the Downey record because of its very small PGA/PGV ratio (6.7/sec). Because of their unusual characteristics both records are excluded from the later discussed regression analysis, although their effects on regression lines is relatively small as was tested by including and excluding them in regressions on PGA and PGV attenuations.

Figure 1 shows the maximum of the vector resultant of the two components of each record. However, in all analytical studies and in all results

reported from here on, the larger of the two recorded components was used rather than the vector resultant.

Attenuation of Ground Motion Parameters

The following ground motion parameters were evaluated for the CSMIP records:

PGA: Peak ground acceleration of record

$RMSA_{max}$: Maximum value of cumulative root-mean-square function of acceleration record

PGV: Peak ground velocity of record

I_{sm}: Arias Intensity of strong motion portion of record, $I_{sm} = D_{sm}(RMSA_{sm})^2$

D_{sm}: Duration of strong motion portion of record, using the definition proposed by McCann and Shah, 1979.

It was attempted initially to look at spacial variations of these parameters, but it was concluded that the CSMIP records represent too small a sample set to draw definite conclusions on spacial variations. Trifunac, 1988, has reported on spacial variations of PGA, using the records from 68 stations of the Los Angeles Strong Motion Accelerograph Network. He came to the conclusion that the motions were largest to the south and north-west of the epicenter. It is planned to combine the CSMIP and USC records to check whether the combined set confirms the contours obtained by Trifunac from the USC set alone.

The CSMIP records are utilized here to evaluate attenuation with epicentral distance alone, without regard to geographic location. It is recognized that such an attenuation disregards variations in geological and site conditions. Although the surface geology of the Los Angeles basin is rather complex, most of the area is covered with a layer of recent or quaternary alluvium. Only records at alluvial sites are used in this study.

Regression analysis was performed on all five parameters listed above. For the first four parameters the following relationship between the parameter y and the distance r is assumed:

$$\log y = a + d \log r + kr \qquad (1)$$

where r = distance from station to the hypocenter of the earthquake, with the focal depth estimated as 14 km (Hauksson, et al., 1988)

a,d,k = regression parameters.

This equation is of the form proposed by Joyner and Boore, 1988, without consideration of a site soil correction factor. Also, Joyner and Boore set the value of d equal to -1.0, whereas in this study d was a free regression parameter. Results of the regression analysis, plotted versus epicentral distance, are shown in Fig. 2.

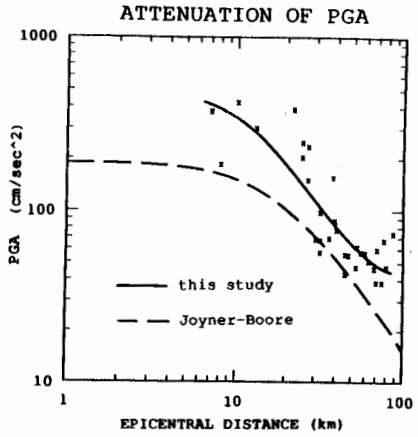

(a) Regression of PGA

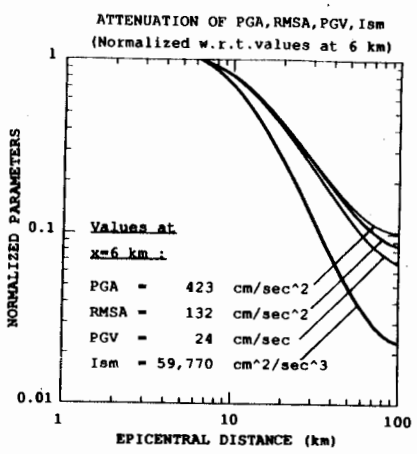

(b) Normalized Regression Lines for PGA, RMSA, PGV, and I_{sm}

Fig. 2. Attenuation of Ground Motion Parameters with Epicentral Distance

Figure 2(a) shows the data points for PGA values and the corresponding regression line as well as the regression line from Joyner and Boore for a magnitude 5.9 earthquake (they used a focal depth of 8 km in their regression). The figure shows that the Whittier Narrows earthquake generated ground motions that were considerably higher at all epicentral distances than predicted by Joyner and Boore.

Figure 2(b) illustrates the relative attenuation of the four basic ground motion parameters. The rate of attenuation for PGA, RMSA, and PGV is very similar, whereas the Arias Intensity I_{sm} attenuates at a much faster rate.

Regression was also performed on the strong motion duration D_{sm}, but using a second order polynomial. The data points and regression line shown in Fig. 3 indicate a clear trend towards an increase in duration with epicentral distance. The strong motion duration becomes an important parameter when cumulative damage is evaluated, an issue that is part of this study but is not addressed in this paper.

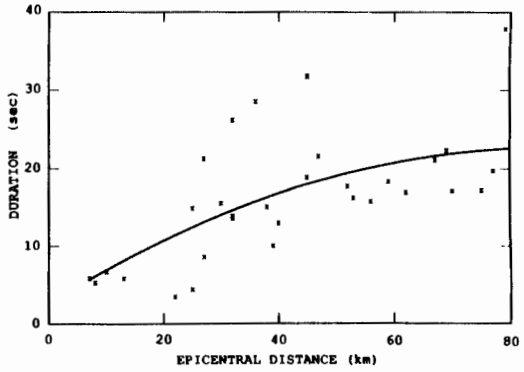

Fig. 3. Attenuation of D_{sm}

EVALUATION OF SEISMIC DEMAND AND CAPACITY OF BUILDING STRUCTURES

It is the main objective of this study to gain a clear understanding of the seismic demands imposed by the Whittier Narrows earthquake on buildings in the larger Los Angeles area The predictions will serve as a basis for assessing the global damage potential of the earthquake as well as the performance of a small number of actual buildings.

For this purpose, seismic demands are predicted from the CSMIP ground motions and capacities of generic code designed structures are estimated.

The global damage potential is assessed through combining the information on demand predictions and capacity estimations.

Seismic Demand Predictions

Seismic performance depends on a number of demand parameters, which may be conveniently classified as follows:

Elastic Strength Demand, $F_{y,e}$. The elastic response spectra provide the needed information on this parameter, which serves to assess the force level at which brittle failure modes have occurred in this earthquake.

Ductility Demand, μ. This parameter is defined as the ratio of maximum deformation over yield deformation for a system with a yield strength smaller than the elastic strength demand $F_{y,e}$.

Inelastic Strength Demand, $F_y(\mu)$. This parameter defines the required yield strength of an inelastic system whose ductility demand is equal to μ.

Strength Reduction Factor, $R_y(\mu)$. This parameter defines the reduction in elastic strength that will result in a ductility demand of μ.
Thus, $R_y(\mu) = F_{y,e}/F_y(\mu)$.

Energy and Cumulative Damage Demands. Repeated cyclic loading is known to have a detrimental effect on inelastic response characteristics. Many cumulative damage models have been proposed in the literature, the simplest one being of the form (Krawinkler, 1987)

$$D = C \sum (\Delta\delta_{pi})^c \qquad (2)$$

where D = cumulative damage
C, c = structural performance parameters
N = the number of inelastic excursions experienced in the earthquake
$\Delta\delta_{pi}$ = the plastic deformation range of excursion i.

For bilinear systems this expression reduces to the total hysteretic energy if the coefficient C is taken as the yield strength F_y and the exponent c is taken as 1.0. In this study the cumulative damage demands using exponents of c = 1.5 and 2.0 were evaluated, as well as the hysteretic energy, damping energy, and input energy.

Time history analysis of bilinear Single Degree of Freedom (SDOF) systems was performed to predict these seismic demands, using all of the CSMIP records. The natural period and yield level of the systems were varied to cover the full range of interest. The strainhardening stiffness and damping were kept constant at 10% of elastic stiffness and 5% of critical, respectively.

Because of space limitations, only elastic and inelastic strength demands ($F_{y,e}$, $F_y(\mu)$) are discussed here. Two examples of spectra of these demands are illustrated in Fig. 4. The solid lines represent site specific

distance for the elastic demand and the inelastic demand for $\mu = 2.0$. The shapes of the spectra are relatively smooth and change very little with distance. The elastic spectra (Fig. 6(a)) exhibit one consistent large protuberance in the short period range, with a peak that moves with distance from 0.15 sec. at 10 km to 0.35 sec. at 80 km. The high values of elastic strength demand in the short period range of near-source spectra help to explain the large damage experienced by stiff masonry buildings in Whittier and other nearby communities. Superimposed in Fig. 6(a) are graphs of the UBC Code values for the product ZC (for soil types S1, S2, and S3), which are a measure of the elastic strength demand for severe earthquakes implied by code design.

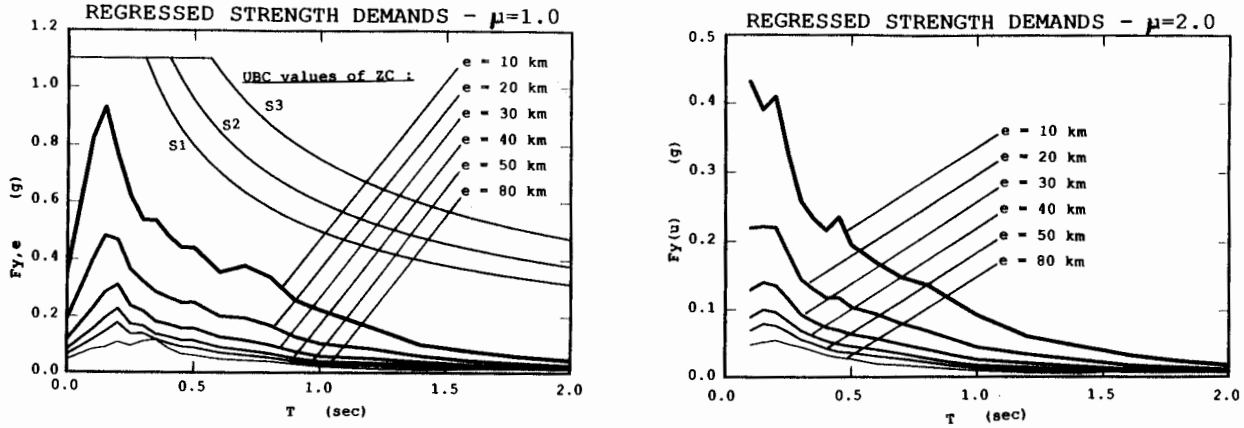

(a) Elastic Strength Demands

(b) Inelastic Strength Demands for $\mu = 2.0$

Fig. 6. Attenuation of Regressed Strength Demand Spectra

The inelastic strength demand spectra attenuate at a rate that is very similar to that of the elastic spectra. Regardless of distance, these spectra show a relatively high demand for structures with a natural period of 0.25 sec. or smaller. This can be seen from Fig. 6(b) and other spectra for $\mu = 3.0$ and 4.0 which are not shown here.

Figure 6 shows clearly that the strength demands of the Whittier Narrows ground motions are large, particularly near the source. If one would consider modern code seismic design forces as a measure of strength capacity (e.g., V/W = ZC/Rw in the 1988 UBC), then the damage potential of the ground motions appears to be very large. However, damage observations do not confirm high ductility demands for modern structures for the reasons discussed in the next section.

Strength Capacity of Building Structures

It is easy to show, and to some degree intended by code design, that actual structures have a significantly larger lateral strength than is indicated by the code seismic design forces. Structures have overstrength due to a variety of sources, including effects of gravity loads on member strength, stiffness (drift) requirements, increase in structure strength due to redistribution of internal forces in the inelastic range, as well as contributions of structural and nonstructural elements that are not considered as part of the lateral load resisting system.

spectra for μ equal to 1, 2, 3, and 4, whereas the dashed lines represent spectra obtained from a regression analysis discussed next.

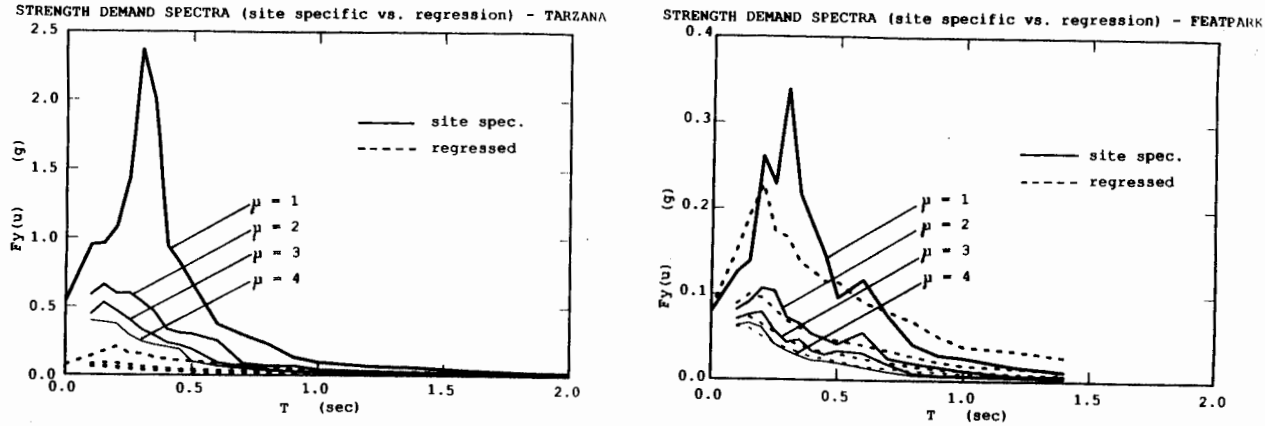

(a) Tarzana Record (b) Featherly Park Record

Fig. 4. Site Specific and Regressed Strength Demand Spectra

A global assessment of damage potential cannot be achieved from site specific spectra whose details may be affected considerably by local site conditions. In order to smoothen local site effects and obtain continuous expressions for distance dependent strength demands, regressionanalysis was performed on each spectral ordinate as a function of hypocentral distance. Equation (1) was again utilized for this regression analysis.

A typical example of a regression line and the corresponding data points are shown in Fig. 5 (for T = 0.2 sec and μ = 4.0). The regression line is similar to that for PGA but, again, the data show considerable scatter. This example is shown because the period of 0.2 sec. is in the most sensitive part of the spectra where the scatter is largest.

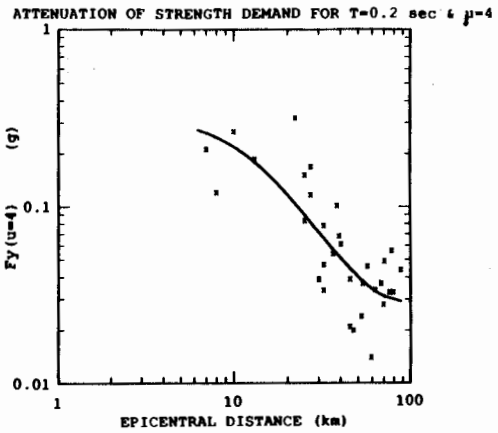

Fig. 5. Attenuation of Strength Demand (T = 0.2 sec., μ = 4.0)

Regressed strength demand spectra at any selected epicentral distance are then obtained from the values of the regression lines for different periods at the selected distance.

Figure 4(a) clearly shows the unusual strength demands of the Tarzana record. The site specific demands exceed the demands obtained from regression by about a factor of 10 in the short period range. The same is not observed in the Featherly Park record (Fig. 4(b)) which is at a similar epicentral distance (40 km vs. 44 km) but to the S-E of the epicenter rather than the N-W. For this record, site specific and regressed demands are similar, particularly for the inelastic strength demands.

An illustration of the attenuation of strength demands is presented in Fig. 6, which shows the variation of regressed strength demand spectra with

In the simplest case, structural behavior can be modeled as shown in the diagram of Fig. 7 (Osteraas and Krawinkler, 1989). In this figure, E represents the seismic design loading, E_1 is the capacity at the member strength level, and E_2 is the capacity at the structure strength level including overstrength. When ductility demands of structures are evaluated, due consideration must be given to this overstrength.

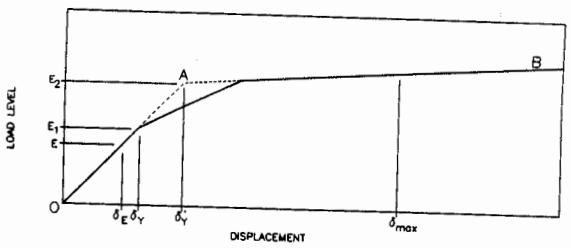

Fig. 7. Simplified Structural Model

The overstrength available in real structures varies widely, dependent on the material and type of structural system, structural configuration, number of stories, and detailing. Although general rules for assessing overstrength cannot be developed for all structures, the need exists to estimate overstrength in order to assess the damage potential of ground motions. Such an attempt has been reported by Krawinkler and Osteraas, 1988, for certain generic types of steel building structures. Efforts are being made as part of this study to estimate overstrength for a limited set of generic reinforced concrete buildings. It would be desirable to do the same for masonry buildings, but not much success can be expected from this exercise because of the great variation in lateral resistance of these structures. Thus, they have to be addressed on a case by case basis.

Information is presently available on the real strength, including overstrength, for three types of generic steel structures designed according to the 1988 UBC (Krawinkler and Osteraas, 1988). These structures are 3-bay by 5-bay buildings of two or more stories, designed as all moment resisting frame structures with Rw = 12 (MF), perimeter frame structures with Rw = 12 (PF), and braced frame structures with two braced bays and Rw = 8 (BF). The bay width was assumed to be 24 ft, altough it was found that the results were rather insensitive to the assumed bay width. For the designed structures the overstrength factor E_2/E is highest for the MFs and lowest for the BFs, decreases with the number of stories, and is as high as 6 for 2-story MFs. Braced frames (BFs) were only used to a period of 0.9 sec. since this period corresponds to the height limitation of 160 ft.

These structures can be viewed as well designed structures that follow basic code requirements, have no excessive waste in their member sizes, but have also no undesirable features such as plastic hinges in columns or weak connections. The information on strength capacity for these generic structures is combined in the next section with the previously discussed strength demands to assess damage potential.

Damage Potential of Ground Motions

Figure 8 shows the strength capacities E_2 of the three generic types of steel structures superimposed on the spectra of strength demands for different ductilities at an epicentral distance of 10 km. It can be seen that, even with the large overstrength available in the generic structures, there are period ranges in which each one of the structure types is expected to experience inelastic deformation. It is fortunate that the overstrengths are highest in the short period range where the strength demands are highest. As can be seen from the figure, for the epicentral distance for which this

figure applies, i.e., 10 km, the global ductility demands are not expected to exceed a value of 2.

The attenuation of ductility demands can be evaluated by comparing Fig. 8 with Fig. 9 which shows similar information at an epicentral distance of 20 km. Capacity curves are shown in this figure only for the perimeter frame (PF). In addition to the E_2 curve, the E_1 curve (see Fig. 7) for this structure type is shown as well. Figure 9 indicates that at this distance localized inelastic deformations have to be anticipated for PF structures with periods of less than 0.5 sec. The figure also contains a curve identifying the code seismic design force level for this structure type denoted by E. The differences between E and the capacity curves E_1 and E_2 illustrate the overstrength present in PF structures.

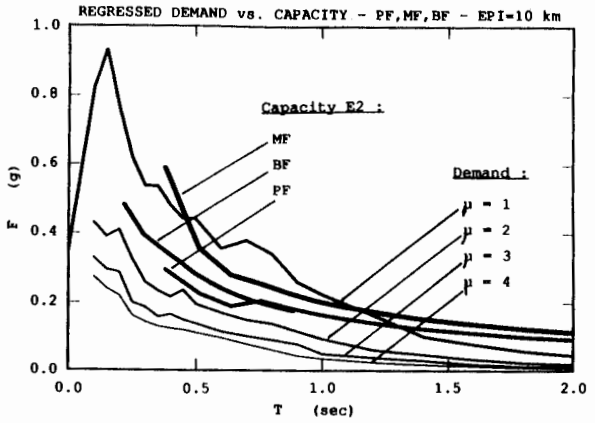

Fig. 8. Strength Demands and Capacities for Generic Types of Steel Structures (e = 10 km)

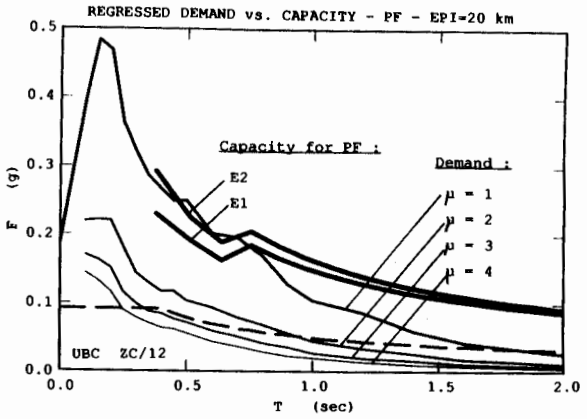

Fig. 9. Strength Demands and Capacities for Perimeter Frame Structures (e = 20 km)

The information of the type presented in Figs. 8 and 9 can be utilized to derive estimates of ductility demands for different types of steel structures as a function of epicentral distance. Figure 10 shows two typical examples, for PF, MF, and BF structures with periods of 0.5 and 0.9 sec. The figure shows global ductility demands (δ_{max}/δ_y' in Fig. 7) as well as local ones (δ_{max}/δ_y in Fig. 7).

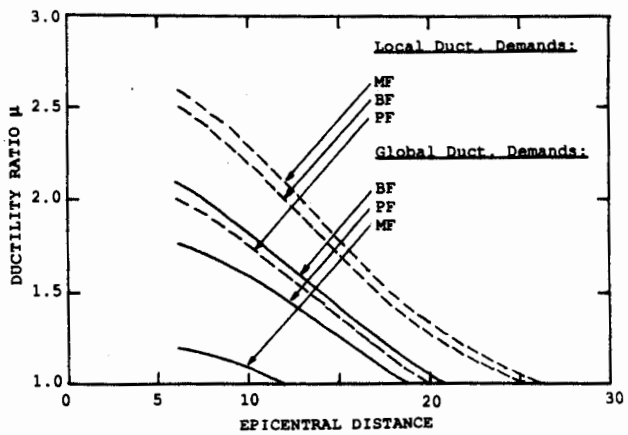

(a) For a Natural Period of 0.5 Seconds

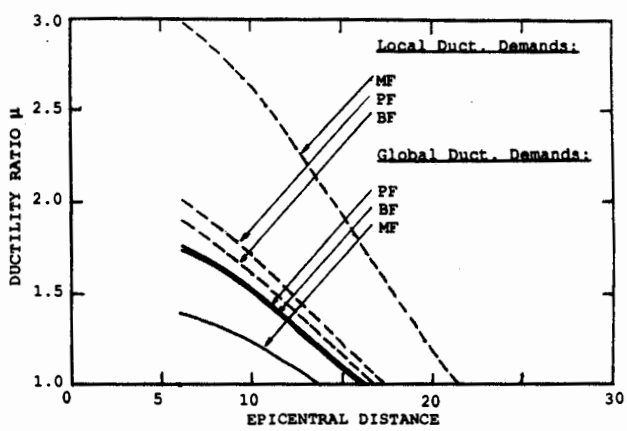

(b) For a Natural Period of 0.9 Seconds

Fig. 10. Variation of Ductility Demands with Distance for Three Types of Steel Structures

Information of the type presented in Fig. 10 permit an assessment of the damage potential of the Whittier Narrows earthquake. It is conluded that this earthquake was indeed a severe test for modern structures located near the source. At specific sites, at which localized site conditions led to greater amplification of motions than is indicated by the regressed spectra, the ductility demands may even have been considerably higher.

CONCLUDING REMARK

Regression analysis on ground motion and seismic demand parameters was employed to obtain information that permits a global assessment of the damage potential of ground motions. A realistic assessment of damage potential can be obtained provided that the real strength of structures, including overstrength, is considered. Even when the overstrength is considered, this study has shown that the October 1, 1987 Whittier Narrows earthquake produced seismic demands that were more severe than expected from a magnitude 5.9 earthquake.

ACKNOWLEDGEMENTS

This study was supported by the California Department of Conservation through a research grant provided by the California Strong-Motion Instrumentation Program.

REFERENCES

1. McCann, M.W., and Shah, H.C., 1979, "Determining Strong-Motion Duration of Earthquakes," Bulletin of the Seismological Society of America, Vol. 69, No. 4, August 1979.

2. Trifunac, M.D., 1988, "The Whittier Narrows, California Earthquake of October 1, 1987 - Note on Peak Accelerations During the 1 and 4 October Earthquakes," Earthquake Spectra, EERI, Vol. 4, No. 1, February 1988.

3. Hauksson, E., et al., 1988, "The 1987 Whittier Narrows Earthquake in the Los Angeles Metropolitan Area, California," Science, American Association for the Advancement of Science, Vol.239, March 1988.

4. Joyner, W.B., and Boore, D.M., 1988, "Measurement, Characterization, and Prediction of Strong Ground Motion," Proceedings of Earthquake Engineering & Soil Dynamics II, GT Div/ASCE, Park City, Utah, June 27-30, 1988.

5. Krawinkler, H., 1987, "Performance Assessment of Steel Components," Earthquake Spectra, EERI, Vol. 3, No. 1, February 1987.

6. Krawinkler, H., and Osteraas, J., 1988, "Steel Building Design," Seminar on Evolving Earthquake Hazard Mitigation Practices, 1988 Annual Meeting, EERI, Mesa, Arizona, Feb. 4, 1988.

7. Osteraas, J., and Krawinkler, H., 1989, "The Mexico Earthquake of Septemner 19, 1985 - Behavior of Steel Buildings," Earthquake Spectra, EERI, Vol. 5, No. 1, February 1989.

IMPLICATIONS OF STRONG MOTION DATA FOR DESIGN OF REINFORCED CONCRETE BEARING WALL BUILDINGS

Jack P. Moehle
Associate Professor of Civil Engineering
University of California at Berkeley

ABSTRACT

A study is made of the performance of two reinforced concrete bearing wall buildings subjected to recent California earthquakes. The buildings are analyzed to verify modeling techniques. The buildings are compared with similar buildings in Chile, and based on the comparison, conclusions are drawn from the Chilean practice regarding likely performance in strong US earthquakes. Design recommendations are made.

INTRODUCTION

Observations of building performances following previous earthquakes have revealed comparatively good performances for reinforced concrete shear wall buildings. These observations extend not only to the combined frame-wall system that has been a popular form of construction in recent years, but also to the bearing wall system in which the walls act as both the vertical and lateral load resisting system. Despite the good performance record of reinforced concrete shear wall buildings, current codes [eg., the Uniform Building Code (UBC) (1)] effectively penalize such buildings in design. A study of the performance of bearing wall buildings during recent earthquakes and of their inherent response characteristics has been undertaken so that more consistent recommendations can be developed.

The study is founded largely on the measured responses and observed performances of shear wall buildings during recent earthquakes. The measured responses have been obtained from two multistory bearing wall buildings located in California that were subjected to low to moderate intensity ground motions. The measured data are used to calibrate analytical models of bearing wall buildings. Having developed confidence in the modeling procedure, responses of several similar buildings subjected to the 1985 Chile earthquake are studied and compared with observed performances. Comparison is made between the Chilean and US bearing wall buildings, and between the Chilean and expected US earthquakes. Conclusions are drawn regarding the expected performance of US bearing wall buildings in the US. Design recommendations consistent with the expected performance are presented.

BEHAVIOR OF TWO BEARING WALL BUILDINGS DURING RECENT CALIFORNIA EARTHQUAKES

Description of the Buildings

The two buildings under study are designated in this paper as Building 1 and Building 2. (These are identified in the CSMIP as CSMIP

Building SN 356 and CSMIP Building SN 385, respectively.) The buildings are each ten stories tall. Plan views of the two buildings are in Fig. 1. The vertical and lateral force resisting system for both buildings consists of reinforced concrete bearing walls coupled by thin slabs. The walls in Building 2 are precast with hollow mandrels into which concrete and reinforcement are cast in the field, apparently achieving an effectively monolithic construction. Slabs in Building 1 are post-tensioned and in Building 2 are precast panels with topping. All walls are continuous over height except within Building 1 for which the two interior corridor walls are discontinued at the sixth floor.

Building 1 was constructed in 1971/72. Building 2 was constructed in 1974. Details appear to be consistent with those in common practice at the time of construction. Materials in Building 1 are: 3000-psi NWC in the walls; 4000-psi LWC in the slabs; Grade 60 reinforcement for all bars larger than No 5, otherwise, Grade 40 reinforcement. Materials in Building 2 are: 5000-psi precast walls with 4000-psi mandrels (4600 psi assumed average); LWC slabs; Grade 60 reinforcement throughout.

The total weight of Building 1 was calculated to be 24,000 kips. The total weight of Building 2 was calculated to be 23,000 kips.

Computed Building Strengths

Base shear strengths of the two buildings were calculated in each of two principal directions considering (a) flexural mechanisms extending over the height, and (b) wall shear strength computed according to the UBC. Values are listed in Table 1.

Dynamic Analytical Model

Linear-elastic properties of the buildings were modeled using conventional software. Lacking specific information on soil conditions, all analytical models were given fixed bases at the foundation model.

Given the symmetry in the floor plan of Building 1, a simple 2-dimensional model was prepared for each direction. The model of the transverse direction considered contributions only of walls alined in that direction. The model in the longitudinal direction considered two frames (one to model the exterior column lines and another to model the corridor walls). In both models, gross-section properties were assumed for all elements. Effective widths of coupling slabs were computed using the results of Qadeer, et al. [2] (the resulting slab width was typically equal to wall width plus six slab depths). A rigid floor diaphragm was assumed. Responses of the 2-D models were computed using the program SAP-80.

Because Building 2 had some assymmetry in plan, a complete 3-D model was prepared using the program ETABS. Member modeling assumptions were essentially the same as those assumed for Building 1.

Computed periods for the models are in Table 2. The fundamental periods are approximately N/20, where N is the number of stories in the building. For comparison with the values in Table 2, Eq. 12-3 of the UBC gives a fundamental period of 0.58 sec for each building.

Ground Motions at Building Sites

Response records for Building 1 were obtained for the Morgan Hill and Mt. Lewis earthquakes. Only the former is considered here. Response records for Building 2 were obtained for the Whittier-Narrows earthqukae and aftershocks. Only the former is considered in this paper. Instrument and processing details can be obtained from the CSMIP. Ground acceleration histories (obtained from instruments in the ground floor of the buildings) are plotted in Fig. 2.

Measured and Computed Responses

Responses to the measured horizontal ground accelerations were computed for each of the buildings using the gross-section models described previously. For the 3-D model of Building 2, the two horizontal components were considered to act simultaneously. Viscous damping equal to five percent of critical was assumed for all calculations.

Computed and measured roof relative displacements are compared in Fig. 3. (Measured relative roof displacement is computed as the difference between measured absolute displacements at the roof and the base. For relative transverse displacements of Building 1, as described by Mahin, the error margin is one-third of the measured displacement. Thus, because it is not possible to accurately gage responses for the transverse direction for this building, no transverse displacement plots are shown.)

From the data in Fig. 3, it is apparent that the computed building periods are too short. Some error is likely to arise because effects of soil-structure interaction have not been considered. For buildings of the proportions considered, soil-structure interaction effects are expected to result in approximately ten percent increase in the computed period. The measured discrepancies thus appear to be beyond what can be attributed to soil-structure interaction.

Another likely source of error lies in the assumption that element stiffnesses could be based on gross-section quantities. At the present time, there is no well-defined technique by which to gage the degree of cracking that occurs in a structure over time. In the absence of load, some initial cracking can be expected due to shrinkage and temperature effects. A modest reduction in stiffness would be expected due to this effect. Under high lateral loads, load-induced cracking will result in more significant reduction of stiffness. Analyses of the effective stiffness of typical walls in the study buildings under the action of applied moments and axial loads indicates a fully-cracked stiffness of approximately 40 percent of the gross-section stiffness. Such a reduction could be expected for Building 2, which was subjected to moderate earthquake excitation. The stiffness reduction for Building 1 might be less, as the degree of shaking was less. Lacking a well-defined reduction, a stiffness of approximately 70 percent of gross section might be reasonable. (Clearly more study of this problem is warranted, and possible using the CSMIP data.)

Figure 4 compares measured and computed roof displacements for the

two buildings with stiffness taken as 70 percent of gross section for Building 1 and 40 percent of gross section for Building 2. The degree of correlation is greatly improved. Periods and response amplitudes are closely matched in both directions.

It is noted that the computed and measured periods in Fig. 4 compare reasonably throughout the entire duration of response. The implication is that, cracking aside, the response of the buildings during these earthquakes was basically elastic. This conclusion is consistent with the relatively high base-shear strengths of the buildings (Table 1). Likely performance during more severe motions is gaged by comparison with experiences with bearing wall buildings in Chile.

PERFORMANCE OF BEARING WALL BUILDINGS IN CHILE

Given the frequency of strong earthquakes, the Chileans have developed a formula for building design that is remarkably different from that in the US. The typical building in Chile is a reinforced concrete bearing wall building. The structures are designed for lateral forces similar to those prescribed in the US. However, in sharp contrast with US practice, the Chilean engineers have learned through experience that this form of construction can survive strong earthquakes without ductile details and without inspection during construction.

The success of the Chilean "formula" for design was apparent following the 1985 Chile earthquake [3]. The city of Vina del Mar, with over 400 reinforced concrete buildings over 5 stories, was subjected to a ground motion having peak acceleration of 0.36 g and duration of strong shaking in excess of one minute. The success of the Chilean construction is apparent in the cost of repair, which averaged 35 cents per square foot. A cost this low is unusual for an event of this magnitude.

As part of the study of bearing wall building performance, a detailed study of the Chilean buildings has been undertaken. Details of the study are reported elsewhere [4].

Five-percent damped response spectra for the 1985 Chile earthquake and for representative US design earthquake motions are compared in Fig. 5. It is noted in relation to that figure that the Chile motion has response ordinates representative of those that might be expected in the US. Thus, it has been concluded [4] that the Chilean earthquake provided a representative test of bearing wall construction for the US.

Figure 6 compares computed strengths and periods of several Chilean buildings and the two California bearing wall buildings with inelastic spectra for the ATC soil type 1, which is similar to the spectrum of the Chilean earthquake. For these buildings, it is estimated that the maximum displacement ductility demand of approximately three is likely to have resulted in the Chilean earthquake. The comparison of spectra in Fig. 5 suggests that similar results would be expected in a California earthquake. For a displacement ductility of three, results reported by Paulay [5] indicate a curvature ductility of eight or less

for the usual bearing wall.

Moment-curvature relations of typical reinforced concrete bearing walls have been computed using standard techniques (Fig. 7). For reinforcement ratios less than or equal to one percent, the available curvature ductilities in the absence of confinement reinforcement exceeds the required ductility by a safe margin.

CONCLUSIONS

Based on a study of California bearing wall buildings and of similar buildings in Chile, the following have been observed:

1. Periods and responses of reinforced concrete bearing wall buildings cannot be adequately gaged on the basis of uncracked section properties, even when the earthquake loading is not severe (as in the Morgan Hill earthquake).

2. By modifying the periods of the two study buildings in the range between the cracked and uncracked periods, good correlation with measured behavior was obtained.

3. Simlarities in strength of the two study buildings and of similar Chilean buildings were noted. Also, the similarity between design US motions and the 1985 Chilean earthquake was observed. By observation and by analysis, it is reasonable to conclude that US bearing wall buildings would perform in a strong US earthquake with similar success as the Chilean buildings, even in the absence of the ductile details required in the US. Reductions in detailing may be appropriate.

ACKNOWLEDGEMENT

The writer thanks Dr. J. Wallace, currently at the University of Clarkson, formerly a Research Assistant at the University of California at Berkeley, and Mr. Jose Martinez-Cruzado, Research Assistant at the University of California at Berkeley, for conducting the building analyses and providing data for this paper.

REFERENCES

1. Uniform Building Code, International Conference of Building Officials, Whittier, California, 1988.

2. Qadeer, Aslam, and Smith, "The Bending Stiffness of Slabs Connecting Shear Walls," ACI Journal, June 1969, pp. 464-473.

3. "The 1985 Chile Earthquake," EERI Spectra, February, 1986.

4. J. W. Wallace, "The 1985 Chile Earthquake: Implications for Design of Bearing Wall Buildings in the US," PhD Dissertation submitted to the Graduate College, University of California at Berkeley, January 1989.

5. T. Paulay, "The Design of Ductile Reinforced Concrete Structural Walls for Earthquake Resistance," EERI Spectra, October 1986.

Table 1 - Computed Base Shear Strengths

	Shear Strength		Flexural Strength	
	Trans.	Long.	Trans.	Long.
Building 1	0.20W	0.47W	0.32W	0.22W
Building 2	0.41W	0.37W	0.32W	0.29W

Note: W = 24,000 kips for Building 1,
23,000 kips for Building 2.

Table 2 - Computed Periods, sec

	Trans.	Long.	Tors.
Building 1	0.32	0.50	---
Building 2	0.31	0.34	0.28

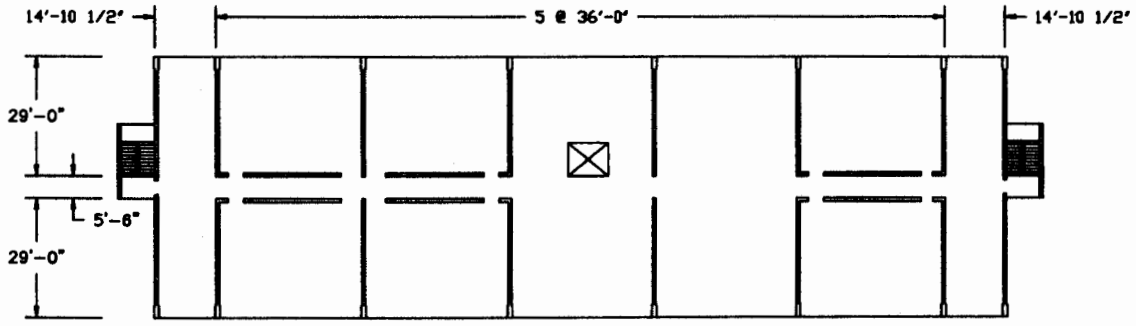

(a) Building 1

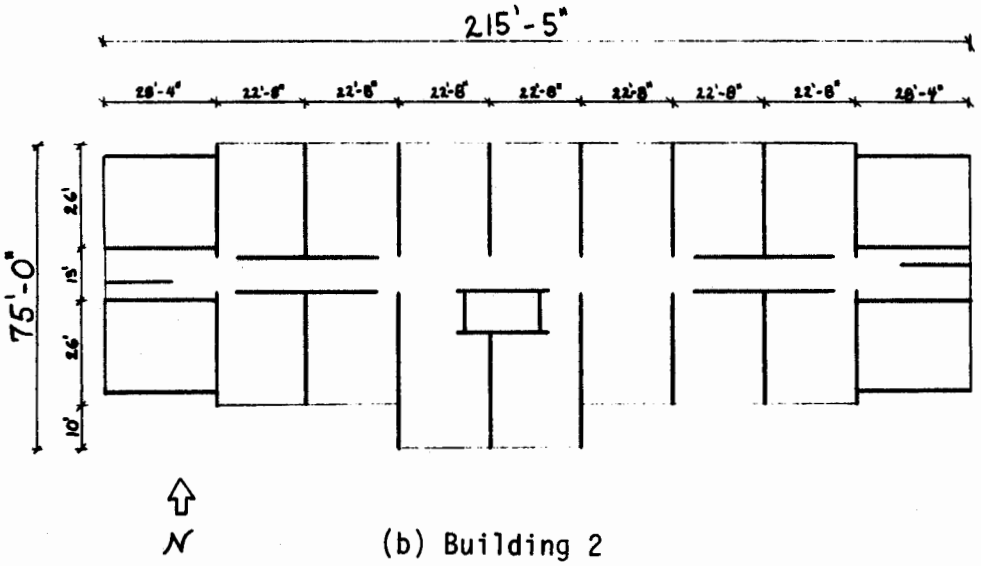

(b) Building 2

Fig. 1 Building Plans

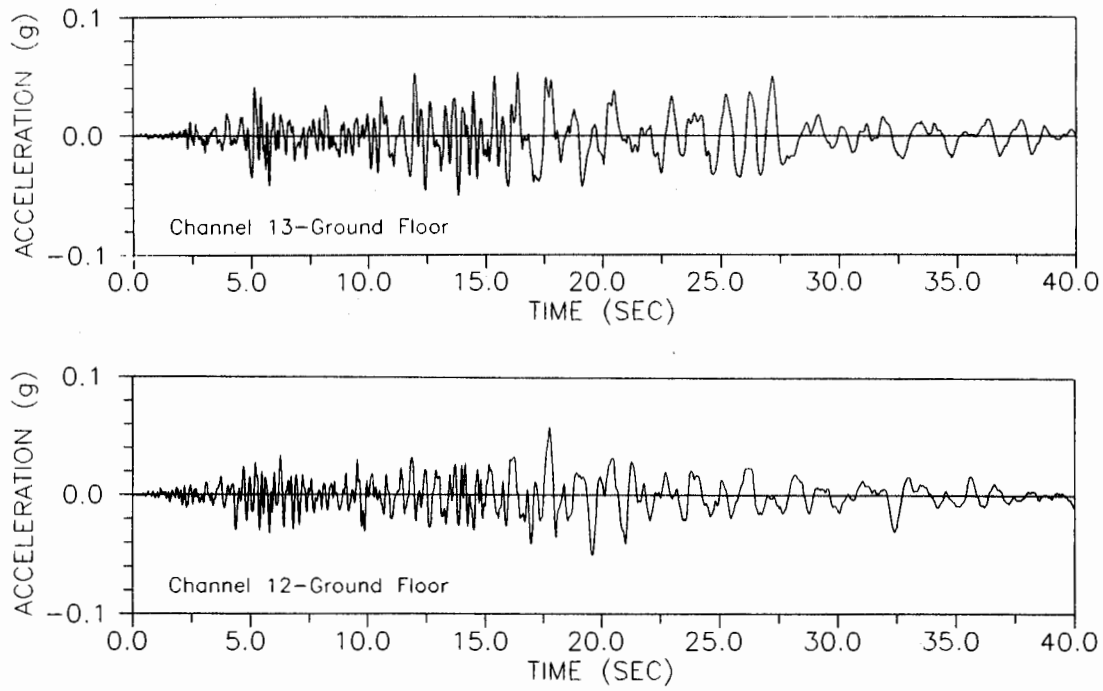

(a) Building 1

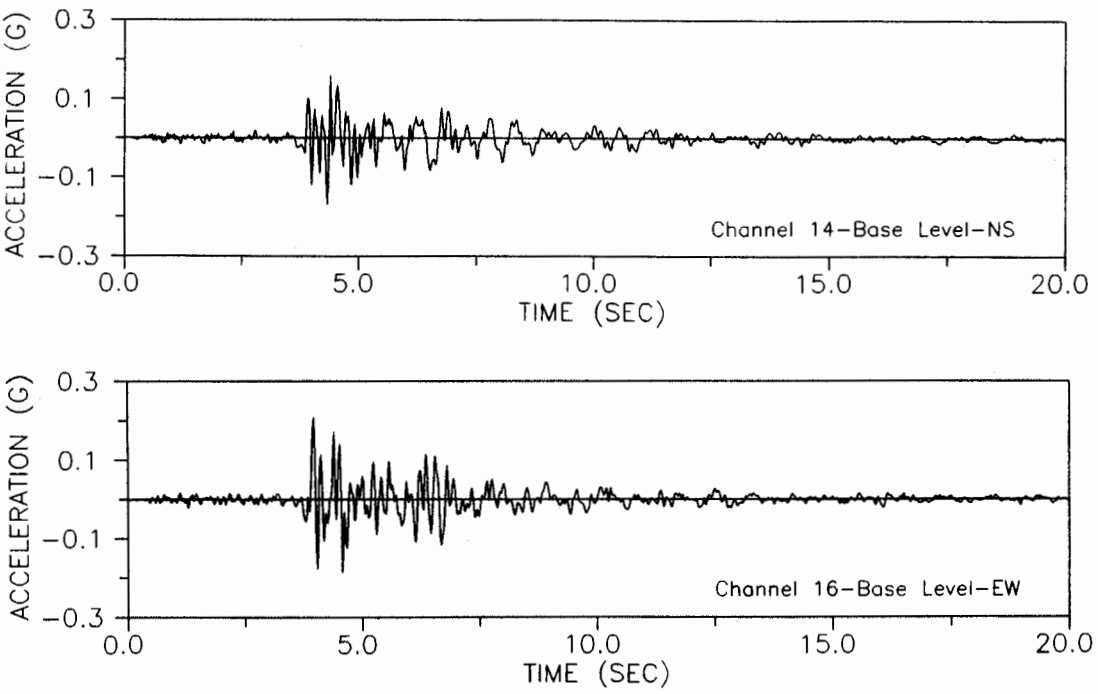

(b) Building 2

Fig. 2 Measured Base Accelerations

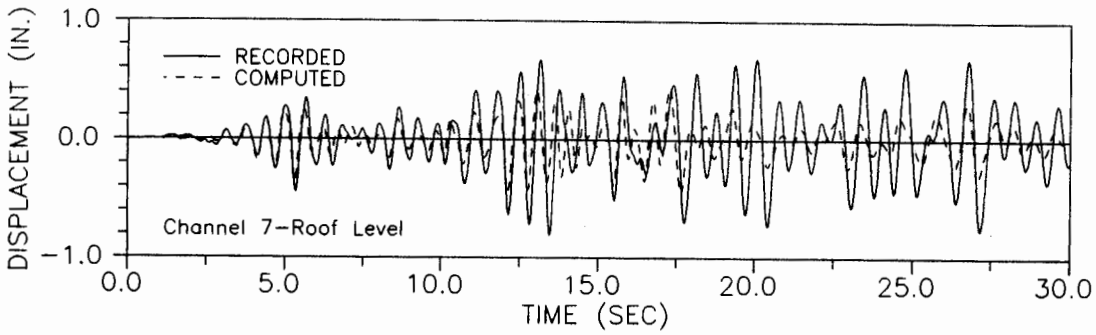

(a) Building 1, Longitudinal

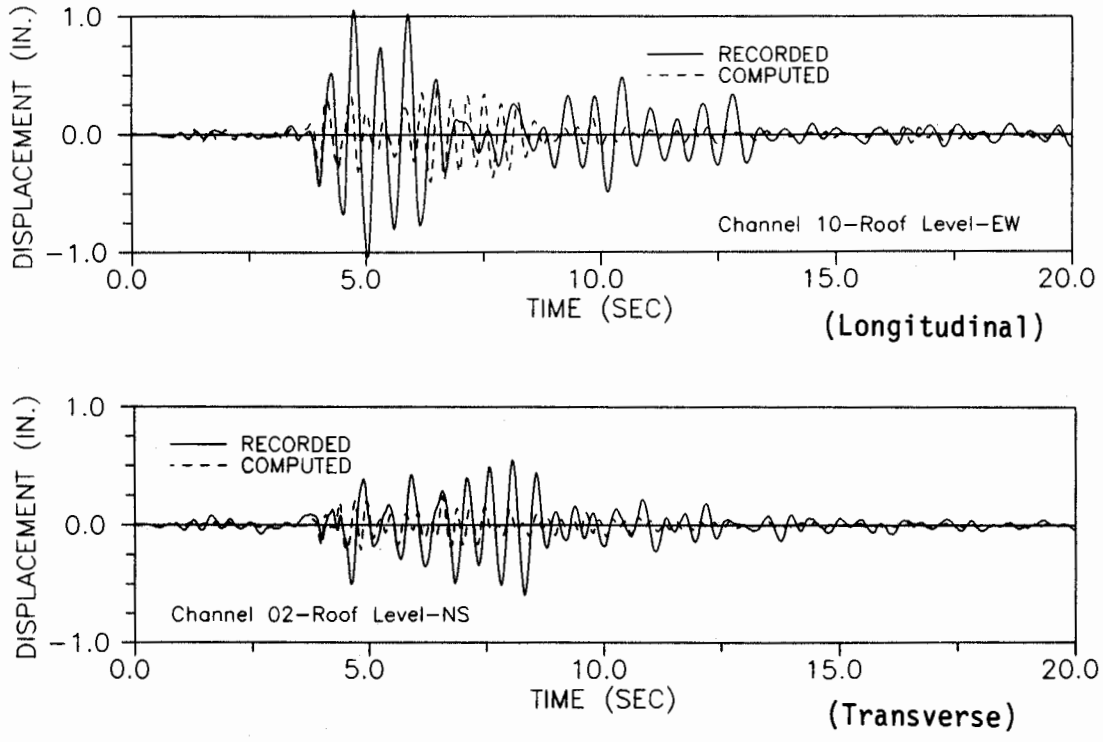

(b) Building 2

Fig. 3 Measured and Computed Roof Responses, Gross-Section Model

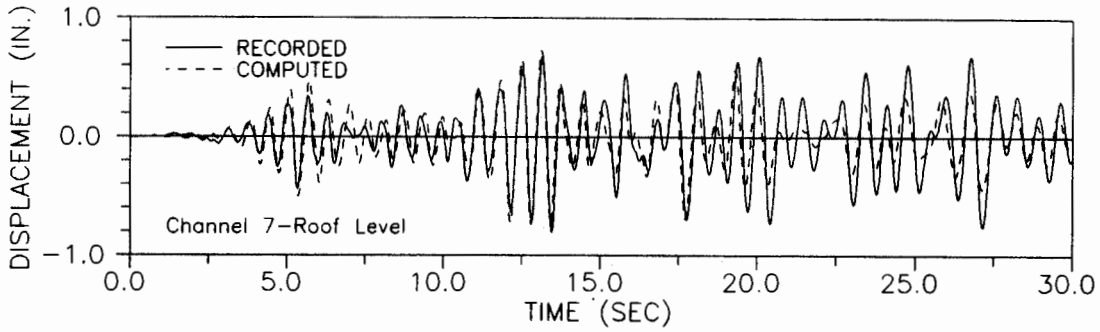

(a) Building 1, Longitudinal

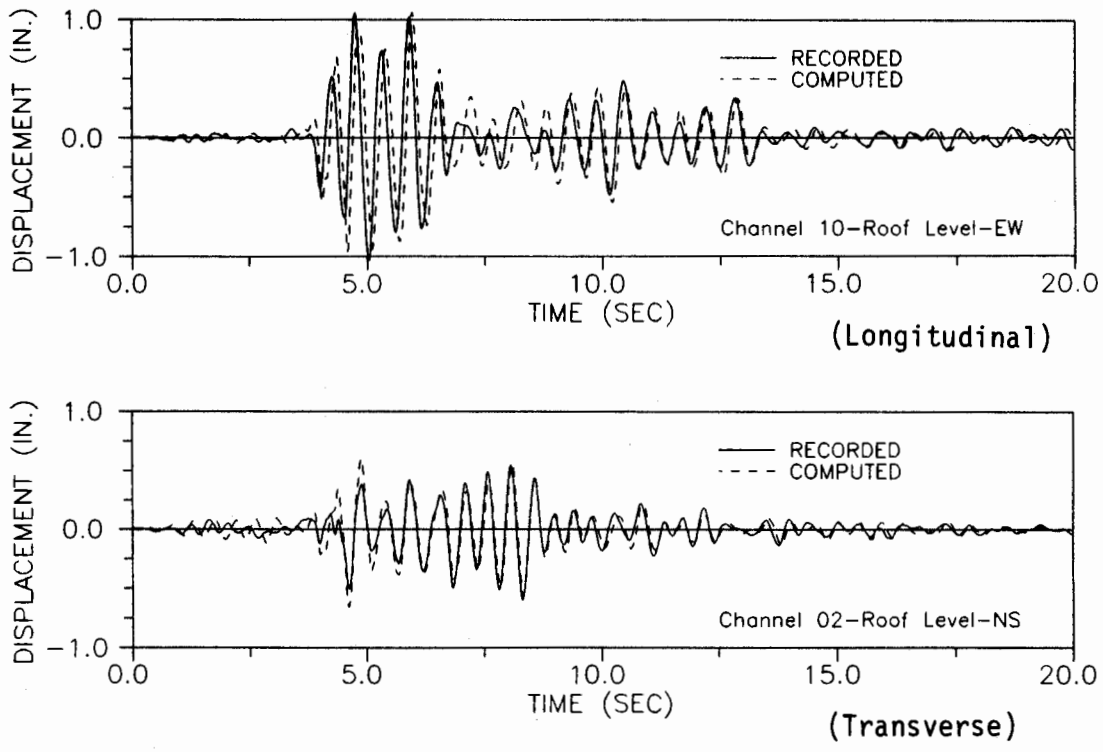

(b) Building 2

Fig 4 Measured and Computed Roof Responses, Cracked Model

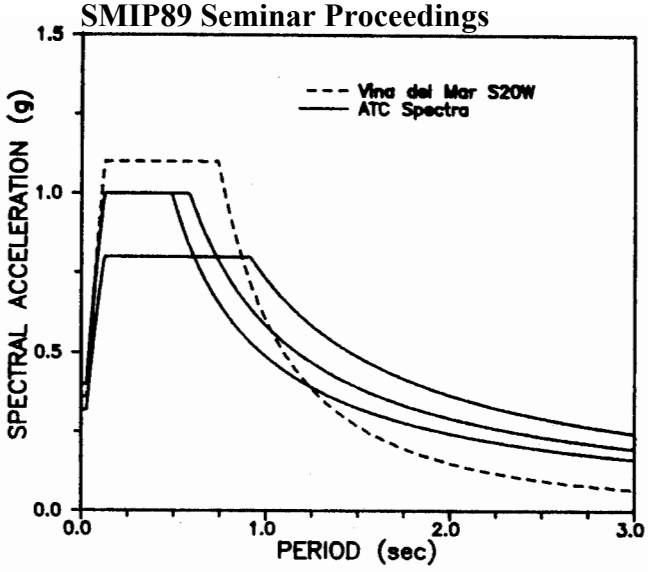

Fig. 5 Comparison of Chile and ATC Spectra

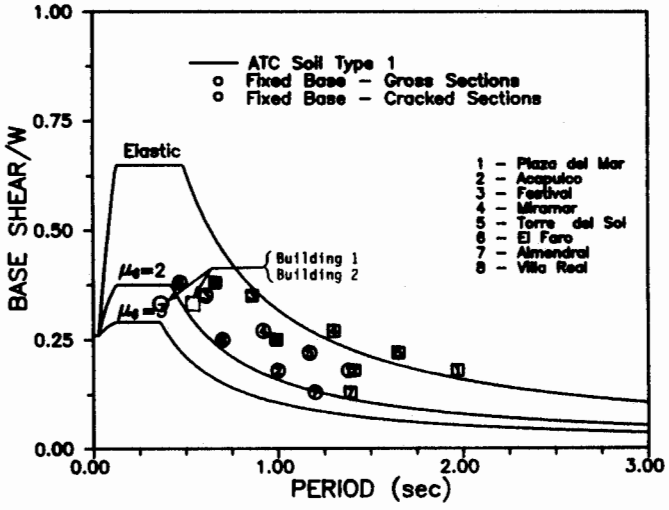

Fig. 6 Comparison of Ductility Demands

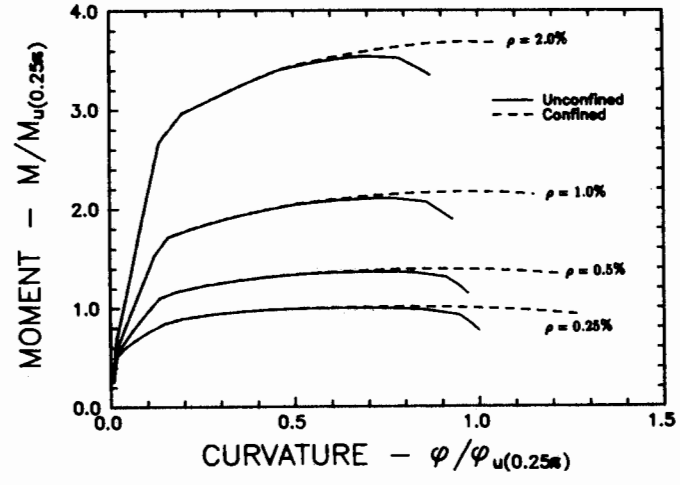

Fig. 7 Computed Moment-Curvature Relations for Bearing Walls

CORRELATION STUDIES OF SEISMIC RESPONSE OF REINFORCED CONCRETE MOMENT RESISTING FRAMES

Filip C. Filippou
Department of Civil Engineering
University of California Berkeley

ABSTRACT

This study focuses on the correlation of analytical predictions with the measured seismic response of two reinforced concrete moment resisting frames during the October 1, 1987 Whittier Narrows earthquake. The first building is a five story warehouse with a flat slab and a perimeter frame and the second is a twenty story hotel with moment resisting frames in both directions. Both buildings have a regular, rectangular, symmetric layout. To study the seismic response three dimensional models of the two buildings were subjected to the accelerations recorded at the base. The study assesses the effect of modeling assumptions on the fundamental period and the response of the buildings.

INTRODUCTION

On October 1, 1987 an earthquake measuring 6.1 on the Richter scale took place in the greater Los Angeles area with the epicenter located near the town of Whittier. Damage was moderate over a broad area and extensive in certain locations such as downtown Whittier. A preliminary report by the firm EQE, Inc. estimated total damage in excess of $100 million [1]. On October 4, 1987 an aftershock measuring 5.3 on the Richter scale with its epicenter located almost at the same point as the main event shook the area. A large number of structures in the greater Los Angeles area were instrumented as part of the California Strong Motion Instrumentation Program (CSMIP). These yielded a wealth of data on the seismic response of various types of structures.

The objective of this study is the utilization of the records obtained during the Whittier earthquake and its aftershock in assessing the capabilities of present state-of-practice analytical models to predict the seismic response of reinforced concrete buildings in the elastic range. The study attempts to show the effect of modeling assumptions on response prediction and their ramification in the earthquake resistant design of structures. A brief evaluation of current procedures for establishing the equivalent static lateral loads due to earthquake excitations is also presented.

Attention is focused on a particular type of structure in order to facilitate the comparison of response and the drawing of conclusions. The structural type of interest in the reinforced concrete moment resisting frame. Two such buildings were selected in the first phase: the first is a five story warehouse with a flat slab and a relatively stiff perimeter frame. The second is a twenty story hotel with moment resisting frames in both directions. Both buildings have a regular, rectangular, symmetric layout. The intent of the selection was to eliminate irregular buildings from consideration where torsional effects could be significant and concentrate on modeling assumptions for regular multistory buildings. In the following a brief description of the layout, the structural system and the instrumentation of each building is given. Subsequently, a discussion of modeling assumptions and the development of the three dimensional analytical model is presented followed by correlation studies of analytical predictions with measured response. A discussion of the results in light of current earthquake resistant design provisions and preliminary conclusions from this study complete the presentation.

FIVE STORY PERIMETER FRAME

The first building selected for this study is a five story plus basement warehouse located in Los Angeles at a distance of approximately 14 km from the epicenter of the main event and about 12 km from the epicenter of the aftershock. The building has a rectangular layout measuring 280' by 360.5'. Gravity loads are carried by a 11 3/4" thick flat slab resting on circular columns of 32" diameter. The lateral force resisting system consists of a perimeter ductile moment-resisting frame with rather deep beams and columns. The foundation consists of spread footings. The structure was designed in accordance with 1970 Los Angeles Building Code. Fig. 1 shows the typical floor plan and framing system.

The building was extensively instrumented with all instruments functioning well and triggering during, both, the main event and the aftershock. Thus a wealth of data is available for in-depth studies of the building response. Four instruments were placed in the basement of the building. Two of these recorded the N-S accelerations along the east and the west wall, one the E-W accelerations at the east-wall and one the vertical accelerations imposed on the building. Three instruments were placed in each of the following floors: second, third, and topmost (roof). The instrumentation layout is shown in Fig. 2. The presence of three instruments measuring lateral accelerations in the basement and on each of several floors facilitates the study of the torsional response, if any, of the building. By comparing the two N-S acceleration records at the base of the building it is readily concluded that no rotational excitation is imposed at the base of the building, since the two records are almost identical. This fact also gives confidence about the accuracy of the recorded excitations.

It is interesting to note that the comparison of roof displacement response histories recorded in the N-S direction at the east and west wall of the building clearly shows the effect of torsional response (Fig. 3). This effect is not very significant for such a regular, symmetric building, but is not negligible either. In order to predict the three dimensional response of the building including the effects of torsion, a three dimensional model was developed. Initially, the model only accounts for the stiffness of the perimeter frame assuming that the lateral stiffness of the frame composed of the flat slab and the interior columns is relatively small. This is not true, however, and subsequent refinements will account for the lateral stiffness of the flat slab. It is interesting to point out the relatively large story height of 24 feet which leads to a fundamental period of vibration of about 1.45 sec in the N-S direction and 1.30 sec in the E-W direction. The maximum base acceleration was 0.18g in the E-W and 0.14g in the N-S direction.

The following considerations played an important role in the development of the three dimensional building model:

- In order to avoid complications in the response caused by the building foundation the model was assumed to fixed at the top of the basement walls. Unfortunately, no acceleration records are available at this level. Accounting for the relatively large in-plane stiffness of the basement walls it is assumed that the base acceleration propagates unaltered to the top of the basement. The analytical studies support the validity of this assumption.
- The depth of the members of the perimeter frame is considerable. The depth of the beams and the width of the columns is 66"=5.5 ft while the clear of the beams amounts to 22.5 ft in the transverse direction and 29.5 ft in the longitudinal direction. More importantly, the clear column height measures 19.5 ft. The span to depth ratio, thus, ranges from 3.5 in the case of columns to 5.5 in the case of beams in the longitudinal direction. Special attention needs to be devoted to the shear deformations of the members and the distortion of the beam-column joint region. The effect of this parameters is discussed in detail below.

- The mass of the floor slab is considerable. It makes up about 65% of the total mass of the building, the remainder contributed by the members of the perimeter frame (27%), the large interior columns (6%) and two small staircases located in the perimeter of the building.
- The building is so perfectly regular and symmetric that the small torsional response is caused by non-symmetric distribution of stiffness due to cracking of members and by the presence of two small staircases located in the perimeter of the building. The former effect is very difficult to evaluate. To account for the latter box-type columns are used to model the stiffness of the staircases.
- Initially, properties of structural members are based on gross uncracked concrete sections. This will be revised in subsequent refinements to account for the effect of cracking.

The program SAP89 developed by E.L. Wilson [3] is used in all following studies, which were all performed on a microcomputer.

	Study in Ref. [2]	Final model	Rigid panel zones	Neglect shear deformations	Remarks
Mode Number	Period [sec]	Period [sec]	Period [sec]	Period [sec]	
1	1.39	1.43	1.27	1.37	N-S
2	1.22	1.27	1.12	1.29	E-W
3	0.76	0.87	0.77	0.85	Rotation
4	0.46	0.47	0.42	0.46	N-S
5	0.40	0.41	0.36	0.42	E-W
6	0.26	0.29	0.25	0.28	Rotation

Table 1 Comparison of periods of vibration of first six modes of vibration of 5-story perimeter frame

Table 1 summarizes the periods of first six modes of vibration of the structure obtained in four cases: first a study conducted in ATC-2 Report and three cases with the present three-dimensional model investigating the flexibility of beam-column joint panel zones and the effect of shear deformations in structural members. The final model includes the effect of shear distortions and accounts for the flexibility of panel zones through a panel zone factor of 0.5, which is halfway between a fully rigid panel zone (factor=0) with member stiffness based on clear span dimensions and a completely flexible panel zone (factor=1.0), in which case the center-to-center dimensions of members are used.

It is interesting to point out that the fundamental period of vibration of the building is predicted equal to 1.08 sec in, both, N-S and E-W, directions by formula (12-3) of the 1988 Uniform Building Code.

In conducting the dynamic response analyses presented in the following the mass and stiffness properties of the final model in Table 1 are used. The damping ratio is assumed equal to 5% of critical in all vibration modes with ten modes being used in the analysis.

The correlation of the predicted response with measured data is presented in Figs. 4-6. Fig. 4 shows the roof displacement response history at the west wall in the N-S direction. Fig. 5 shows roof the displacement response history at the west wall in the E-W direction and Fig. 6 compares the two calculated response histories in the N-S direction to highlight the small torsional response that is obtained due to the non-symmetric arrangement of two staircases in the building. It can be concluded that the analytical model is capable of very accurately predicting the elastic response of this building to a moderate ground motion.

TWENTY STORY MOMENT FRAME

The second building used in this study is a twenty story hotel with basement located in the Hollywood area at a distance of 28 km from the epicenter. This building experienced a smaller ground excitation than the five story warehouse building, because of the larger epicentral distance. The maximum ground acceleration at the base was 0.11g in the N-S direction and 0.09g in the E-W direction. The lateral load resisting system consists of ductile moment resisting frames in, both, the N-S and the E-W direction. Two way slabs carried the gravity loading to the girders of the frame. The slab is 4" thick, with the exception of the corridors where the thickness is increased to 6". Of particular interest is the fact that 110 pcf lightweight concrete of 3,000 psi nominal strength was used for the slab and beams above the first floor. The columns are also of lightweight concrete with a nominal strength of 4,000 psi in the first ten floors and 3,000 psi in the floors above the tenth. Normal weight concrete is only used in the members of the basement and the first floor (lobby). A transverse section of the building is shown in Fig. 7.

The same building has been the subject of a study in connection with San Fernando Earthquake of February 9, 1971 published in [4]. The building, which was completed in 1967, was subjected to peak ground acceleration of 0.18g during that earthquake and suffered only minor architectural damage totaling $2,100 [4]. The field observations and the ensuing study did not indicate any structural damage. It is interesting to point out that two a dimensional planar frame model in the two principal directions of the building was used in the studies reported in [4].

	Study in Ref. [4]	Final model	Remarks
Mode Number	Period [sec]	Period [sec]	
1	2.21	2.31	Transverse
2	2.15	2.05	Longitudinal
3	——	1.91	Rotation
4	0.79	0.79	Transverse
5	0.74	0.70	Longitudinal
6	——	0.64	Rotation

Table 2 Comparison of periods of vibration of first six modes of vibration of 20-story frame

In this study a three-dimensional model of the entire structure was developed. All structural members, including staircases, were included in the model. Modeling of the twenty story building was a major effort, since the final structural model consists of 3,855 members, 1,767 joints and almost 5,000 degrees of freedom. In spite of its large size the model was analyzed on a personal computer with a 30 MB hard disk.

Many of the same modeling considerations as discussed in the case of the five story warehouse also played an important role here. Since the structural members were not deep in this case, distortions due to shear are negligible and were not accounted for. The effect of partially rigid joints is, however, again significant. Table 2 shows the periods of the first six mode shapes and compares the results of this study with those of Ref. [4].

The correlation of the predicted response with measured data is presented in Figs. 8 and 9. Fig. 8 shows the 16th-floor displacement response history at the west wall in the N-S direction. Fig. 9 compares the two measured 16th-floor displacement response histories in the N-S direction to show the significant torsional response that is obtained in this case. Even though Fig. 8 indicates a satisfactory agreement between predicted and measured displacements of the 16th-floor further studies are required to establish the cause of the significant torsional response.

CONCLUSIONS

The three dimensional model of a five story perimeter frame building yields very satisfactory agreement between calculated and measured response values. This seems to support the assumptions made in the development of the analytical model. The agreement is not as good in the case of a twenty story moment resisting frame, in large part due to the significance of the torsional response which is not represented by the model. Further studies are currently under way to shed light on the relation of modeling assumptions with actual building stiffness and mass distribution.

ACKNOWLEDGEMENTS

This study is supported by a grant from the Strong Motion Instrumentation Program of the Department of Conservation of the State of California. This support is gratefully acknowledged. The views expressed in the paper are those of the author and do not reflect the opinion of the sponsoring agency. The assistance of Drs. Shakal, Huang and Ventura is greatly appreciated. I would also like to thank graduate student David Sze for his tireless efforts in the preparation of the data of the analytical models. Finally, my most sincere thanks go to Professor E.L. Wilson for providing a copy of his powerful microcomputer program and for much advice during the course of the study.

REFERENCES

[1] A.F. Shakal, et. al., "CSMIP Strong-Motion Records from the Whittier, California Earthquake of October, 1, 1987. Report No. OSMS 87-05, California Department of Conservation, Oct. 1987.

[2] Applied Technology Council, "An Evaluation of A Response Spectrum Approach to Seismic Design of Buildings", Report No. ATC-2, San Francisco, Sept. 1974.

[3] E.L. Wilson, "SAP-89: A Series of Computer Programs for the Static and Dynamic Finite Element Analysis of Structures", Users Manual, University of California, Berkeley, Report, January 1989.

[4] L.M. Murphy, Editor, "San Fernando, California, Earthquake of February 9, 1971, U.S. Department of Commerce, Washington, D.C. 1973.

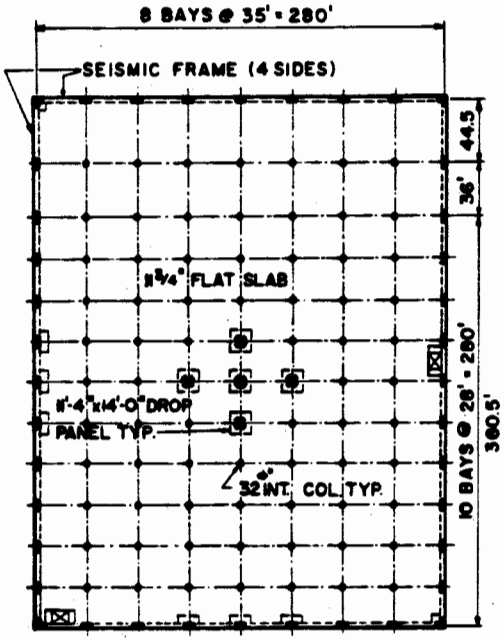

FIG. 1.0.1. Typical Floor Plan.

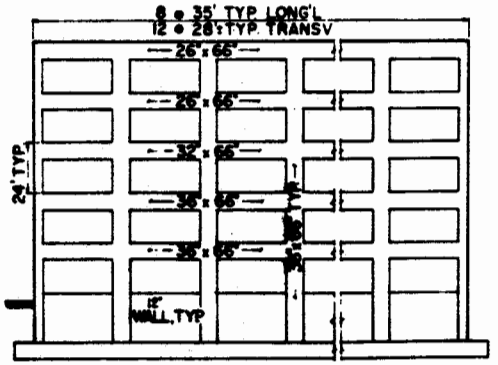

FIG. 1.0.2. Frame Elevation.

FIG. 1

SENSOR LAYOUT

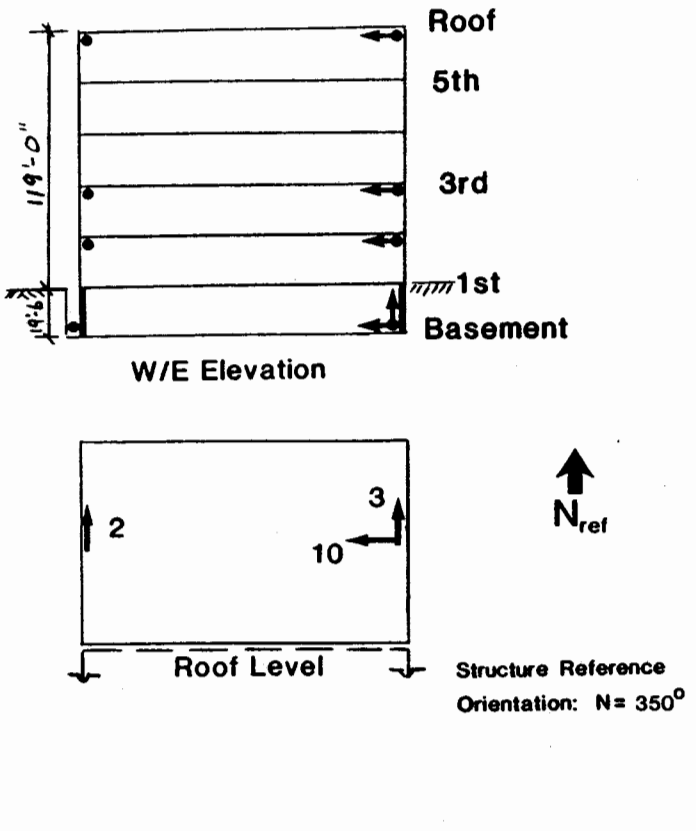

FIG. 2

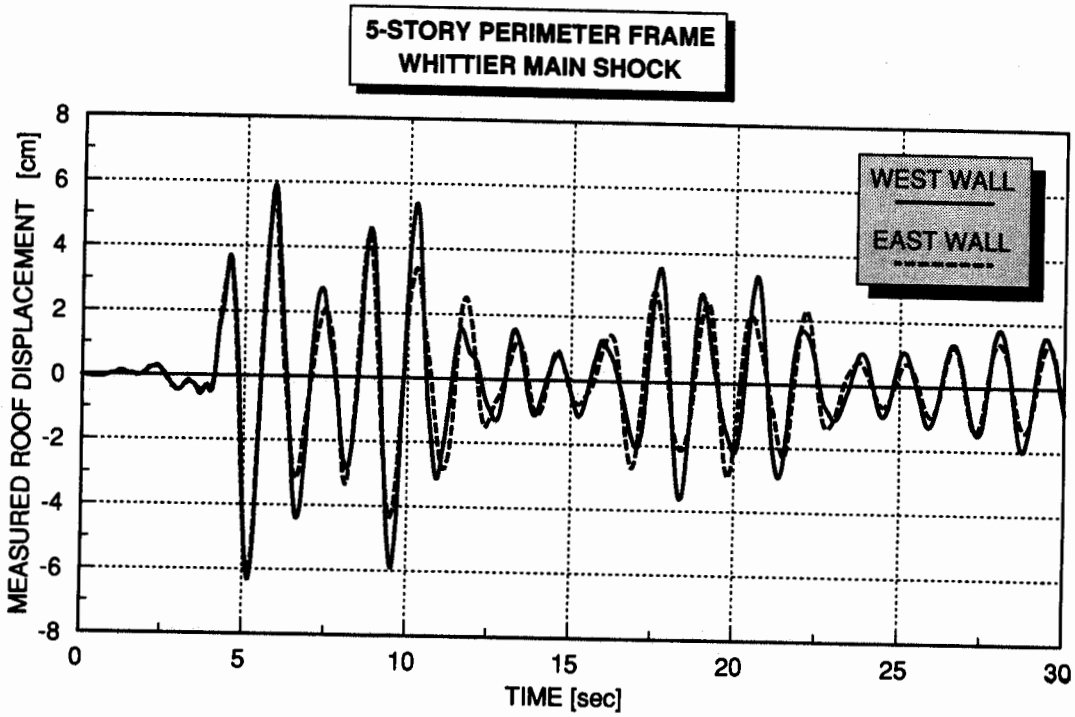

FIG. 3 COMPARISON OF ROOF DISPLACEMENT RESPONSE AT EAST AND WEST WALL, N-S DIRECTION, 5% DAMPING

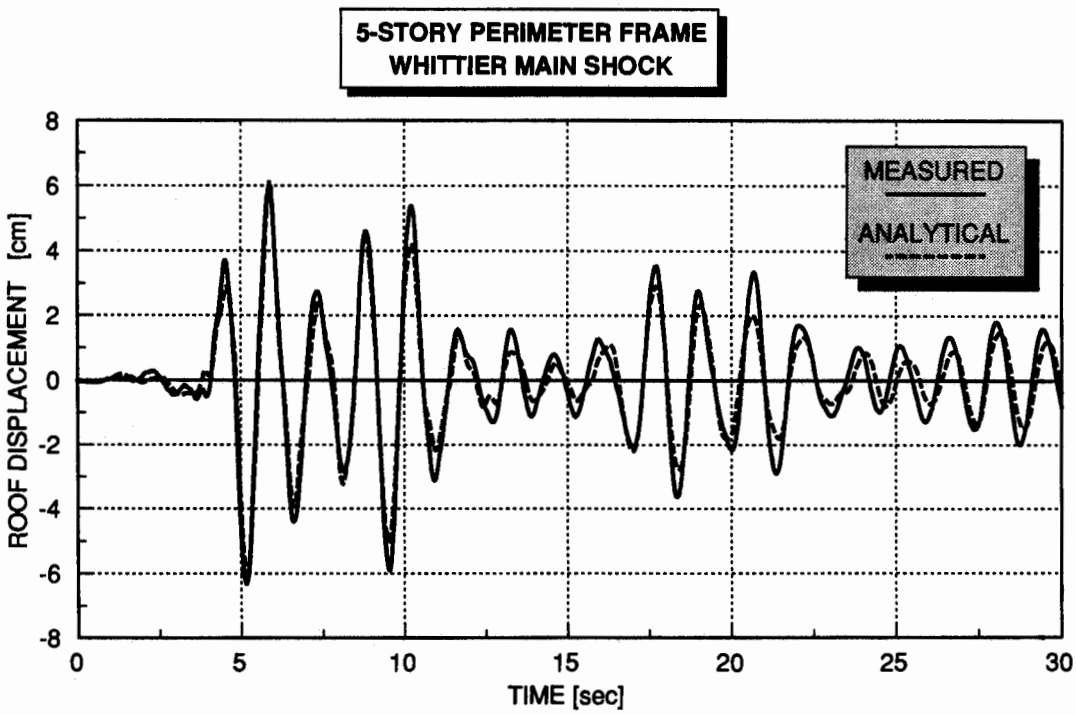

FIG. 4 ROOF DISPLACEMENT RESPONSE AT WEST WALL N-S DIRECTION, 5% DAMPING

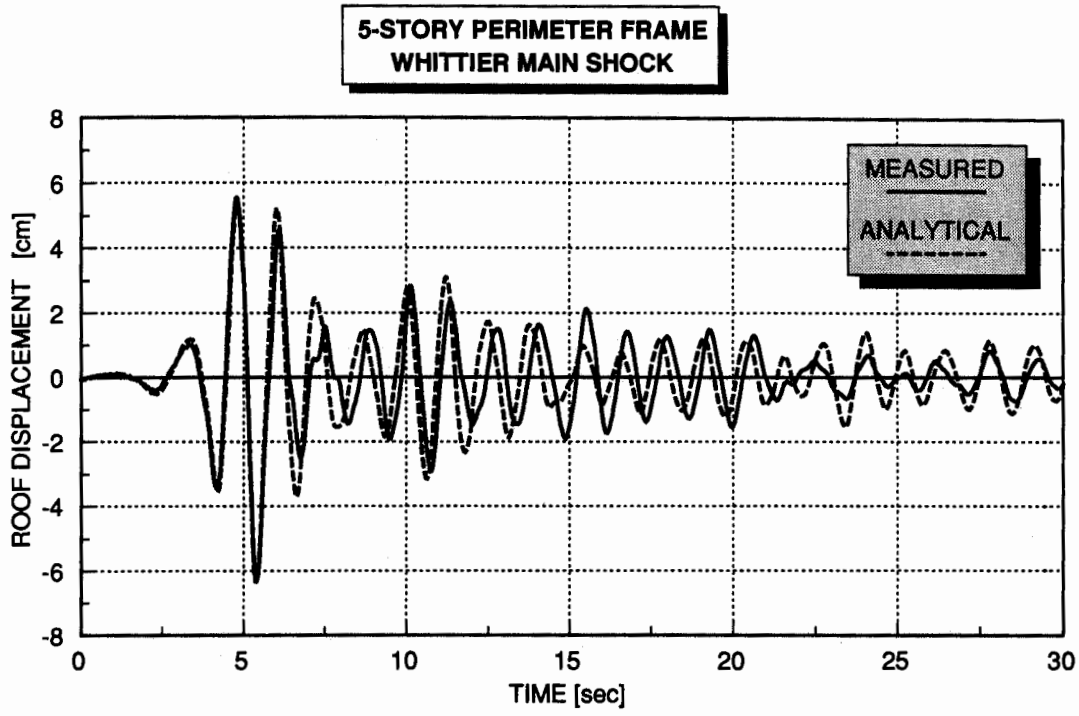

FIG. 5 ROOF DISPLACEMENT RESPONSE AT WEST WALL E-W DIRECTION, 5% DAMPING

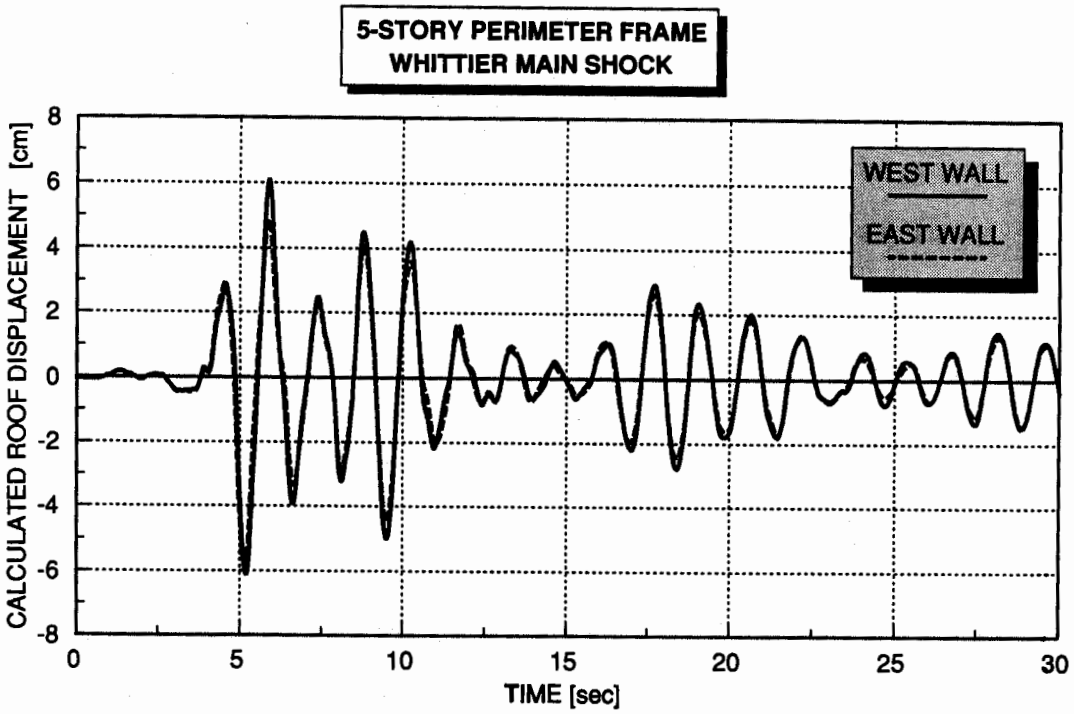

FIG. 6 COMPARISON OF ROOF DISPLACEMENT RESPONSE AT EAST AND WEST WALL, N-S DIRECTION, 5% DAMPING

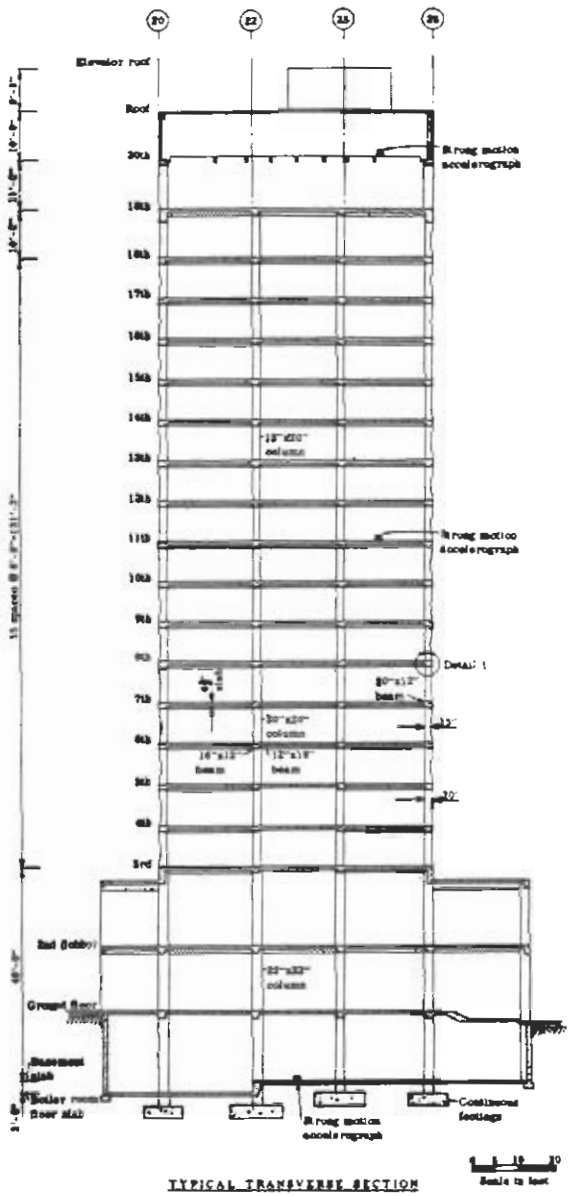

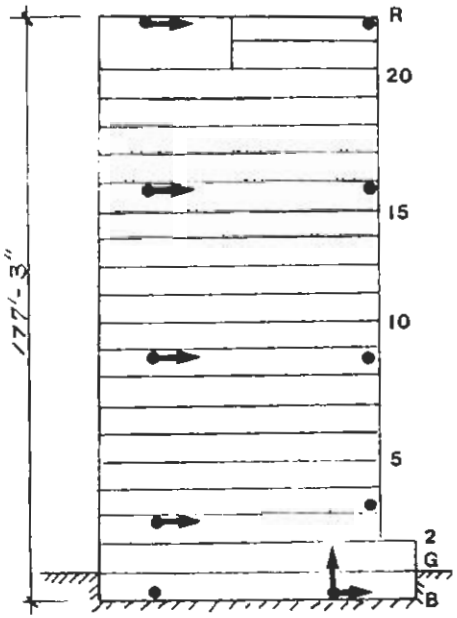

SENSOR LAYOUT

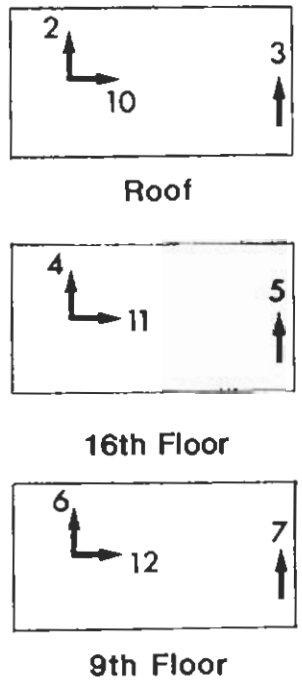

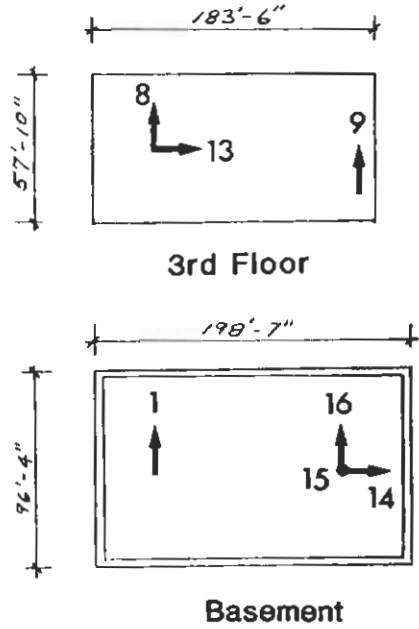

Structure Reference
Orientation: N= 0°

FIG. 7

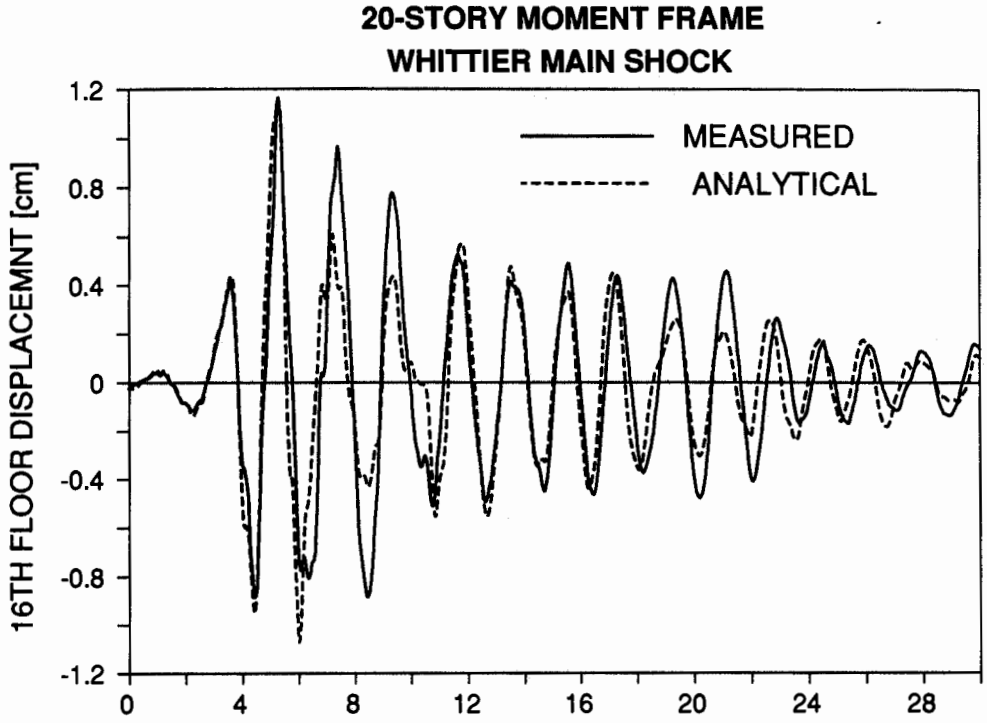

FIG. 8 COMPARISON OF 16 FLOOR DISPLACEMENT RESPONSE

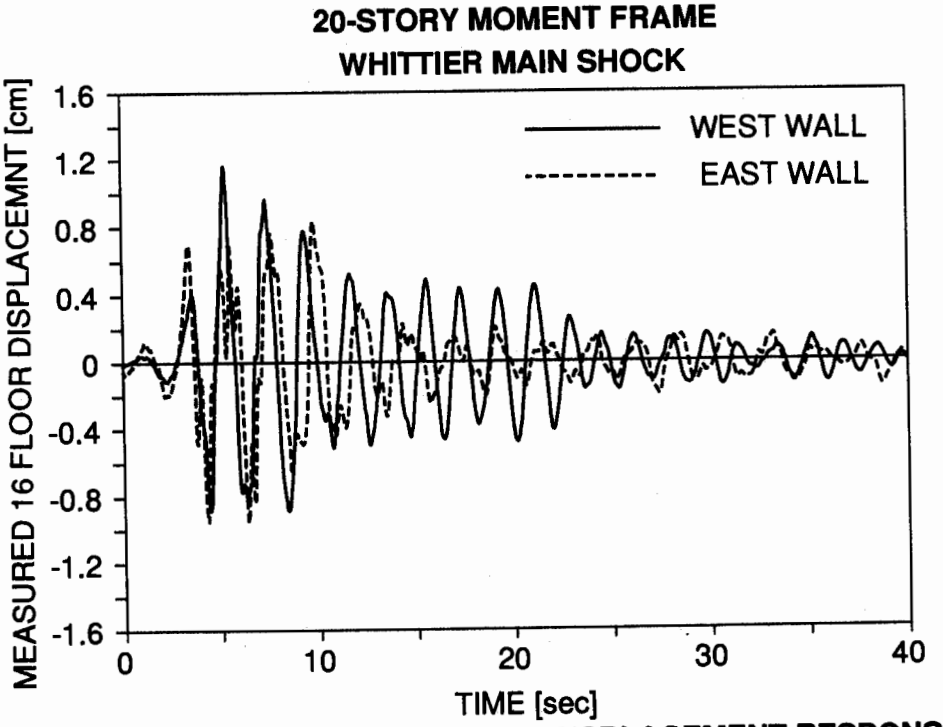

FIG. 9 COMPARISON OF 16 FLOOR DISPLACEMENT RESPONSE AT EAST AND WEST WALL, N-S DIRECTION

SEISMIC RESPONSE OF THE PUDDINGSTONE AND COGSWELL DAMS IN THE 1987 WHITTIER NARROWS EARTHQUAKE

by

R. B. Seed[1], J. D. Bray[2], R. W. Boulanger[2] and H. B. Seed[3]

(1) Assistant Professor, (2) Graduate Research Assistant, (3) Professor,
Department of Civil Engineering, Univ. of California at Berkeley

ABSTRACT

The 1987 Whittier Narrows Earthquake (M_L = 5.9) shook two dams, the Puddingstone and Cogswell Dams, which were instrumented as part of the California Strong Motion Instrumentation Program (CSMIP). The resulting recorded accelerograms provided a valuable opportunity to investigate and evaluate the accuracy and reliability of conventional geotechnical procedures for evaluation of dynamic response characteristics of earth and rockfill dams. This paper presents the results of these studies, which provide insight regarding current techniques for dynamic soil property evaluation and the applicability of one-, two- and three-dimensional analytical procedures to evaluation of the dynamic response of these types of dams.

THE PUDDINGSTONE DAM

The Puddingstone Dam, located approximately 16 miles northeast of Whittier, California, actually consists of three earth dams. Figure 1 shows a schematic plan view of the main dam (Dam No. 1), and Figure 2 shows a cross-section through the maximum height embankment section of the main dam. The main dam is a rolled earth fill embankment with a maximum height of 148 feet and a crest length of 1,085 feet. Two smaller saddle dams (Dams No. 2 and 3) with heights of 49.5 and 60 feet also serve to retain the reservoir. This study concerns only the main dam (Dam No. 1).

The Puddingstone dam was constructed during 1926 and 1927 of locally available crushed weathered shale. The resulting compacted material, which comprises the main portions of all three homogeneous earth embankment dams, is a sandy silty clay with weathered shale fragments. Typically, the soil is composed of 60 to 90% fines of medium to high plasticity (CH-MH), with LL ≈ 55 to 70 and PI ≈ 26 to 32, and 10 to 40% sand and gravel sized particles. As shown in Figure 2, the toe of the main dam is drained with a triangular toe drain section composed of large boulders and gravel.

Seismic Instrumentation and the Recorded Motions:

A total of 18 strong motion accelerographs were installed at six locations on and near the main dam, as shown in Figure 1. At most locations, motions were recorded in three orthogonal directions: vertically, longitudinally (parallel to the main dam axis) and transverse to the main dam axis. This paper will concentrate on the transverse motions, as these are the motions of primary engineering interest. Sensors 1-6 and 13-18 were sited to record "bedrock" motions. These sensors were actually installed on shallow, stiff soil deposits or on protrusions of low-grade rock, so that they do not record true rock motions. They will be referred to as "near" rock sites. Sensors 1, 2, 3 and 16, 17, 18 were co-located, and produced nearly identical records for the Whittier Narrows Earthquake. Sensors 7-12 were sited on the main dam's crest and downstream face.

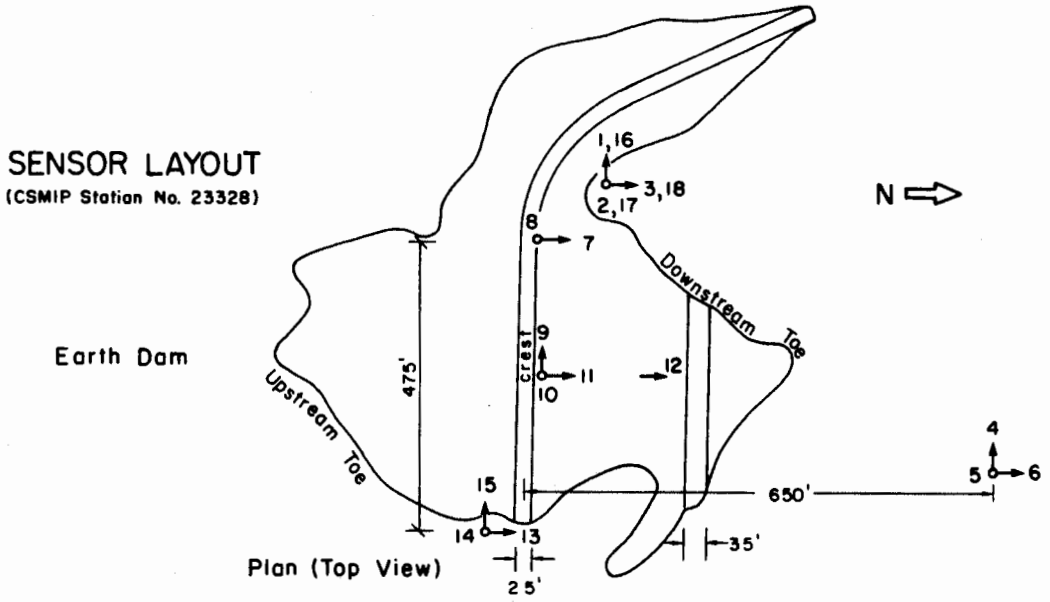

Fig. 1: Plan View of Puddingstone Main Dam Showing Sensor Locations

The Whittier Narrows Earthquake of October 1, 1987 provided an excellent record of the seismic response and performance of Puddingstone Dam. This magnitude 5.9 earthquake on the newly discovered Whittier Fault located approximately 16 miles from the dam site produced strong motions with peak ground accelerations of the "near" rock sites ranging from 0.04 g to 0.08 g. Puddingstone Dam suffered no significant damage as a result of the earthquake shaking. Unfortunately, one of the sensors (Station 7) did not operate. Hence, the variation of strong motions in the transverse direction along the crest of the dam cannot be studied. On the other hand, Sensors 11 and 12 in conjunction with the recorded "near" rock motions provide an excellent opportunity to study the variation of strong motions transverse to the dam at the center of the crest and at the mid-height downstream slope of the dam at its maximum cross-section, and thus to study the dam's response characteristics of principal engineering interest.

Figure 3 shows the response spectra for the transverse components of the motions recorded at the three "near" rock sites (Channels 3, 6 and 13). All three motions are largely similar, and the peak accelerations recorded at all three stations were on the order of $a_{max} \approx 0.07$ g. A closer inspection, however, showed a higher concentration of energy at higher frequencies in the motion recorded on Channel 3, corresponding to the most "rock-like" recording among the three, so this motion was taken as the apparent rock motion for these

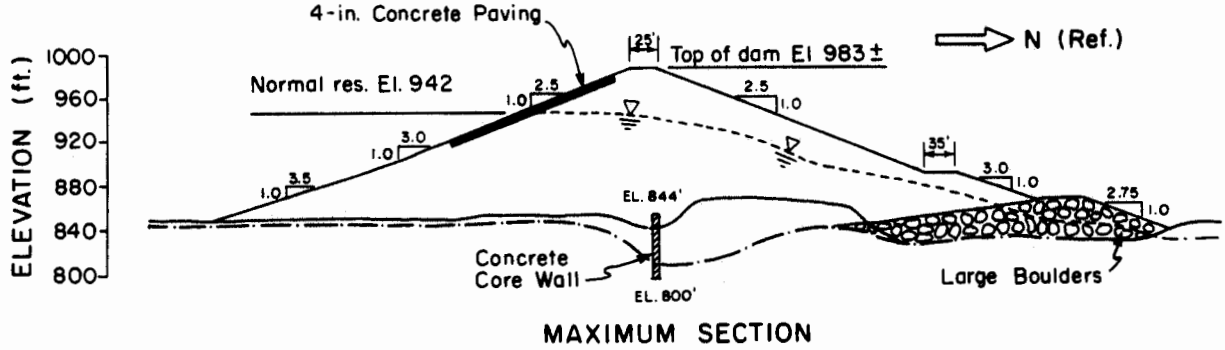

Fig. 2: Cross-Section Through the Maximum Height Section of Puddingstone Dam

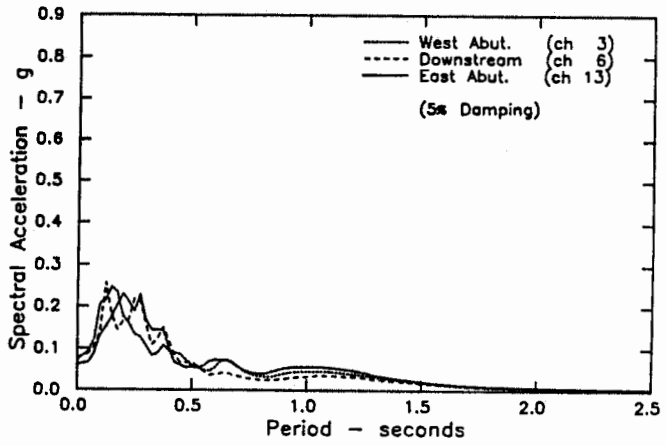

Fig. 3: Response Spectra for the Recorded Transverse Motions at the East and West Abutment, and Downstream of Puddingstone Dam

studies. Subsequent comparative studies involving analyses using each of the three "near" rock transverse recordings confirmed that the best overall dam response could be achieved with the use of the Channel 3 recording as an input motion.

Figure 4 shows the response spectra for the recorded transverse motions (a) "near" rock [Channel 3], (b) at the middle of the downstream face [Channel 12], and (c) at the center of the crest [Channel 11], clearly demonstrating the response amplification as the dam was excited. The peak accelerations of these three recorded motions are 0.07 g, 0.18 g and 0.19 g respectively.

Analyses of Dam Response:

All analyses of dynamic response performed as part of these studies used the equivalent linear method to model strain dependent moduli and damping characteristics. One-dimensional (columnar) response analyses were performed using the program SHAKE (Schnabel, et al., 1972), and two-dimensional (plane strain) finite element analyses were performed using the program FLUSH (Lysmer, et al., 1975).

Information regarding soil properties within the main Puddingstone embankment section were available from a 1973 study of the dam. These data were used as a basis for evaluation of dynamic shear moduli (G). Shear moduli at small strains (G_{max}) were

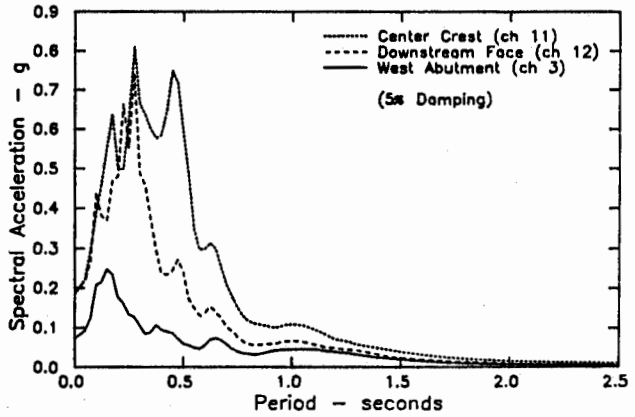

Fig. 4: Response Spectra for the Recorded Transverse Motions at the Crest, Mid-Face (Downstream) and Abutment of Puddingstone Dam

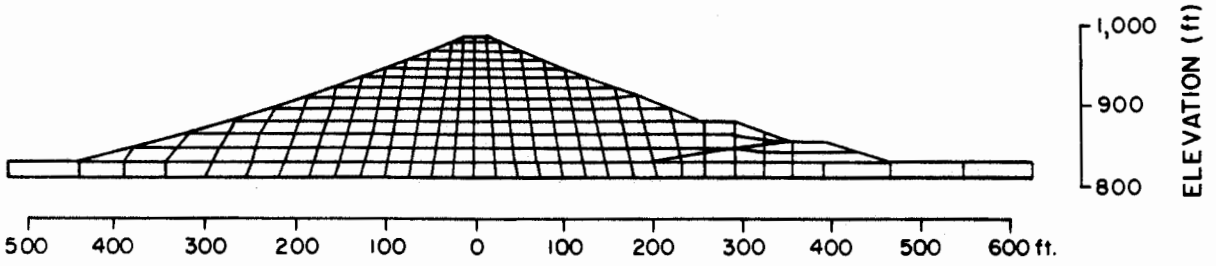

Fig. 5: Finite Element Mesh Used to Model Puddingstone Dam

evaluated using a variety of techniques (Bray et al., 1989), and an average value of G_{max} = 4,000 kips/ft^2 was selected for use in all analyses presented herein. A full parameter study using a range of moduli is presented by Bray et al. (1989). Moduli varied slightly with confinement, and $G_{max} \approx$ 3,600 kips/ft^2 was used at the crest and faces, and $G_{max} \approx$ 4,400 lb/ft^2 deep within the interior of the embankment. A shear modulus vs. shear strain relationship for the sandy silty clay comprising the main embankment section was selected, based on recent studies by Sun et al. (1988), and is presented in Table 1. A review of the damping vs. shear strain data presented by Sun et al. (1989) and Seed et al. (1984) suggested that sandy silty clays typically have somewhat higher than average damping ratios relative to the relationships they suggested for cohesive soils, so the upper bound damping ratios proposed by Sun et al. (1988) for cohesive soils were used, as shown in Table 1. This damping curve is intermediate between the average curves recommend for cohesive soils and sandy soils in these two references. Dynamic properties of the cohesionless toe drain were relatively unimportant, and were modelled using modulus degradation and damping vs. shear strain relationships recommended for gravelly soils by Seed et al. (1984), with $(K_2)_{max}$ = 90. The abutment rock shear wave velocity was modelled as v_s = 5000 ft/sec.

Figure 5 shows the finite element mesh used for 2-D finite element (FEM) analyses of Puddingstone Dam. Comparative analyses showed that a frequency cut-off above 12 Hz provided a negligible loss of accuracy in performing these analyses. Figure 6 shows a comparison between the response spectra for the resulting predicted crest and mid-downstream face motions vs. those actually recorded. The predicted peak acceleration of a_{max} = 0.21 g at the crest agrees well with the recorded peak of a_{max} = 0.19 g, and the predicted crest response spectra is in good general agreement with the observed crest motions. The predicted peak acceleration of a_{max} = 0.15 g at the downstream face station also agrees well with the recorded a_{max} = 0.18 g, and the spectral response

Table 1: Dynamic Shear Moduli and Damping Ratios vs. Shear Strain Used for Puddingstone Analyses

Shear Strain (γ)	Normalized Dynamic Modulus $\left(\frac{G}{G_{max}}\right)$	Damping Ratio
10^{-4}%	1.00	2%
10^{-3}%	0.99	4%
10^{-2}%	0.86	7.5%
10^{-1}%	0.40	15.0%

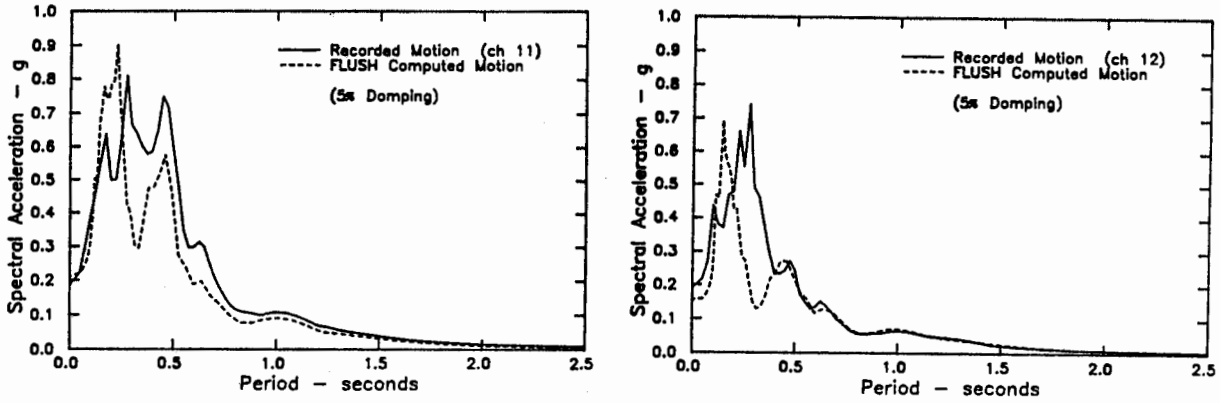

Fig. 6: Comparison Between Predicted and Observed Response Spectra: 2-D FEM Analyses of Puddingstone Dam

agreement is fairly good here too. Overall, these 2-D FEM analyses provided a good prediction of the observed response, with an accuracy level amply sufficient as to provide a good basis for engineering analyses.

Similar analyses were performed using 1-D analyses of "representative" columnar sections through the crest and downstream face, and the results are shown in Figure 7. As expected, these analyses greatly under-predicted both the peak acceleration and the spectral response at the crest station, but they provided a somewhat better (but still only fair) prediction of the observed response at the downstream face station.

COGSWELL DAM

Cogswell Dam, located 20 miles north of Whittier, was designed as a conventional Concrete-Faced Rockfill Dam of the old fashioned type. At the time of its construction (1931-34) the conventional way of placing the rockfill in such a dam was by dumping and sluicing the rock with large volumes of water. Because of the scarcity of water at the Cogswell site, the sluicing part of the usual procedure was omitted and the rockfill was dumped in 25 ft lifts with no compaction, leading to a very loose condition of the fill.

The entire rockfill section, some 280 ft high with average side slopes of 1.3:1 upstream and 1.3:1 to 1.6:1 downstream was placed in this manner between Spring 1931

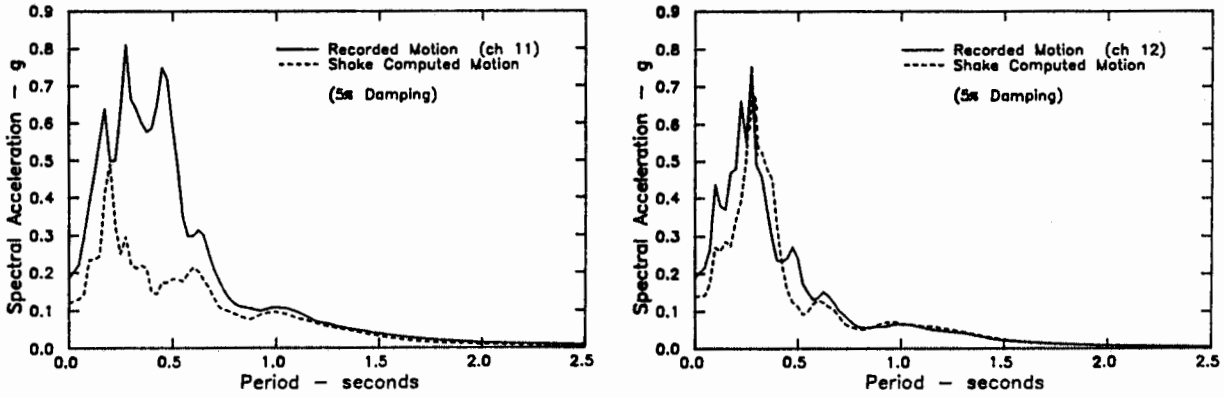

Fig. 7: Comparison Between Predicted and Observed Response Spectra: 1-D Columnar Analyses of Puddingstone Dam

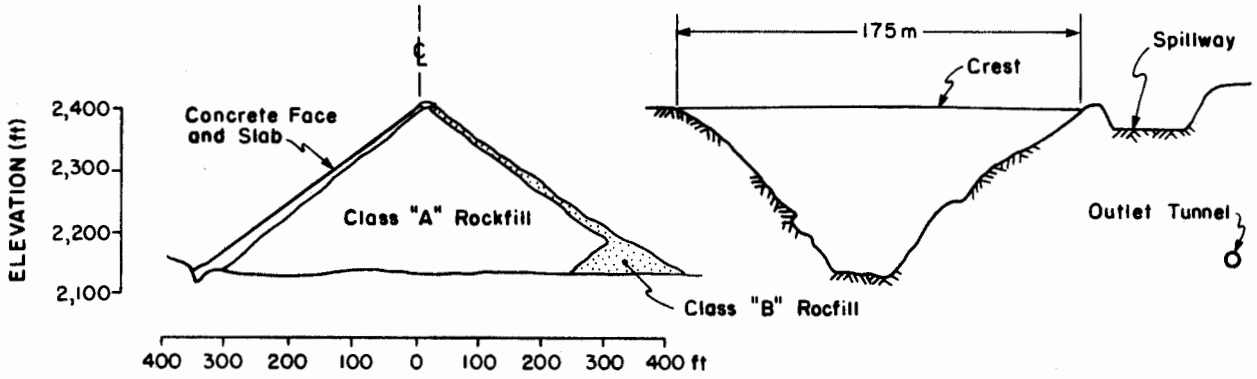

Fig. 8: Cross-Section Views of the Maximum Height Sections of Cogswell Dam

and Fall of 1933. At this stage construction began on placement of the concrete-facing with the intention of completing this work by Spring of 1934. Heavy rains in December 1933 through March 1934 interfered with this plan. The heavy rains also wetted the fill and led to large settlements which disrupted the facing already constructed and caused deformations of the dam. During one particularly severe rainstorm of December 31, 1933 the crest of the dam settled about 5 ft, and throughout the four months of rain the total settlement of the crest was as much as 15 ft. This led to a need to re-shape the dam and reconstruct the upstream facing. It was decided to use a temporary timber facing until settlements had essentially ceased, and then to replace the timber with a gunite facing. In the event, the timber was left in place for about 10 years before it was replaced by the gunite facing.

Figure 8 shows a transverse cross-section through the maximum height section of the completed dam as it stands today, and a longitudinal cross-section along the crest showing the geometry of the steep-walled, V-shaped canyon.

Seismic Instrumentation and the Recorded Motions:

A total of 9 strong motion accelerographs were installed at three locations on and near the dam, as shown in Figure 9. At each location, motions were recorded in three orthogonal directions: vertically, longitudinally (parallel to the main dam axis) and transverse to the main dam axis. Again, this paper will concentrate on the transverse motions, as these are the motions of primary engineering interest. The right abutment sensors were well sited to record abutment "rock" motions, and the transverse motions recorded at this station were used as input motions for the analyses described herein.

Figure 10 shows the response spectra for the recorded transverse motions at (a) the right abutment, (b) the right crest and (c) the center crest with peak recorded accelerations of a_{max} = 0.06 g, 0.10 g and 0.16 g respectively.

Analyses of Dam Response:

As this steep-faced dam in a narrow, V-shaped canyon has a low crest length vs. maximum crest height ratio of only $L/H \approx 2.1{:}1$, this dam was judged likely to respond in a highly complex three-dimensional fashion not amenable to analysis by 2-D techniques, and this proved to be the case. Nonetheless, relatively simple analyses sufficed to provide valuable information regarding the dynamic response properties of the rockfill comprising this embankment.

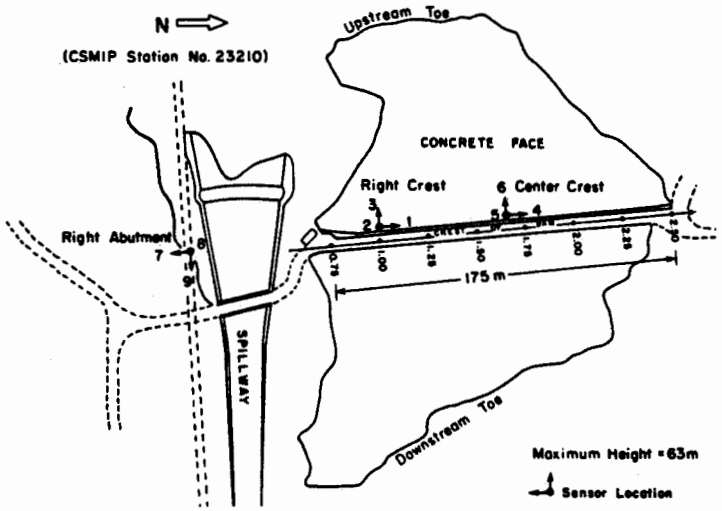

Fig. 9: Plan View of Cogswell Dam Showing Sensor Locations

The response recordings obtained at Cogswell Dam provided a valuable opportunity to obtain field data regarding the dynamic response characteristics of rockfill materials. Only limited data regarding their behavior exists, as they cannot be adequately evaluated using laboratory testing techniques, and field shear wave velocity measurements in coarse rockfills are fraught with difficulty.

Since the geometry of Cogswell Dam would require fully three-dimensional analyses to accurately reproduce the full observed response, analyses to evaluate the rockfill response characteristics concentrated on the predominant period of the observed response. Mejia and Seed (1981, 1984) proposed a relationship between the predominant frequency of a fully 3-D dam in a V-shaped canyon vs. an infinitely long dam with the full maximum crest section (based on 2-D, plane strain analysis) as a function of dam height (H) over crest length (L). Their relationship was based on 2-D and 3-D back-analyses of the response of several such dams, and was supported by similar theoretical analyses by Ambraseys (1960). For Cogswell Dam, with H/L = 2.1:1, the plane section 2-D period would be approximately 1.65 times the actual 3-D period.

Two approaches were taken to evaluate the observed 3-D period. The recorded crest response motion had a predominant period of 0.33 seconds, as shown in Figure 10. Because of the broad band spectral crest response with its multiple peaks, however, there

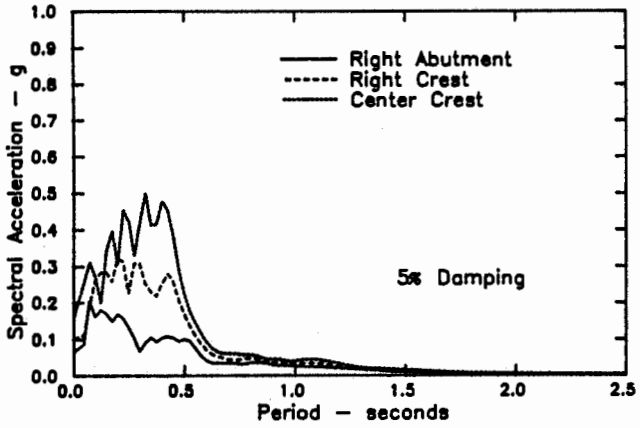

Fig. 10: Response Spectra for the Transverse Motions Recorded at Cogswell Dam

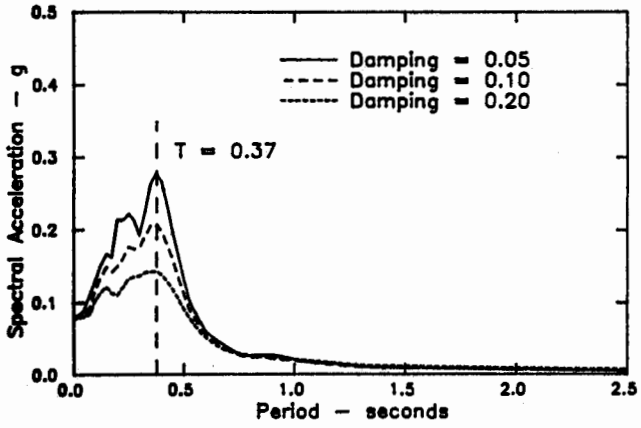

Fig. 11: Crest Transverse Response Spectra from t = 7.5 sec to 10.0 sec.

was some question as to whether this represented interaction with the high frequency input motions, in which case a slightly lower peak on the spectral response might better represent the dam's predominant period at the observed strain levels. Accordingly, a section of the crest response accelerogram representing the initial period of decay of strong shaking was analyzed, and found to have a predominant period of approximately 0.37 seconds, as shown in Figure 11. The dam's predominant period was thus taken to be $T_p \approx 0.33$ to 0.37 seconds. By scaling for 3-D geometry effects, the corresponding maximum plane section (2-D) predominant period would then be T_p (2-D) $\approx$ 0.54 to 0.61 seconds.

The dynamic shear modulus degradation curve (the G/G_{max} vs. shear strain relationship) and the damping ratio vs. shear strain relationship used to model the rockfill were the modulus degradation curve and upper bound damping curve recommended by Seed et al. (1984) for gravelly soils. Having thus selected a dimensionless modulus degredation curve, it then remained to give it scale by selection of a value for the paramter $K_{2,max}$ which would then establish G_{max} as

$$G_{max} = 1000\, K_{2,max}\, (\sigma_m')^{\frac{1}{2}} \qquad \text{(Eq. 1)}$$

Three approaches were taken to evaluate $K_{2,max}$ based on the Cogswell Dam response recordings. Ambraseys and Sarma (1967) developed a relationship for estimating the predominant period of 2-D planar dam sections as

$$T_p \approx 2.61 \times H/V_s \qquad \text{(Eq. 2)}$$

where V_s is the average shear wave velocity (based on G_{avg}, the average shear modulus) within the embankment, and H is the embankment height. For the levels of shear strain likely to have been induced within the Cogswell embankment by the Whittier Narrows Earthquake, the representative G_{avg} is likely to have been about 55% of G_{max}, so that the $K_{2,max}$-values necessary to produce a T_p of about 0.54 to 0.61 seconds are $K_{2,max} \approx$ 110 to 130.

A second, more robust estimation of $K_{2,max}$ was achieved by performing 2-D, plane strain response analyses of Cogswell Dam using the mesh shown in Figure 12. Using the abutment recording as an input motion, and varying $K_{2,max}$ over a range from $K_{2,max}$ = 95 to 240 (the full likely range) produced varying predominant periods, as shown in Figure 13. The values producing the desired 2-D predominant periods of $T_p \approx$ 0.54 to 0.61 seconds were $K_{2,max} \approx$ 120 to 150, in good agreement with the values estimated above.

Figure 14 shows response spectra for crest motions calculated using $K_{2,max}$ = 120, 180 and 240. Similar spectra were produced for other choices of $K_{2,max}$. As shown in Figure 14, all 2-D analyses over-predicted the actually observed 3-D response (see Figure 10 for comparison). A careful evaluation of these calculated crest response spectra,

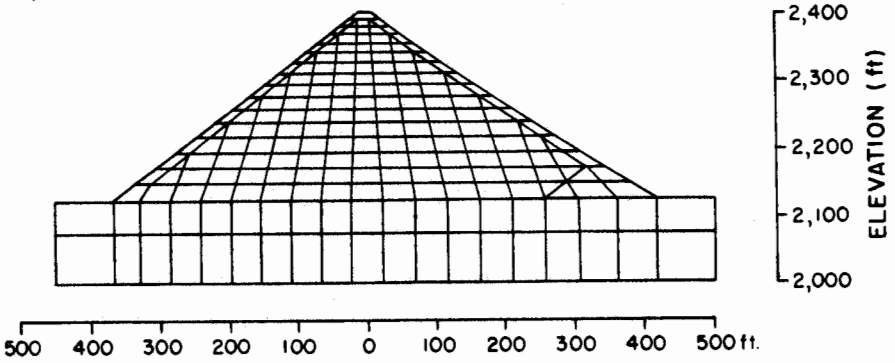

Fig. 12: Finite Element Mesh Used to Model Cogswell Dam

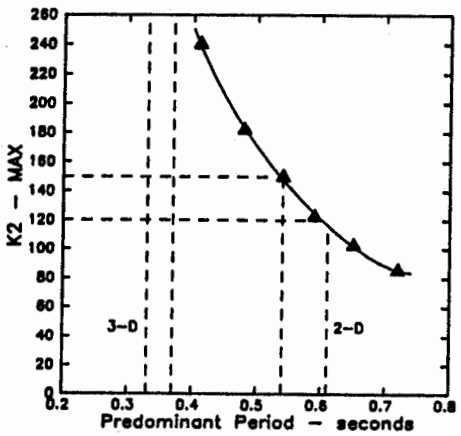

Fig. 13: Predominant Period vs. $K_{2,max}$

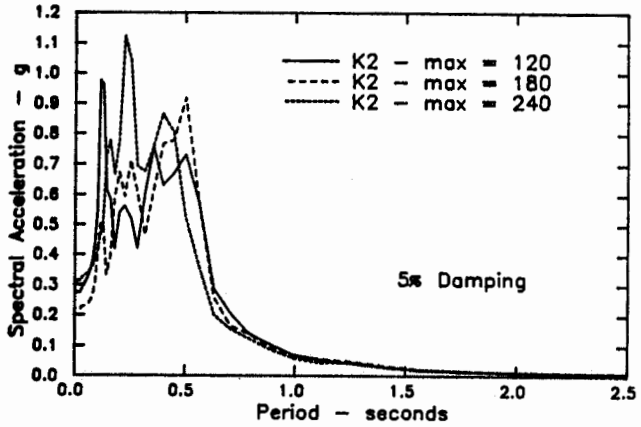

Fig. 14: Crest Response Spectra Calculated with Different Values of $K_{2,max}$

however, with allowance for 2-D vs. 3-D period response shifts, suggested that optimum overall spectral response modelling was achieved with $K_{2,max} \approx 150$ to 180.

Overall, based on these studies, it was concluded that best modelling of the recorded response of the Cogswell Dam rockfill embankment was achieved with $K_{2,max} \approx 150$. This compares well with the value of $K_{2,max} \approx 100$ to 130 developed by Lai and Seed (1985) by similar back analyses of the recorded response of two similar rockfill dams, as they used the modulus degredation curve recommended by Seed et al. (1984) for sands. Considering the representative shear strain levels in their analyses, and substituting the modulus degredation curve for gravelly soils used in this study, their corresponding estimates would have been $K_{2,max} \approx 130$ to 170, in very good agreement with the value developed in these studies for a similar, loosely dumped and sluiced rockfill mass.

SUMMARY AND CONCLUSIONS

Good agreement between the observed response characteristics of Puddingstone Dam and response characteristics predicted using both simple empirical methods as well as 2-D finite element analyses, based on established methods for evaluation and modelling of strain-dependent dynamic shear moduli and damping, provides good support for these modelling and analytical techniques. Proper interpretation of the analytically predicted response characteristics requires appropriate consideration of three-dimensional effects not modelled in the 1-D and 2-D analyses performed. These effects were only moderate, however, for this dam in a V-shaped canyon with a crest length vs. dam height ratio of $L/H \approx 4.5:1$, and the 2-D finite element analyses provided response predictions for both the crest and downstream face motions which were in sufficient agreement with observed response as to provide a good basis for engineering analyses. Even the simpler 1-D analyses provided good approximate predictions of peak accelerations for the downstream face, though these simpler analyses were unable to provide a reasonable prediction of the observed crest response.

The Cogswell Dam response recordings provided an excellent opportunity to obtain additional insight into the parameters suitable for modelling strain-dependent dynamic moduli for rockfills. Only very limited previous data from several similar back-analyses of observed rockfill dam response exist. Analyses of the observed dam response characteristics resulted in selection of a value of $(K_2)_{max} \approx 120$ to 150 as best modelling the behavior of this loosely-dumped and then sluiced rockfill, in good general agreement with the values of $(K_2)_{max}$ suggested by Lai and Seed (1985) and Seed et al., (1984) based

on previous, similar back-analyses of the response of several loosely dumped rockfill dams of similar composition.

Although a good estimate of $(K_2)_{max}$ could be obtained from the response recordings, the geometry of Cogswell Dam (a steep-faced dam in a steep-walled, V-shaped canyon with a crest length vs. dam height ratio of L/H ≈ 2.1:1) was shown not to be amenable to reliable 2-D analysis. This finding was in good agreement with previous studies which suggest that dam response is increasingly affected by abutment constraints for dams in V-shaped canyons with L/H < 3:1, and that 3-D analyses are required for accurate and comprehensive prediction of the strong motion response characteristics of such dams.

ACKNOWLEDGEMENTS

These studies were supported by the California Department of Conservation, Division of Mines and Geology, Grant No. 8-8067, and this support is gratefully acknowledged. The authors also wish to thank the engineers of the California Division of Safety of Dams (DSOD), for their assistance in background reviews for the two dams studied, Dr. Joseph Sun of Kleinfelder Associates for his assistance with the initial processing of the recorded accelerograms, and Professor John Lysmer of U.C. Berkeley whose advice and counsel regarding the dynamic analyses performed was invaluable.

REFERENCES

Ambraseys, N. N. (1960) "On the Shear Response of a Two Dimensional Wedge Subjected to an Arbitrary Disturbance," Bulletin of the Seismological Society of America, Vol. 50, Jan., 1960, pp. 45-56.

Boulanger, R. W., Seed, R. B., Seed, H. B. and Bray, J. D. (1989) "Analyses of the Seismic Response of the Cogswell Dam in the 1987 Whittier Narrows Earthquake," report in preparation for the California Strong Motion Instrumentation Program (CSMIP), Dept. of Civil Engineering, University of California at Berkeley.

Bray, J. D., Seed, R. B., Seed, H. B. and Boulanger, R. W. (1989) "Analyses of the Seismic Response of the Puddingstone Dam in the 1987 Whittier Narrows Earthquake," report in preparation for the California Strong Motion Instrumentation Program (CSMIP), Dept. of Civil Engineering, University of California at Berkeley.

Lai, S. S. and Seed, H. B. (1985) "Dynamic Response of the Long Valley Dam in the Mammoth Lake Earthquake Series of May 25-27, 1980," Report No. UCB/EERC-85/12, Earthquake Engineering Research Center, University of California, Berkeley, November.

Lysmer, J., Udaka, T., Tsai, C-F. and Seed, H. B. (1975) "FLUSH - A Computer Program for Approximate 3-D Analysis of Soil-Structure Interaction Problems," Report No. EERC 75-30, Earthquake Engineering Research Center, University of California, Berkeley, November.

Mejia, L. H. and Seed, H. B. (1981) "Three Dimensional Dynamic Response of Earth Dams," Report No. UCB/EERC-81/15, Earthquake Engineering Research Center, University of California, Berkeley, September.

Mejia, L. H. and Seed, H. B. (1984) "Comparison of 2-D and 3-D Dynamic Analyses of Earth Dams," Journal, Geotechnical Engineering Division, ASCE, Vol. 109, No. GT11, November, pp. 1383-1398.

Schnabel, P. B., Lysmer, J. and Seed, H. B. (1972) "SHAKE - A Computer Program for Earthquake Response Analysis of Horizontally Layered Sites," Earthquake Engineering Research Center, Report No. EERC 72-12, University of California, Berkeley, December.

Seed, H. B., Wong, R. T., Idriss, I. M. and Tokimatsu, K. (1984) "Moduli and Damping Factors for Dynamic Analyses of Cohesionless Soils," Report No. UCB/EERC-84/14, Earthquake Engineering Research Center, University of California, Berkeley, September.

Sun, J. I., Golesorkhi, R. and Seed, H. B. (1988) "Dynamic Moduli and Damping Ratios for Cohesive Soils," Report No. UCB/EERC-88/15, Earthquake Engineering Research Center, University of California, Berkeley.

INTERPRETATION OF RIO DELL FREEWAY RESPONSE DURING SIX RECORDED EARTHQUAKE EVENTS

K. Romstad, Professor
B. Maroney, Graduate Student
M. Chajes, Graduate Student
Department of Civil Engineering,
University of California, Davis

ABSTRACT

Six earthquakes have been recorded since 1980 on the overpass of Highway 101 at Painter Street in Rio Dell, California, just south of Eureka. Finite element models of the bridge have been constructed and the natural frequency results compared with the recorded motions. Analysis of the experimental data tends to identify the first six modes of vibration. Modeling the backfill-abutment-superstructure interaction is key to the analytical modeling to describe response. Torsional modes of vibration of the individual spans appear heavily influenced by the skew implying use of very simple bridge models should be approached cautiously for such short spans.

INTRODUCTION

Description of Bridge and Instrumentation

The Rio Dell overpass is a two span bridge crossing Highway 101 at Painter Street. The bridge is a monolithic, cast in place, prestressed, concrete, box girder structure with end diaphragm abutments and a two column bent. Both the abutment and bent foundations are supported on piles. The behavior is complicated by a 39° degree skew between the centerline of bent #2 and the centerline of Highway 101 passing beneath and the unbalanced spans of 119 and 146 feet. A strip bearing pad is located at the base of abutment #1 on the west end as part of a designed mechanism to allow for longitudinal movement. The bridge is typical of numerous bridges in California spanning two or four lane separated highways.

The bridge was relatively heavily instrumented in September, 1977 [1,2] and contains twenty strong motion sensors as shown in Figure 1. Channels 12, 13 and 14 measure free field motions (longitudinal, vertical and transverse to the bridge axis respectively) approximately 200 feet northwest of the overpass between the traffic lanes. At the east end of the bridge, triaxial sets of sensors are located both on the embankment (15, 16, 17) and on the end of the bridge deck (9, 10, 11) so that relative motion between the embankment and the deck can be assessed. The west end of the bridge is similarly instrumented except for the absence of a longitudinal sensor on the bridge deck. A triaxial set of sensors (1, 2, 3) is also located at the base of the bent's north column to aid in assessing soil structure interaction. A transverse sensor (7) is located at the base of the deck adjacent to the center bent and vertical sensors are located at midspan of the east (8) and west (6) spans on the north side of the deck. Torsion of the bridge deck cannot be directly assessed since only the north edge of the bridge deck is instrumented.

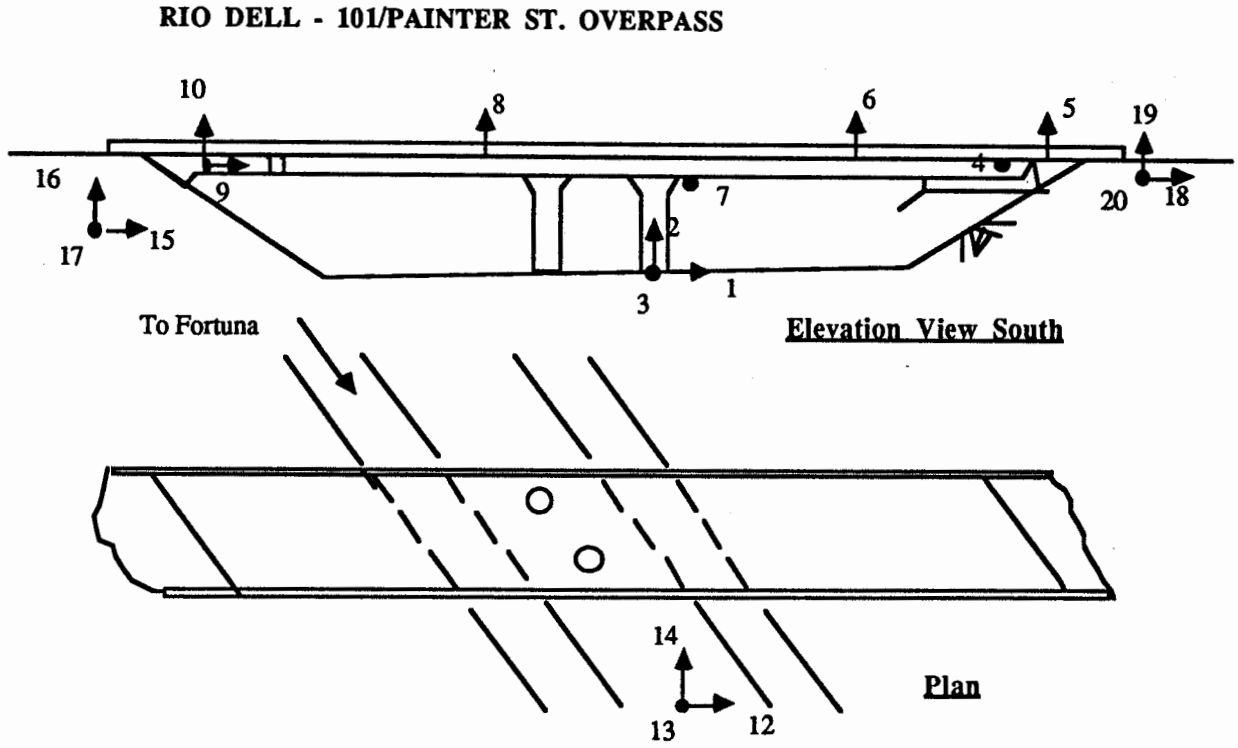

Figure 1 Distribution of Strong Motion Sensors at Painter Street Overpass, Highway 101, Rio Dell, Humbolt County, CA.

Strong Motion Records

Since the overpass was instrumented, it has been shaken by six earthquakes [2] starting with the large (6.9ML) Trinidad offshore earthquake of November 8, 1980 at 72 km from the site. The second earthquake was a smaller (4.4ML) event on December 16, 1982 only 15 km from the site. The other events ranged from 5.1 to 5.5 ML at 27 to 61 km. The six earthquakes are summarized in Table 1. Observation of the free field data in Table 1 shows that the maximum vertical accelerations are less than fifty percent of the maximum transverse accelerations and less than twenty five percent of the maximum longitudinal accelerations. However, the maximum vertical accelerations measured by sensors six and eight on the north end of the deck at the middle of the spans generally equal to or exceed the maximum transverse acceleration measured by sensor 7 of the deck at bent #2. The largest bridge accelerations were caused by caused by the relatively small Rio Dell earthquake of 12/16/82. Unfortunately the free field sensors did not record this event.

TABLE 1

EARTHQUAKES RECORDED BY THE RIO DELL OVERPASS INSTRUMENTATION

Earthquake	Date	Mag. (ML)	Epicent. Distance (km)	Maximum Ground Acceleration C12	C13	C14	Maximum Bridge Acceleration C6	C7	C8
Trinidad	11/08/80	6.9	72	.15g	.03g	.06g	.34g	-	.25g
Rio Dell	12/16/82	4.4	15	-	-	-	.39g	.43g	.59g
Cape Mendocino	08/24/83	5.5	61	-	-	-	.27g	.22g	.16g
Event #1	11/21/86	5.1	32	.46g	.08g	.16g	.24g	.26g	.33g
Event #2	11/21/86	5.1	33	.15g	.02g	.12g	.21g	.36g	.29g
Cape Mendocino	07/31/87	5.5	27	.15g	.04g	.09g	-	.34g	.27g

In Table 2 the complete set of maximum accelerations from all sensors are presented for earthquakes 4, 5 and 6 arranged by direction. These are simply listed here because they contain essentially complete data sets including free field and sensor 7. In each direction the free field motion is given first followed by the base of pier motion. The remaining channels are then listed in sequential order from the west abutment fill to east abutment fill. It is interesting to note the longitudinal accelerations on the abutment fill (15 and 18) and on the structure (11) are essentially the same as the free field motion (12) for all earthquakes. This may indicate the bridge is moving as a rigid body with the ground in the longitudinal direction. In the transverse direction all sensors on the abutment fill (17 and 20) and on the structure (4, 7 and 9) are considerably amplified relative to the free field (14) and base of pier motion (3). All vertical sensors on the fill (16 and 19) and bridge (5, 6, 8 and 10) are amplified relative to the free field (13) and base of pier (2) except sensor 5. This is possibly due to the bearing pad which exist at the base of the abutment.

TABLE 2

MAXIMUM SENSOR ACCELERATIONS FROM EARTHQUAKES 4, 5 AND 6

	Longitudinal Max. Accel. (g/100) Channel					Transverse Max. Accel. (g/100) Channel							Vertical Max. Accel. (g/100) Channel							
Earthquake	12	1	18	11	15	14	3	20	4	7	9	17	13	2	19	5	6	8	10	16
11/21/86*	46	27	45	40	40	16	13	30	23	26	23	23	8	8	18	10	23	33	25	11
11/21/86**	15	11	17	19	17	12	12	25	25	35	30	22	2	5	6	5	20	29	14	4
07/31/87	15	11	20	21	17	9	10	17	18	34	25	26	4	6	19	5	-	26	11	5

Scope of Study

The primary goal of this study is to investigate bridge modeling techniques; particularly relative to the level of sophistication necessary to accurately capture the essential dynamic response characteristics. Emphasis to date has focussed upon the transverse free field motion (C14) which would be expected to induce the largest forces in the bent columns, since the longitudinal motions should be transferred primarily through the deck to the monolithic end walls and into the abutment backfill. The availability of records from six different events of variable magnitudes and originating from several faults over a seven year span should give considerable insight into level of sophistication justified in formulating analytical models.

The primary parameters used to characterize the accuracy of the analytical model are the natural frequencies and modeshapes of the bridge model. If the analytical model of the bridge predicts natural frequencies and mode shapes which agree well with those deduced from the measured motions in the field then it can be expected the stresses and displacements will also be predicted with reasonable accuracy. As a result this study was initially divided into two phases:

1) analysis of the measured field data to deduce the natural frequencies and modeshapes of the "as built" bridge.

2) comparison of analytical models of various levels of complexity with respect to computed differences in natural frequencies and mode shapes, and

Information from the two phases was then compared and calibrated by adjusting abutment springs.

ANALYSIS OF FIELD DATA

A recent paper by Wilson [3] describes the analysis of records obtained on the San Juan Bautista 156/101 Separation Bridge during the 6 August 1979 Coyote Lake event. The amount of actual data for Painter Street is somewhat overwhelming including 109 corrected time history acceleration records and associated Response Spectra and Fourier Amplitude Spectra for the six events. The data has been looked at in a variety of ways and the power spectral density plots will be emphasized herein. Power spectral densities were obtained for individual earthquakes for each sensor both by analyzing the entire time history recorded and by selecting a portion of the record following the last major acceleration pulse when it appeared to approximate free vibration decay.

Figure 2 shows a plot for from earthquake 4 for sensor 8 using both approaches. Both graphs indicate spikes at close to the same points but using the entire record emphasizes the shorter periods (0.14, 0.20) while using the selected interval emphasizes Longer periods (.21, .25, .28). Figures 3 and 4 superimpose functions from the first three earthquakes for sensor 8 using full and partial records and Figure 5 presents the superimposed functions for earthquakes 4, 5 and 6 using the full records. All six earthquakes tend to show a spike at .14-.15 seconds indicating an active natural mode with significant participation of sensor 8. Other spikes tend to be concentrated at about 0.21, 0.25 (smaller) and 0.28-0.30 seconds.

Figure 6 superimposes the power spectral density plots for earthquakes 1, 2, 3, 4 and 5 for sensor 6 located vertically at the center of the west span.. A clearly dominating spike exists between .30 and .32 seconds with smaller spikes at .36 seconds and 0.21 seconds and smaller blips at .16 and .24 seconds. Figure 7 shows a similar plot for sensor 7 and also five earthquakes. Again a dominant mode clearly exists in the 0.28 second range. The smaller spike at about 0.40 seconds is primarily particular to earthquake 2 which recorded the largest accelerations and was nearest to the bridge.

Figure 8 presents a comparison of the average Fourier Amplitude Spectrum for all earthquakes for the transverse motions in the free field (14), at the base of pier (3), on the fill at the top of the east abutment (17), and on the deck (9) adjacent to the east abutment. Note the similarity of the free field and base of pier motions indicating probably only minor soil-structure interaction in this area. Sensors 17 and 9 show considerably amplified motion in the vicinity of 0.28 seconds with the on bridge motion slightly larger than the fill motion. The differences between the free field (14) and the top of abutment motion imply considerable interaction in this area. The similarity of the motions on top of the fill (17, 20) with the motions on the bridge deck (4, 9) adjacent to the abutment are demonstrated in Figure 9. The top of the embankment fill appears to be moving with the bridge deck consistently throughout the events.

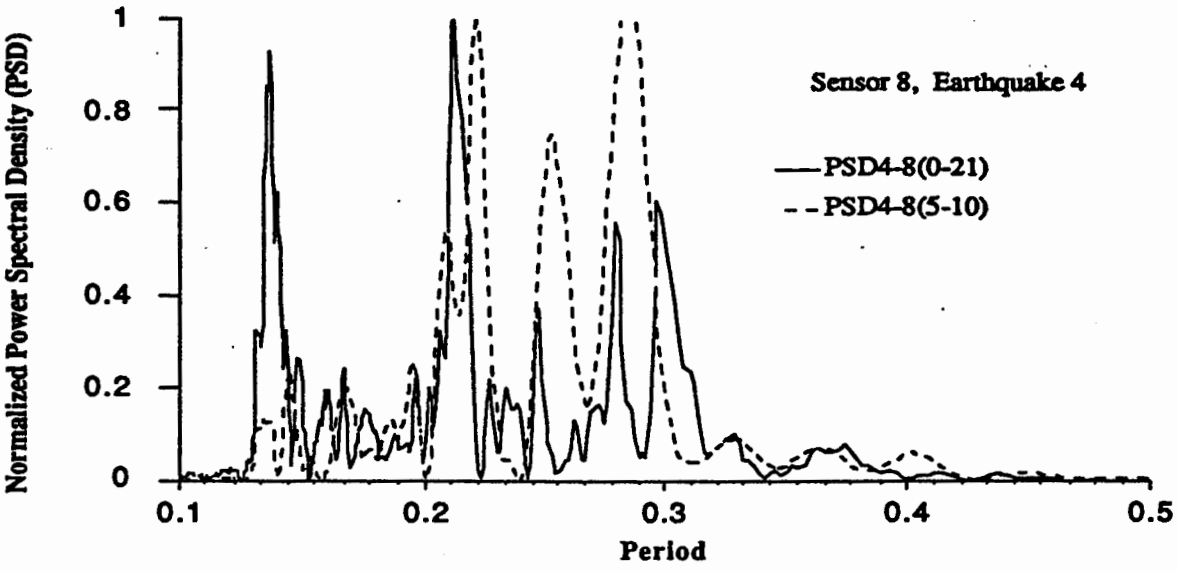

Figure 2 Sensor 8 PSD for Earthquake 4, Two Time Periods

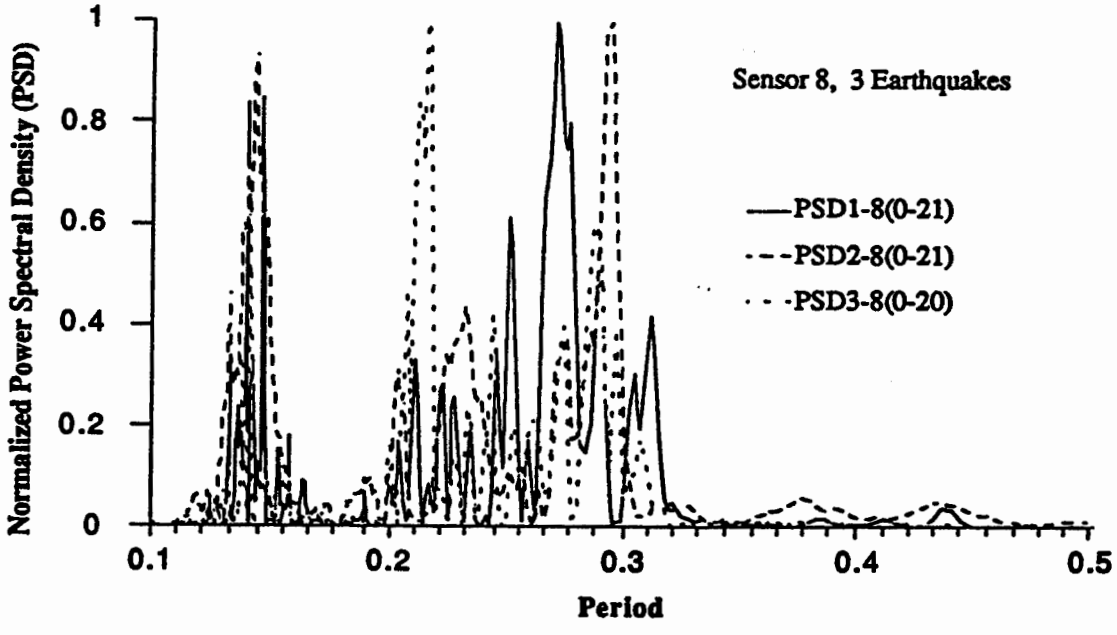

Figure 3 Sensor 8 PSD for Earthquakes 1, 2 and 3, Full Time

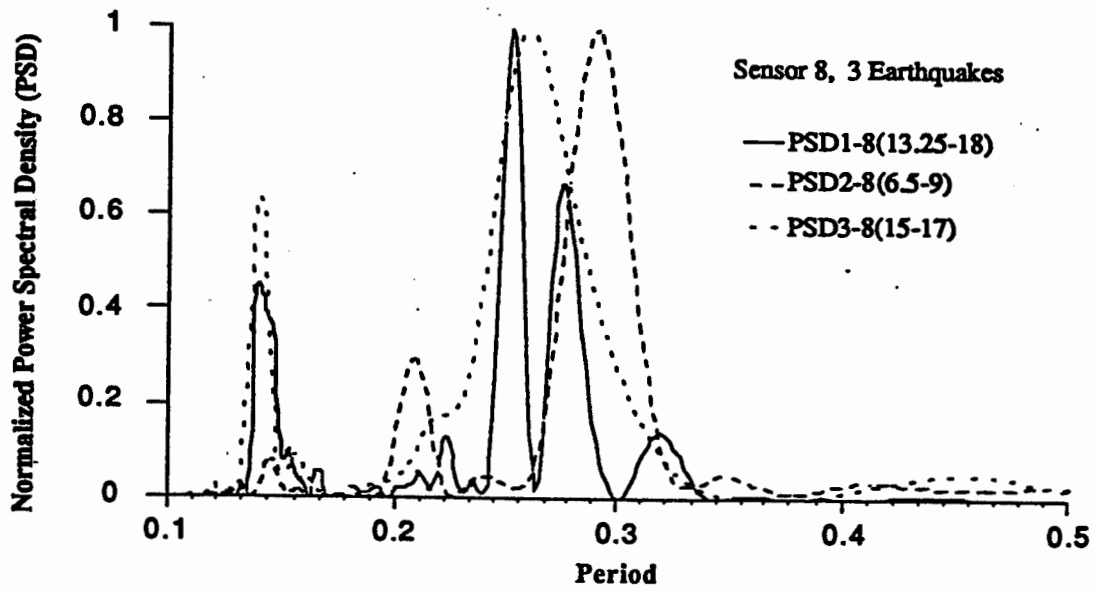

Figure 4 Sensor 8 PSD for Earthquakes 1, 2 and 3, Partial Time

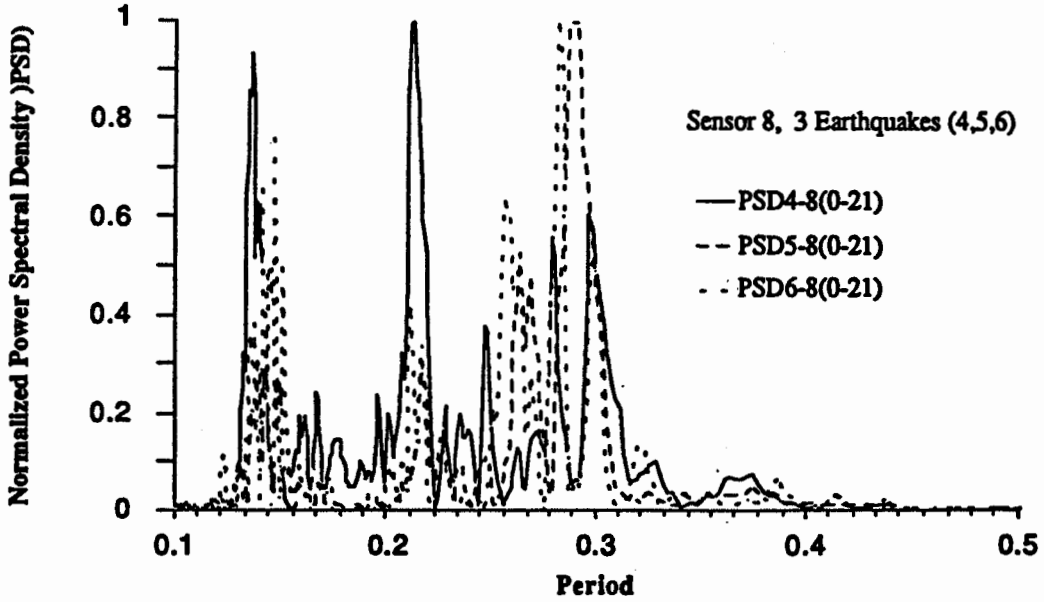

Figure 5 Sensor 8 PSD for Earthquakes 4, 5, and 6, Full Time

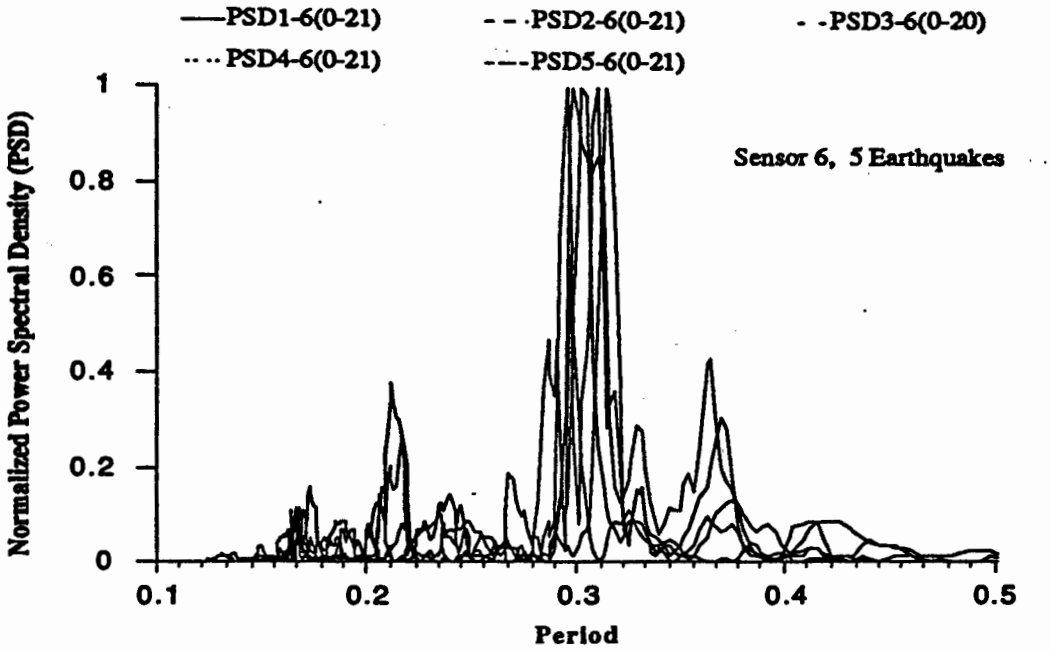

Figure 6 Sensor 6 PSD for Five Earthquakes, Full Time

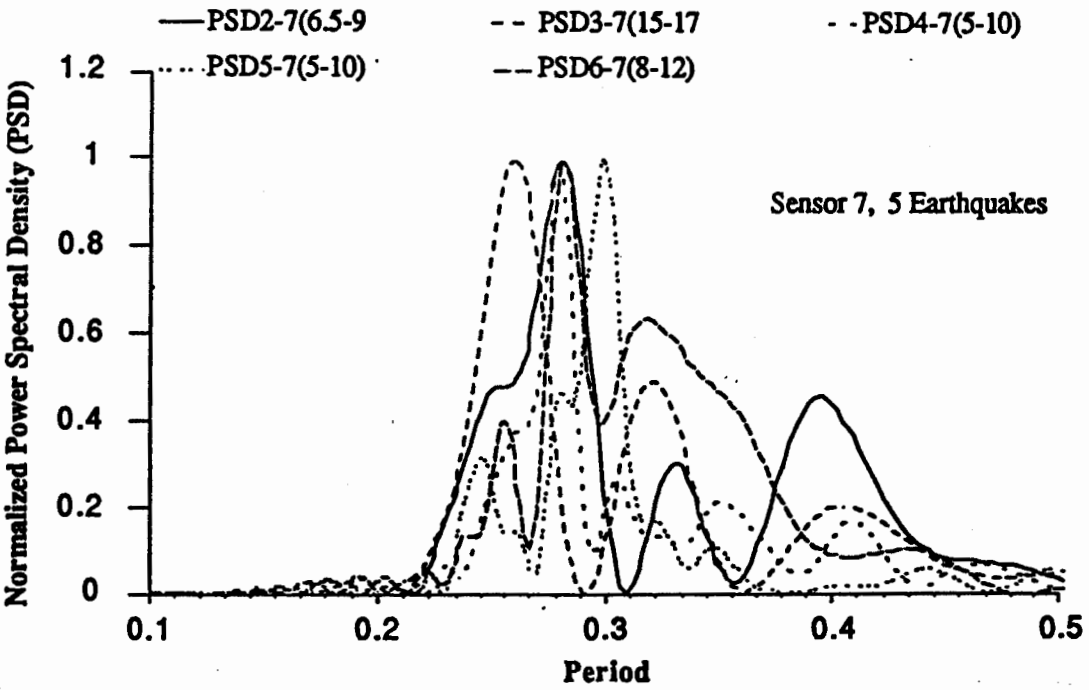

Figure 7 Sensor 7 PSD for Five Earthquakes, Partial Time

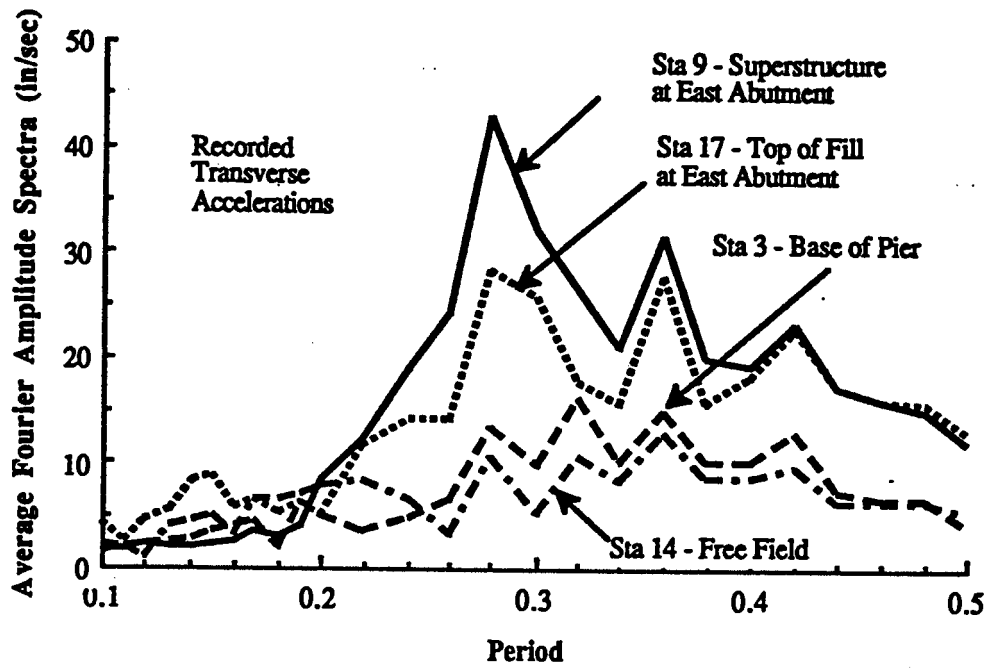

Figure 8 Average Fourier Amplitude Spectrum for 3, 9 and 17

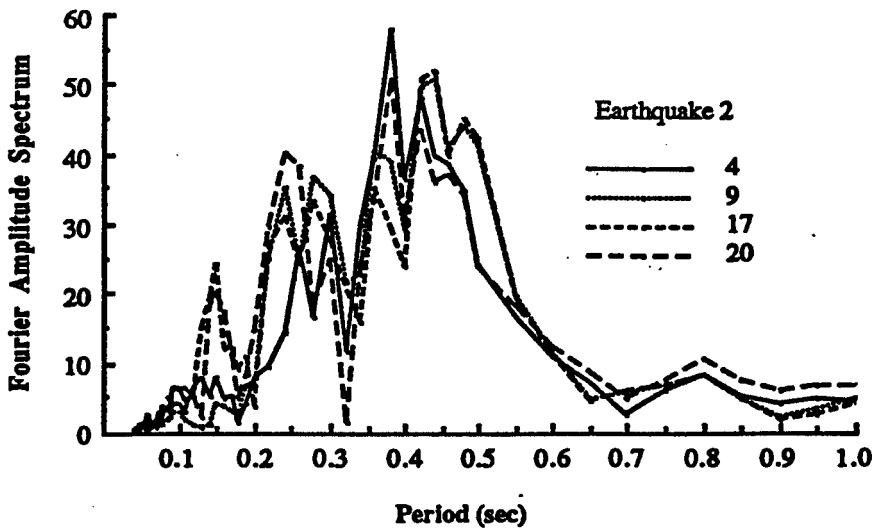

Figure 9 Earthquake 2 Fourier Amplitude Spectrum for 4, 9, 17, 20

ANALYTICAL BRIDGE MODELING

Numerous uncertainties exist in formulating reliable and accurate analytical models to predict the response of concrete bridges to earthquake motions. The Painter Street Overcrossing at Rio Dell is typical of numerous bridges in California which, while apparently simple in form, incorporate most of the uncertainties. The uncertainties investigated included

1) material stiffness modeling of the concrete,

2) finite element model types and mesh size of deck mass and stiffness, and

3) modeling and significance of abutment-backfill and pier foundation-soil interaction springs.

Another major uncertainty present in modeling earthquake response of this type of bridge is estimating the form and magnitude of dissipation of energy (damping) present in the soil foundation superstructure system. We have not yet looked closely at the data to assess energy dissipation or equivalent viscous damping.

Modulus of Elasticity

The modulus of elasticity (E) and shear modulus (G) of the concrete depend upon the actual mix of water, sand, aggregate and cement the contractor used during construction and the age of the concrete. Normally the modulus of elasticity is estimated from the equation

$$E = 33\, w^{1.5} (f_c')^{1/2} \quad (1)$$

where w is the unit weight of the concrete and f_c' is the compressive strength. This is an empirical equation based upon statistical analysis of test data and subject to a local variations. In addition the compressive strength used is normally that specified on the plans and the actual compressive strength found in the field normally exceeds the design strength. In this study we were fortunate to have personnel from the Transportation Laboratory of the State of California take core samples from the bridge and test them in the laboratory. The compressive strength specified on the plans was 3500 psi while the average strength from two laboratory tested core samples was 6400 psi, almost double the design value. The unit weight of the material was measured to be 150 pcf, which gives a modulus of elasticity from equation 1 of 4800 ksi. The actual modulus of elasticity obtained from a stress strain test in the laboratory on one of the core samples was 3800 ksi. This value was used in all subsequent analyses.

Finite Elements Models

A number of finite element models of the Painter Street Bridge were analysized using the computer program STRUDL at the California Department of Transportation Office of Structures computer facilities. The model variations generally differed in the treatment of the stiffness and mass description of the deck and the boundary conditions imposed at the base of the piers and the abutments. Figure 10 illustrates the basic layouts of the two potential models.

The "stick" model in Figure 10 is typical of models used in the dynamic analysis of bridges in California. Using a stick model of the deck means that the torsional, shear, flexural and axial stiffness of the deck are all lumped in a longitudinal one dimensional beam element with six degrees of freedom at each node. This model has the advantage of great simplicity in data preparation and minimal core storage and computation time in the computer. It also permits boundary parameters used to incorporate soil interaction influences. The disadvantages are that rotational inertia effects of the deck about the longitudinal bridge axis, skew and deep beam effects, intermediate diaphragms and deck plate action are not necessarily accurately modeled.

The "grid" model in Figure 10 was chosen to permit the rotational inertia of the deck about the longitudinal axis, skew and deep beam effects and intermediate diaphragms to be directly incorporated and hence serve as an accurate baseline for evaluating the adequacy of the stick model for capturing essential behavior and evaluating a number of the uncertainties present in formulating structural models.

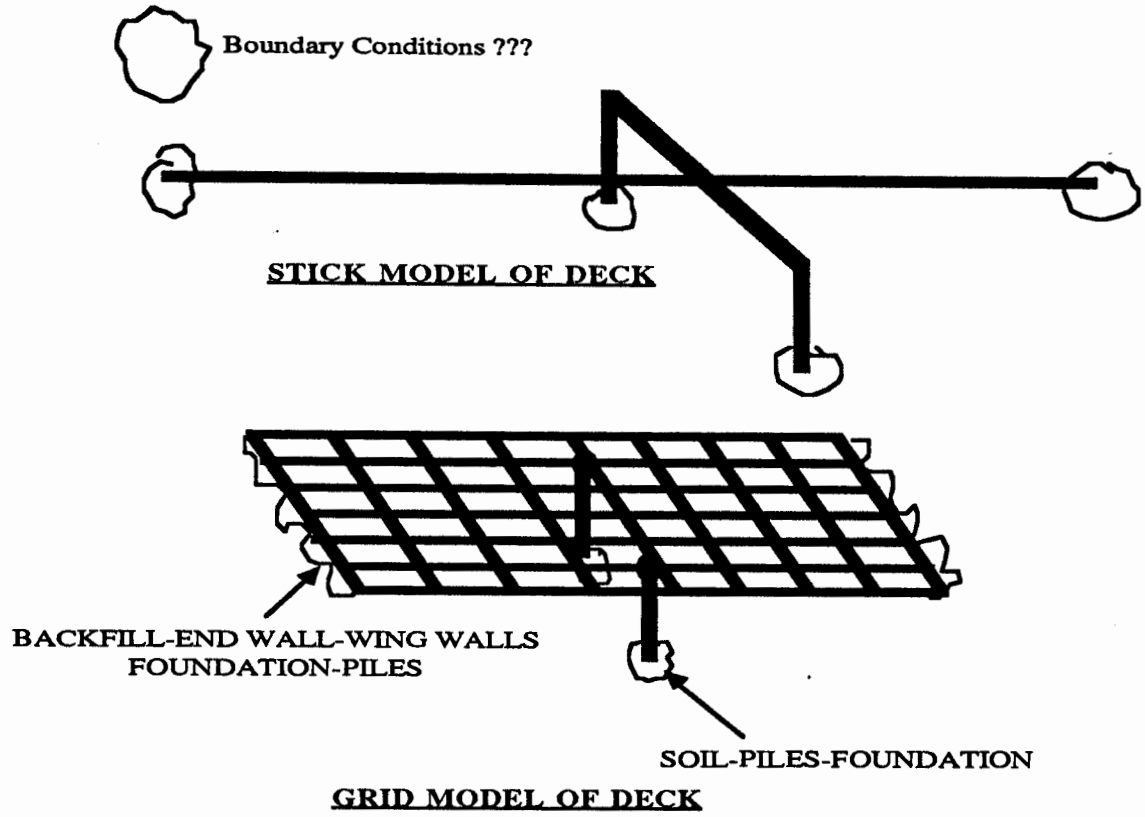

Figure 10 Schematic Finite Element Models of Superstructure

A preprocessor, STRUBAG, used by Caltrans generates STRUDL input coding for the stick model. The finite element model for the finite element grid model had to be laboriously generated point by point. A number of different models for the deck were evaluated in the preliminary analyses in terms of element types, finite element mesh sizes, modeling of the mass variation and choice of cross section properties. The final model for a deck cross section is shown in Figure 3. Each superstructure girder is modeled as a series of longitudinal members with the flanges assumed effective out to one-half the distance to the adjacent girder. The exterior girder elements are assumed to use the entire overhang but not the sidewalk or barrier rail. Transverse diaphragms are also modeled as beams with effective flanges. These properties were then used to determine moment of inertia values for the beams. The web areas were used to determine the effective shear areas and the torsional properties were chosen for the individual beams based upon the torsional stiffness of the entire cross section distributed by tributary area. It was felt the vertical flexural, shear and torsional stiffness of this effectively complicated orthotropic plate would be adequately represented by these beams and their corresponding properties.

A similar model is not adequate for incorporating the transverse stiffness because an intersecting series of beams would not capture the shear stiffness. As a result, plane stress

elements representing the deck were used to fill between the intersecting beams. The element finally selected was the eight node linear strain plane stress element IPQQ in the McDonald-Douglas version of STRUDL. Lower and higher elements were studied and mesh sizes varied to arrive at this selection.

Member section properties were ultimately selected using homogeneous gross sections. It is assumed the sections are only nominally cracked due to shrinkage and temperature because no damage has been observed due to the earthquake. We could find little justification for making more complicated section property calculations.

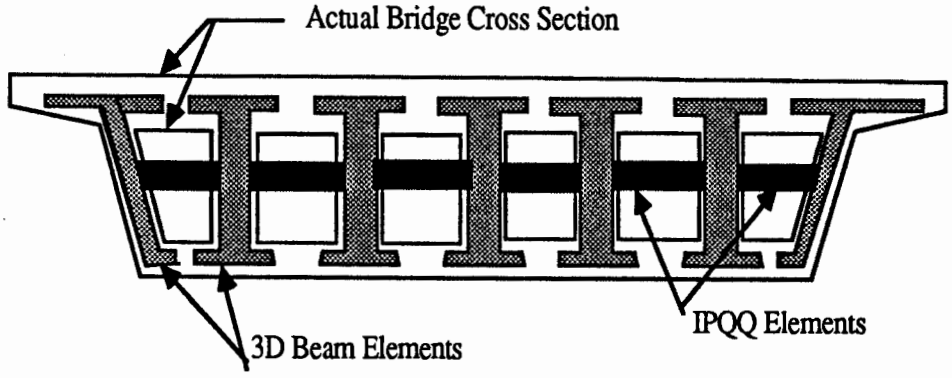

Figure 11 Structural Modeling of Deck in Grid Formulation

Boundary Conditions

Abutment-foundation-backill and pier-foundation interaction springs for use in bridge models have been receiving considerable attention in recent years [5,6,7]. At this point we have not attempted any sophisticated modeling of these interaction influences. In the superstructure we experimented with established spring coefficients for the base of the piers and determined they had little effect on natural frequencies for a range of practical values which tends to be corroborated by the similarity if the measured free field motions with the measured base of pier motions. The most significant boundary condition seems to be clearly the abutment-foundation-backfill condition.

Currently we are assuming the bridge is fixed in all directions at the base of the pier at fixed at the ends of the deck with respect to rotation about all three axes and with respect to translation in the longitudinal and vertical directions. These assumptions, although gross, appear to be reasonable based upon construction conditions and interpretations of the recorded data.

Results

Transverse springs were empirically determined by iteration to yield a computed first transverse period of 0.28 seconds with the relatively sophisticated finite element grid model. Based upon calibrated springs in the transverse direction summing to 39,000 kips/foot the associated first six mode shapes are shown in Figure 12 along with sensor locations. Note that the first vertical mode of 0.36 seconds agrees with the recorded data from sensor 6 while the sixth mode of 0.16 seconds appears to be the mode for by inspecting sensor 8 at about 0.14 seconds. The modes at 0.21 and 0.24 seconds are also visible in the PSD plots for sensors 6 and 8. It appears the finite element model with the calibrated abutment springs in the transverse springs yields a model capable of capturing the essential dynamics of the earthquake response. Much remains to be done!

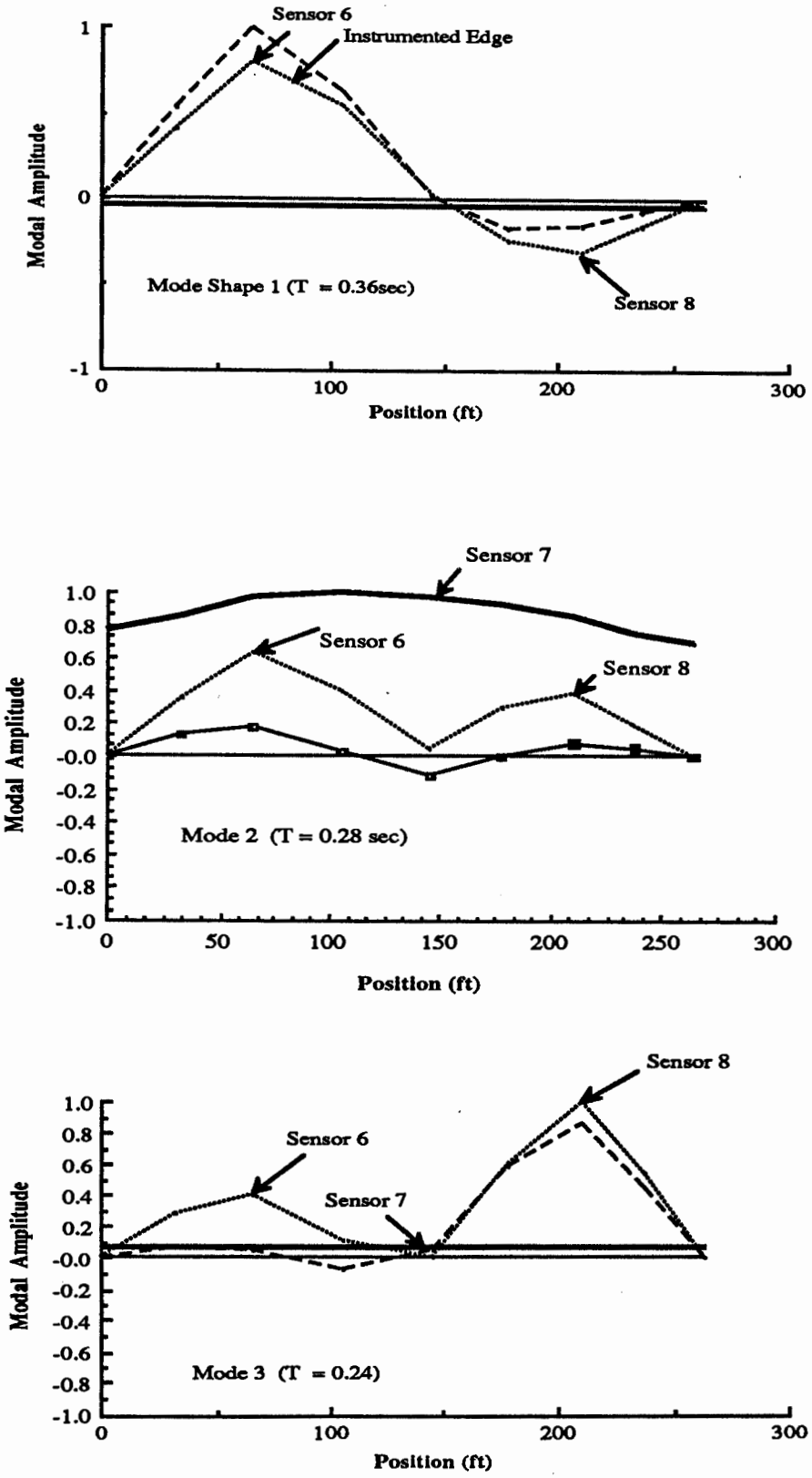

Figure 12 Computed Mode Shapes Using Finite Element Grid Model

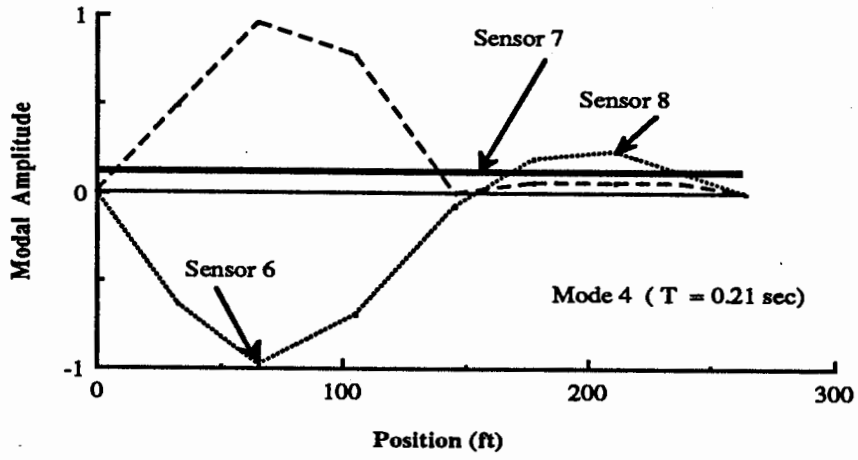

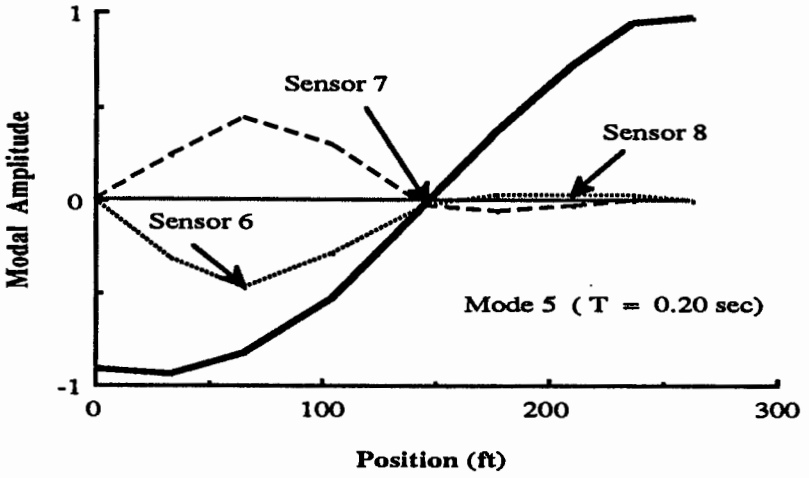

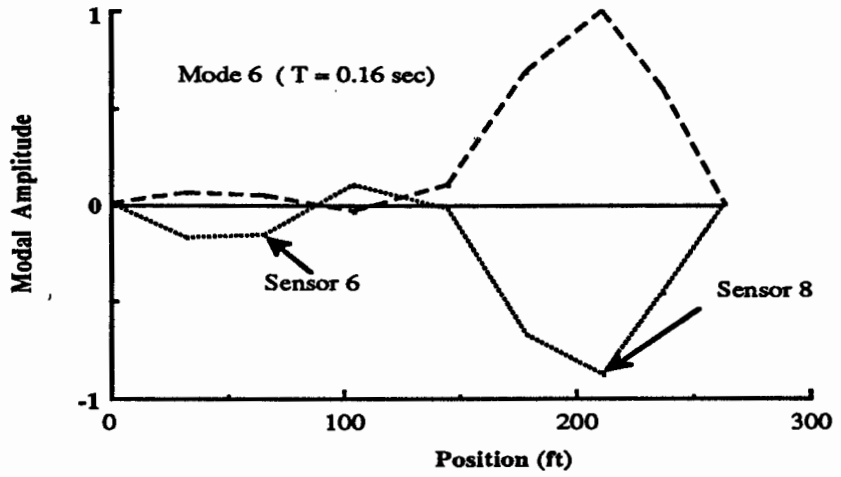

Figure 12 Computed Mode Shapes Using Finite Element Grid Model

Building Vibration Characteristics From Recorded Data

Gerard C. Pardoen
Professor, Civil Engineering
University of California, Irvine

Abstract

This research project is devoted to interpreting the earthquake time history response records of three buildings that experienced strong motion during two recent Southern California temblors. The earthquake response interpretation has been aided by the information obtained from the ambient vibration tests of these buildings as well as developing a linear finite element model of each structural system. In addition some cursory building response results have been gleaned from the spreadsheet analyses of these earthquake records. The buildings and the earthquake records include:

a) Palm Springs Desert Hospital - Roof level excitation of 0.62g was recorded during the 8 July 1986 Palm Springs earthquake.

b) Burbank Pacific Manor - Roof level excitation of 0.54g was recorded during the 1 October 1987 Whittier Narrows earthquake.

c) UCLA Math-Science Building - Roof level excitation of 0.14g was recorded during the 1 October 1987 Whittier Narrows earthquake.

Building Descriptions

Some of the more significant details of each building include:

a) Palm Springs Desert Hospital - This 4 story, 126' x 78' rectangular building has a steel frame for its lateral force resisting system whereas the vertical load carrying system consists of 4"-5" reinforced concrete slabs supported by the steel frame. An elevation and plan sketch of the sensor locations are shown in Figure 1 [1]. Sensor 2 along the south roof wall experienced a peak acceleration of 0.62g whereas sensors 3 and 4 experienced 0.45g and 0.34g motions respectively. A recent site visit noted significant cracks in the basement walls which were attributed to the '86 earthquake.

b) Burbank Pacific Manor - This 10 story, 215' x 75' rectangular residence hall has pre-cast concrete shear walls in both directions for its lateral force resisting system whereas the vertical load carrying system consists of pre-cast and poured-in-place concrete floor slabs supported by pre-cast concrete bearing walls. An elevation and plan sketch of the sensor locations are shown in Figure 2 [2]. Note the plethora of shear walls in the two lateral directions. Sensor 10, located in the middle of the roof and oriented in the longitudinal direction, experienced a peak acceleration of 0.54g whereas the other roof accelerometers,

sensors 2 and 3, experienced 0.33g and 0.34g motions respectively in the transverse direction.

c) UCLA Math-Science Building - This 5 story, 60' x 48' office/classroom addition to the Math-Science building has been the object of several prior experimental and analytical studies [3,4]. The lateral force resisting system consists of a 2 bay by 3 bay moment resisting frame that was added to the roof of an existing two story nuclear reactor building back in 1968. An elevation and plan sketch of the sensor locations are shown in Figure 3 [2]. Sensors 10 and 12 recorded, respectively, 0.14g and 0.11g at the roof level in the N/S direction whereas sensor 11, located in the middle of the roof and oriented in the E/W direction, recorded a peak acceleration of 0.05g.

Ambient Vibration Tests

Ambient vibration surveys represent a relatively inexpensive and rapid means of determining the modal properties of existing structures under low level excitation. The surveys can be used to "calibrate" linear, elastic analytical models as well as to obtain estimates of damping. These surveys are particularly straightforward and meaningful when one "taps" into the in-situ instrumentation network that CDMG has installed in a number of existing structures. Typically the sensors in these buildings have been placed at the most significant vibration locations and, most importantly, the tests can be conducted in an extremely low profile manner so as to provide minimum disruption to the building's occupants.

Such was the case in conducting the ambient vibration tests of the three candidate buildings. Whereas one can normally obtain reasonable information from a single channel recorder, a simple two channel analyzer affords one the opportunity to perform comparison studies such as in-phase and out-of-phase relationships. UCI has been fortunate in that over the last several months the research team has conducted over a dozen field vibration tests (forced and ambient) using its HP 3565 18-channel data acquisition/data reduction system. This prior field experience reduced the "exposure" time within each of the three buildings since most, if not all, strong motion channels could be recorded simultaneously. The HP 3565 system consists of two mainframes that house the input modules for data acquisition, an HP 9000/350 UNIX-based workstation that controls the data acquisition process, and associated peripherals such as plotters, printers, and disk/tape drives. Two experienced people and a pickup truck were sufficient to conduct the ambient vibration tests with the HP 3565.

Whereas the entire array of strong motion sensors can be recorded simultaneously, the "roof-top ambient vibration survey" [5] has been found to provide reasonable modal estimates particularly if one is attempting to "calibrate" a 3D analytical model with two translational modes and one torsional mode. Consider, for example, the roof-top ambient vibration measurements

of the Palm Springs Desert Hospital shown in Figure 4. Clearly the common peak at 2.44 Hz for sensors 2 and 3 denotes a transverse mode whereas the peak corresponding to 2.75 Hz only in the sensor 2 response denotes a torsion frequency. Furthermore the single peak at 2.00 Hz from the sensor 10 measurement denotes the longitudinal fundamental frequency. Similar results for the Burbank Pacific Manor and the UCLA Math-Science Building were obtained.

A satellite calculation of the "roof-top ambient vibration survey" provides a means of determining the center of rigidity using ambient or earthquake recordings [6]. A center of rigidity estimate for the Burbank Pacific Manor was obtained from the autospectrums of sensors 2 and 3 (Saa(f), Sbb(f)) as well as their cross-spectrum (Sab(f)). The procedure assumes that the coherence between the translational and torsional motion is a minimum at the center of rigidity. Since the center of rigidity is not known, then one can express the coherence of the translational-torsional motion in terms of the measured auto- and cross-spectra as well as a non-dimensional length parameter $\underline{L}$ such that

$$|G(f)|^2 = p(\underline{L})Sab(f)\overline{Sab}(f)/[q(\underline{L})Saa(f)r(\underline{L})Sbb(f)] \qquad (1)$$

Here G(f) is the coherence function and $p(\underline{L})$, $q(\underline{L})$, and $r(\underline{L})$ are polynomial expressions (well, sort of) of the unknown non-dimensional length parameter. $\underline{L}$ is defined as the ratio of the center of rigidity distance from sensor 2 to the distance between the sensors. To eliminate a frequency dependent form of $\underline{L}$, the coherence function is integrated over the measurement frequencies to obtain a "coherence length" [6]. The center of rigidity is obtained from a curve such as the one shown in Figure 5 which depicts the coherence length versus $\underline{L}$. The curve's minimum corresponds to the location where the transverse and torsional vibrations have the least coherence.

Analytical Models

An ETABS model [7] of each building has been developed in order to predict the linear elastic response of these structure's to the earthquake ground motion recorded during the event. There are at least three obvious flaws in this procedure. First, the procedure uses the ground motion measured in the building rather than a free field set of records so that soil-structure interaction effects are ignored. Secondly, the linear elastic response may be inadequate for those buildings that experience significant structural motion. Lastly, the fundamental assumption within ETABS that the structure has a rigid diaphragm may distort some of the results.

Despite these flaws there is still merit in performing the analytical-earthquake correlation exercise by subjecting the analytical models to the earthquake ground motion and predicting their linear elastic response at strategic locations within the

upper stories. Such studies, albeit linear theory for a potentially nonlinear structure, usually provide some insight into a building's response. Although ETABS provides the time history motion at the center of mass, the motion at key CDMG accelerometer locations within each building are determined by a post-processing calculation. This analytical effort is being conducted for each of the project's three buildings and is not yet concluded.

The elastic response issue of each building's recorded motion is being investigated from a restoring force-relative displacement diagram [8,9] of a SDOF oscillator. Consider a typical multistory building as shown in Figure 6. If one assumes that the relationship between the relative displacement of the building's roof acceleration ($\ddot{x}$) and the ground acceleration ($\ddot{z}$) can be represented by a SDOF oscillator, then the equation of motion of the building can be expressed as

$$M\,\ddot{x} + F(x,\dot{x}) = -M\,\ddot{z} \qquad (2)$$

The $F(x,\dot{x})$ term in Equation (2) represents the restoring force due to the relative displacement (x) and relative velocity ($\dot{x}$) whereas M is an equivalent mass. Note that the generic form of $F(x,\dot{x})$ can permit a linear or nonlinear restoring force. Equation (2) is founded on the assumption that normally the first mode dominates the earthquake time history response of a building. Alternative forms of Equation (2) are

$$F(x,\dot{x}) = -M\,(\ddot{x} + \ddot{z}) = -M\,\ddot{y} \qquad (3)$$

$$F(x,\dot{x}) / M = -\ddot{y} \qquad (4)$$

Since CDMG provides records of $\ddot{x}$ and $\ddot{z}$ as well as the integrated displacement time histories, then it is a relatively routine matter to "import" these data into a spreadsheet for subsequent analysis. For instance, one need only "import" three records from the processed CDMG Volume 2 data into columnar format of a spreadsheet in order to construct a restoring force-relative displacement diagram; the required data include: (1) roof level acceleration, (2) roof level displacement, (3) ground level displacement. A spreadsheet could form a 4th column of data that is the opposite sign of the roof level acceleration whereas a 5th column would provide the difference between the roof and ground level displacements. A spreadsheet plot of the column 4 data versus the column 5 data thus provides a restoring force-relative displacement curve. Consider, for example, the restoring force-relative displacement diagram for the Palm Springs Desert Hospital shown in Figure 7. Despite the significant 0.62g accelerations experienced at the roof, one could conclude that the hospital's earthquake response was nearly linear with little damping. It should be noted that some earthquake records may have to be filtered in order to eliminate the effects of higher mode frequencies.

Conclusions

Definitive conclusions about the specific earthquake interpretation of all three buildings must wait until the project concludes in the next three months. However, the thrust of the earthquake record interpretation study to date has led the project team to make the following assumptions:

(1) structural engineers might be more inclined to "fiddle" with the CDMG Volume 2&3 data if it could be easily manipulated,

(2) structural engineers usually have access to an AT-class microcomputer for running ETABS and a LOTUS 1-2-3 type spreadsheet.

Given that the CDMG Volume 2&3 data **is** provided in a convenient microcomputer format, then some natural by-products of the current investigation will be public domain software that will enable others to process the earthquake records in much the same manner as reported herein. Calculations such as restoring force-relative displacement curves, relative displacements within a floor to check diaphragm rigidity, center of rigidity estimates, etc. can be performed by others from the Volume 2&3 data.

A provocative recommendation, that others will certainly disagree with, is that an ETABS model should developed for all ETABS-applicable, instrumented buildings within the SMIP network. Even though a building's response might be inelastic or that ETABS rigid diaphragm assumption might be violated, there is some merit in having a 3D elastic model - no matter how inappropriate it might be for a given study - that others could use directly or modify to suit their own needs. The development of such an ETABS model database could be done on a voluntary basis (read free) by those practitioners and researchers interested in advancing the state of SMIP's data dissemination program. The voluntary ETABS model development could be accomplished by assigning 1 building/per year to those consulting firms and universities willing to participate. The database would include an ETABS input and output file on floppy diskette format as well as a 4-5 page standard format report that identifies the modeling characteristics and unusual assumptions.

References

1. "CSMIP Strong-Motion Records from the Palm Springs, California Earthquake of 8 July 1986", Ca. Dept. of Conservation, Div. of Mines & Geology, Office of Strong Motion, Report OSMS 86-05, 1986.

2. "CSMIP Strong-Motion Records from the Whittier, California Earthquake of 1 October 1987", Ca. Dept. of Conservation, Div. of Mines & Geology, Office of Strong Motion, Report OSMS 87-07, 1987.

3. Shanman, R.D., "A Forced Vibration Study of a Completed Five Story Steel Frame Building", MS Thesis, Department of Engineering, UCLA, 1969.

4. Bunce, B.T., "Two and Three-Dimensional Modeling and Dynamic Analysis of the Five Story Math-Science Addition", MS Thesis, Department of Engineering, UCLA, June 1970.

5. Diehl, J.G.,"Roof-Top Ambient Vibration Measurements", Proceedings of the 3rd US National Conference on Earthquake Engineering, Charleston,SC, 1986, pp 1,575-1,585.

6. Safak, E., Celebi, M.,"A Method to Estimate Center of Rigidity Using Vibration Recordings", Submitted for publication in the ASCE Structural Division Journal

7. Wilson, E.L., Hollings,J.P, Dovey,H.H.,"Three-Dimensional Analysis of Building Systems (Extended Version)", EERC-75-13, April 1975, University of California, Berkeley, California

8. McVerry, G.H., Beck, J.L., Jennings, P.C., "Identification of Linear Structural Models From Earthquake Records", Proceedings of the 2nd US National Conference on Earthquake Engineering, Stanford,CA, 1979, pp 515-524.

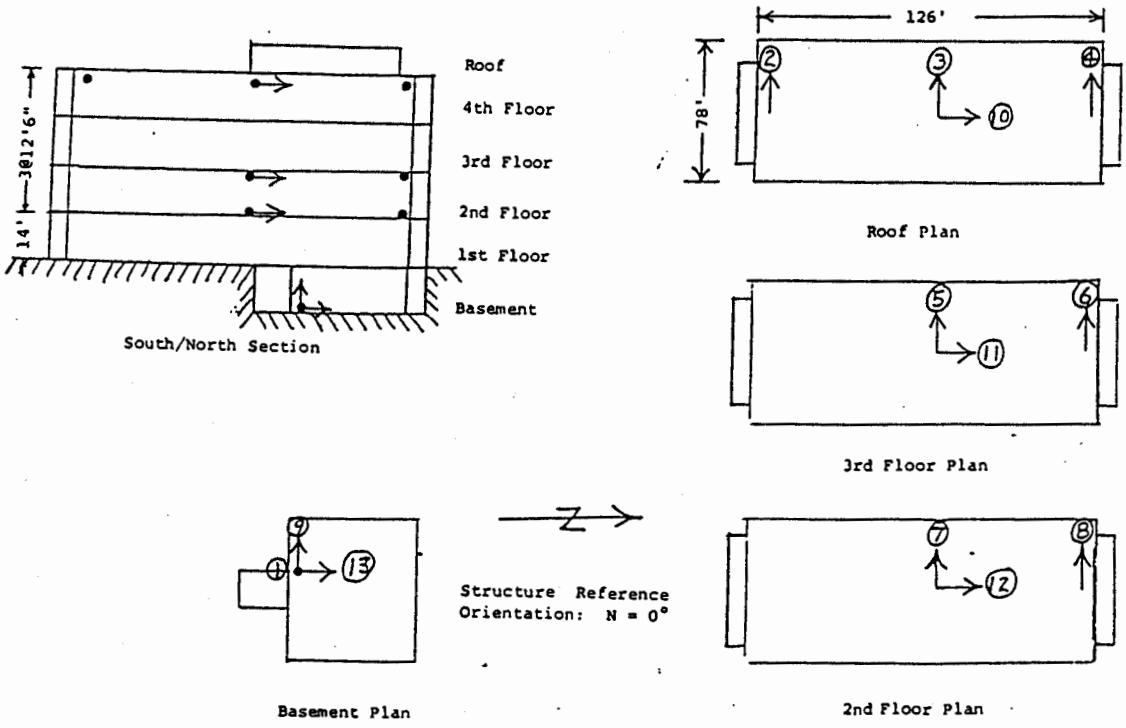

Figure 1 - Sensor Locations @ Palm Springs Desert Hospital

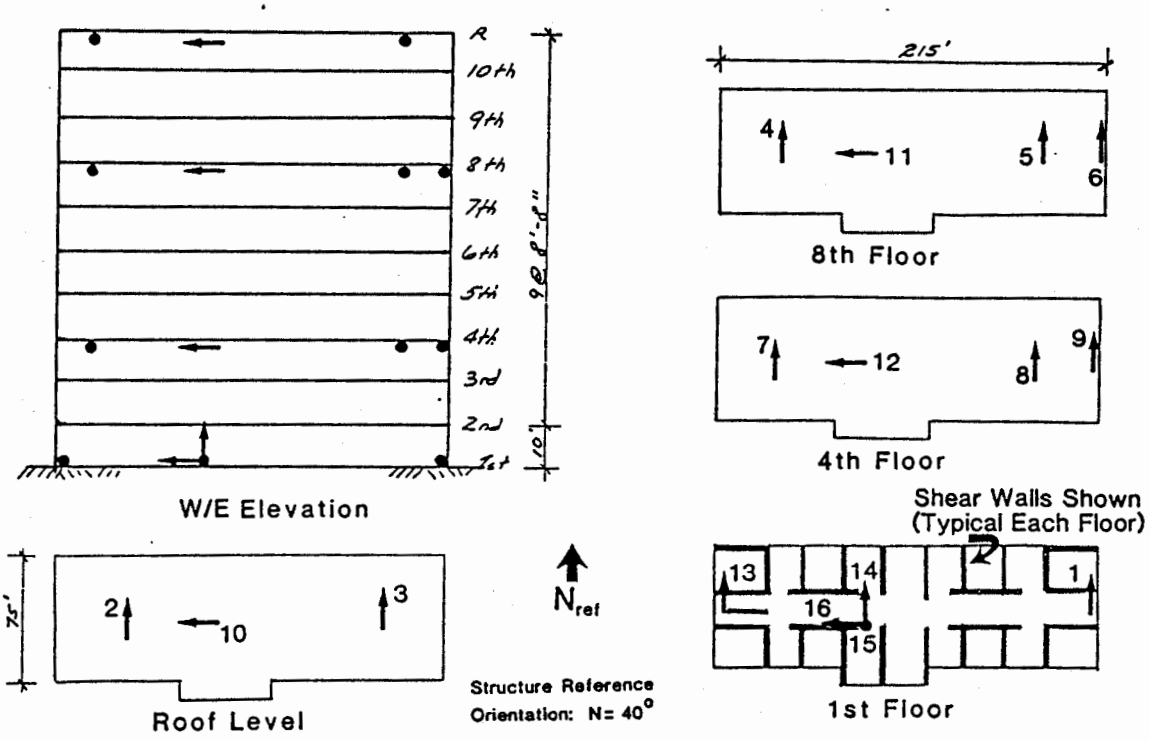

Figure 2 - Sensor Locations @ Burbank Pacific Manor

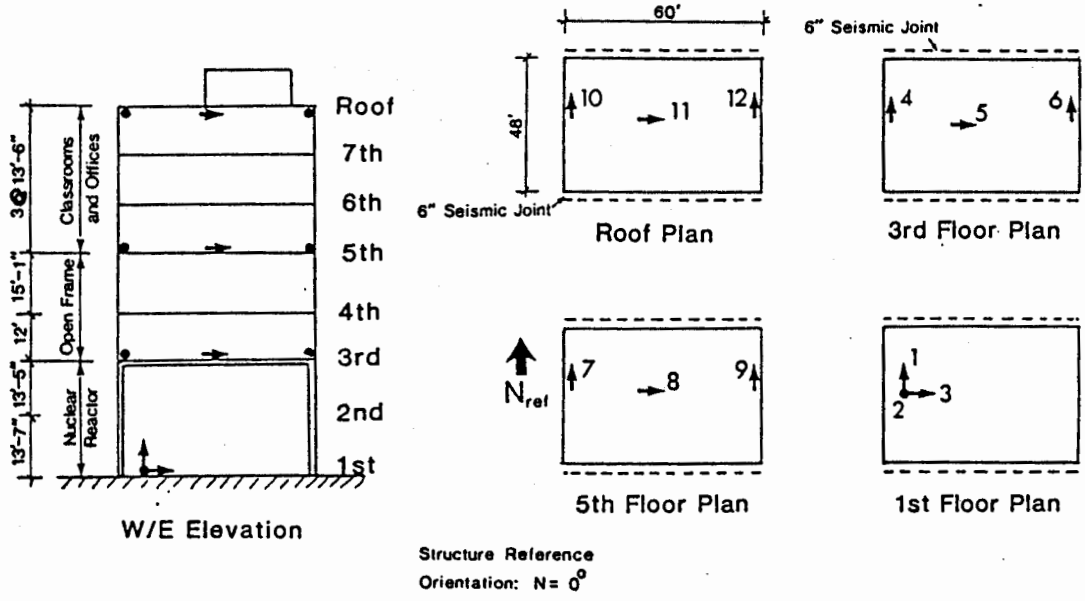

Figure 3 - Sensor Locations @ UCLA Math/Science Building

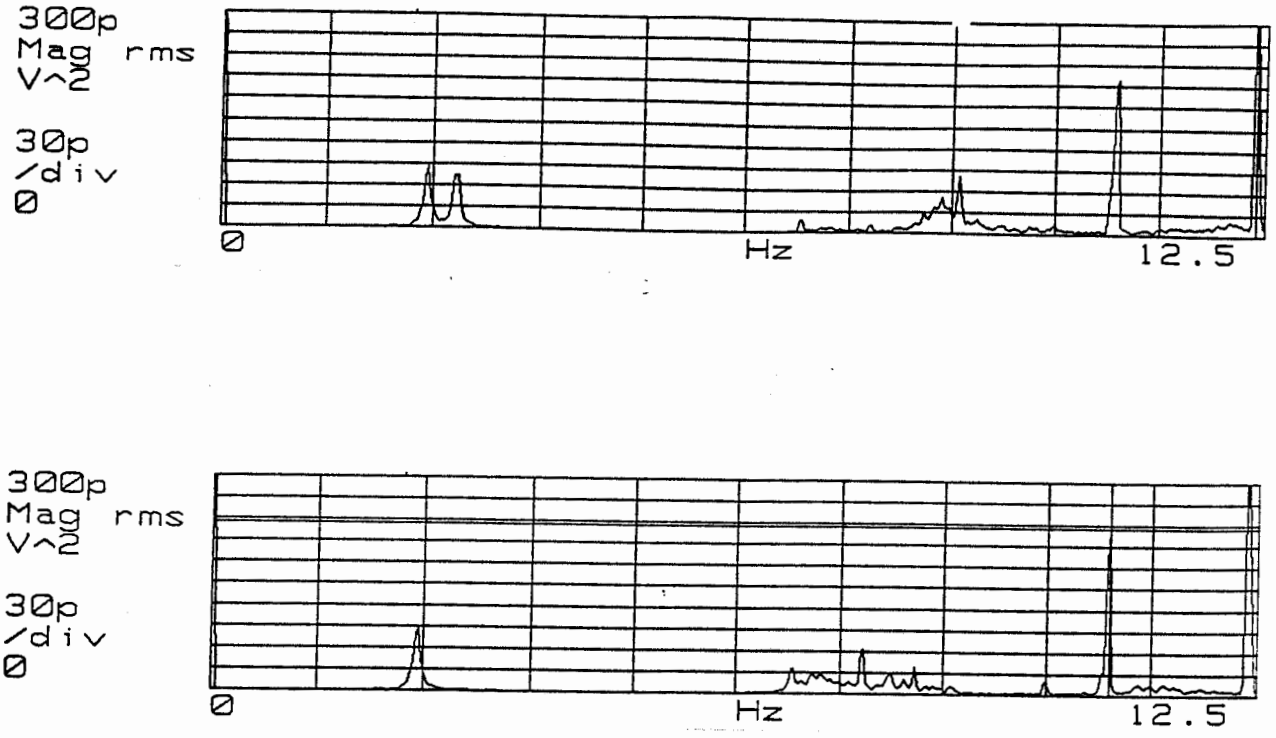

Figure 4a - AVS of Palm Springs Desert Hospital
(Top: E/W Sensor @ Bldg Edge, Bottom: E/W Sensor @ Bldg Center)

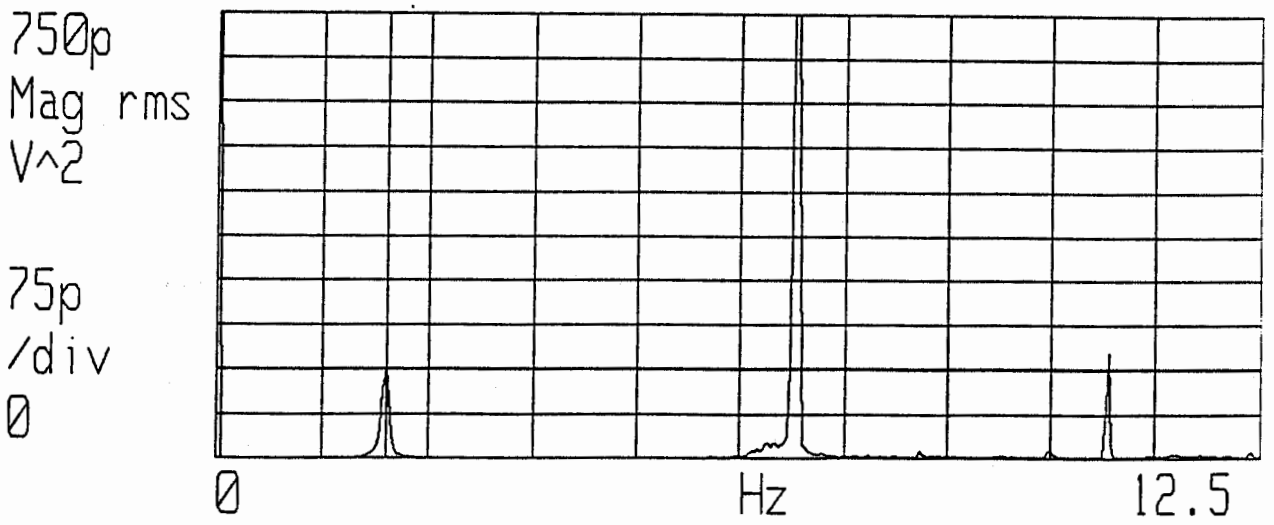

Figure 4b - AVS of Palm Springs Desert Hospital
(N/S Sensor @ Bldg Center)

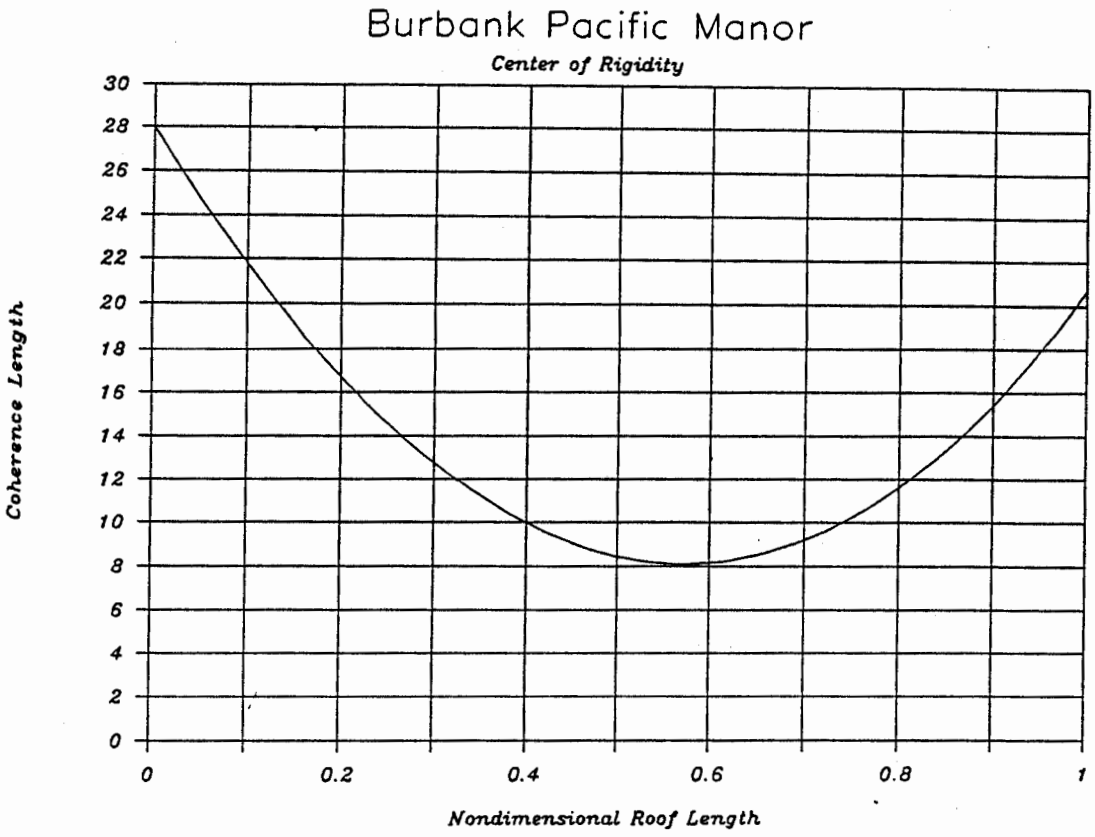

Figure 5 - Burbank Pacific Manor Center of Rigidity

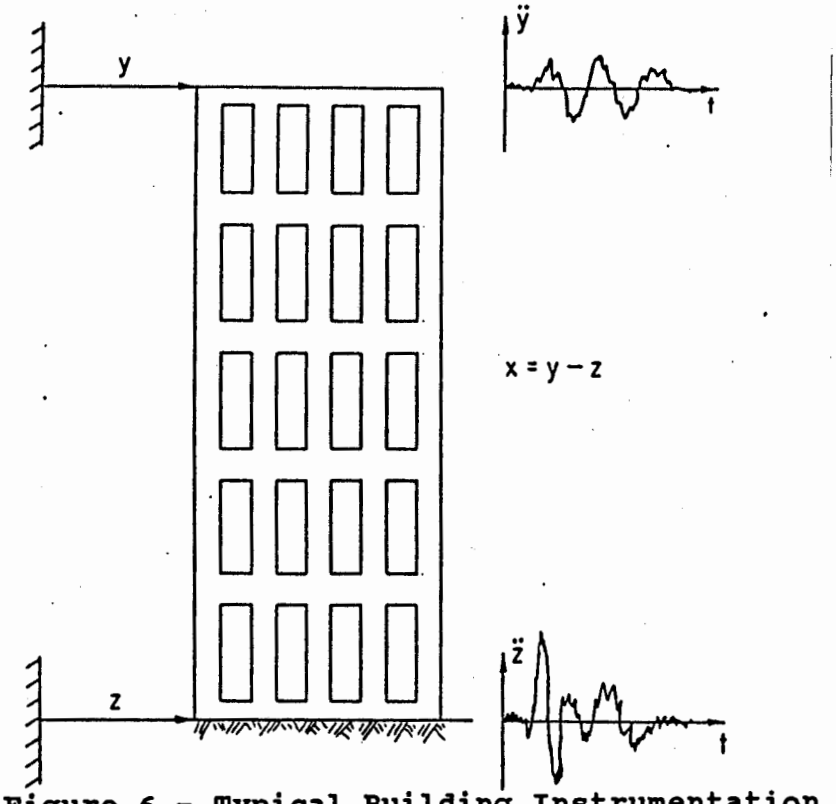

Figure 6 - Typical Building Instrumentation

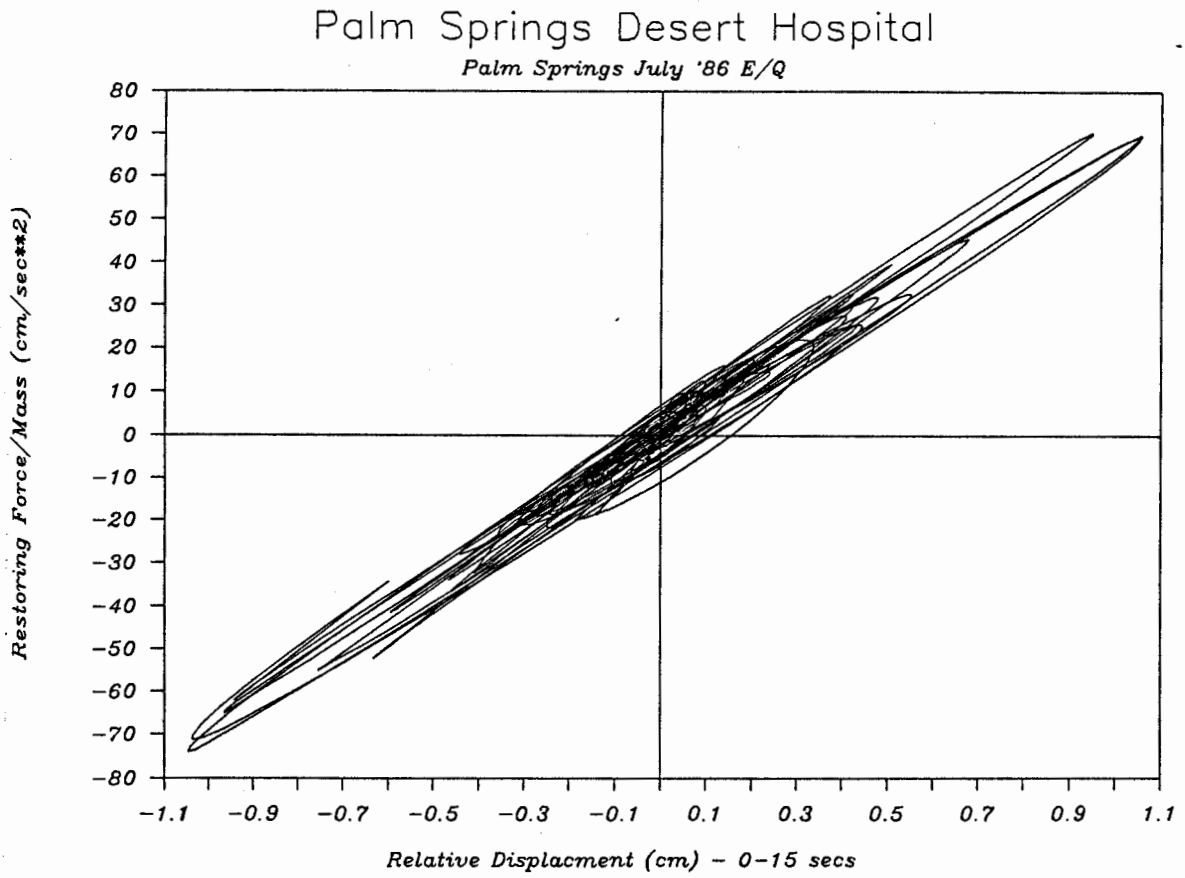

Figure 7 - Palm Springs Desert Hospital
Restoring Force vs Relative Displacement...July '86 E/Q

SOIL-STRUCTURE EFFECTS IN BUILDING RESPONSE

Gregory L. Fenves
Assistant Professor
Department of Civil Engineering
University of California at Berkeley

ABSTRACT

Dynamic interaction between a building-foundation system and the supporting soil can significantly alter the earthquake response of the building depending on the characteristics of the system and the ground motion. The California Strong Motion Instrumentation Program obtained a large number of building response records from the 1 October 1987 Whittier Narrows earthquake. The instrumentation of a 14-story warehouse building included the nearby ground motion. Using this data, this study demonstrates that soil-structure interaction reduces the maximum base shear force in the building.

INTRODUCTION

In the design of building structures to resist earthquake loads or the evaluation of the earthquake response of buildings it is often assumed that the soil supporting the structural system and foundation is rigid. The assumption of a rigid soil does not preclude the use of site dependent ground motion or spectra for input into the building to represent the important effects of the local soil conditions. Assuming a rigid soil, however, neglects the dynamic interaction between a structure-foundation system and the underlying soil. Soil-structure interaction further modifies the input motion and it can significantly alter the earthquake response of structures.

The Whittier Narrows earthquake of 1 October 1987 generated the largest set of strong ground motion records of building response ever obtained from a single event. The California Strong Motion Instrumentation Program (SMIP) collected records from three buildings that included the motion at a ground station close to each building. The recorded ground motion is an estimate of the free-field ground motion, the motion that would occur at the site if the building was not present. Comparison of the free-field ground motion to the basement and building motion can reveal the extent and importance of soil-structure interaction in the dynamic response of the building, foundation, and soil system. Of the three buildings with a free-field instrument, a 14-story reinforced concrete warehouse building was closest to the epicenter and the one which experienced the largest amplitude response. This set of building and ground motion records offers an important opportunity for studying soil-structure interaction effects in building response during a moderate earthquake.

The purpose of this study is to evaluate the records obtained from the warehouse building for soil-structure interaction effects. The results are compared to the National Earthquake Hazards Reduction Program (NEHRP) recommended building code provisions for soil-structure interaction [3].

EVALUATION OF INTERACTION FROM BUILDING RECORDS

The California Strong Motion Instrumentation Program obtained moderate amplitude response records from three buildings with nearby ground motion stations during the 1 October 1987 Whittier Narrows earthquake [4]. Review of the records show that the response of a warehouse building in Los Angeles had significant soil-structure interaction effects. This paper summarizes the investigation of the interaction effects in the building during the earthquake as interpreted from the strong motion records.

Los Angeles Warehouse Building

The Los Angeles warehouse building has been the subject of several investigations using response data collected during earthquakes in 1933, 1952 (Kern County), and 1971 (San Fernando). Figure 1(a) shows the location of the building in relation to the epicenters of previous earthquakes and the 1987 Whittier Narrows earthquake. The availability of both free-field and building records from earthquakes that occurred in the past fifty years, together with the structure's simple design and isolation from other large buildings, make it suited for the study of soil-structure interaction effects.

Figure 1(b) shows location of the triaxial accelerometer in a small shelter structure in the parking lot, 139 ft west of the warehouse building. This instrument records a ground motion that, due to the distance from the building, should not be affected by the dynamic response of the structure and its interaction with the soil. The record approximately represents the free-field motion that would occur at the site if the building was not present. The parking lot instrument, however, is less than one foundation length away from the building in the longitudinal direction, and it is very likely that its motion is affected by interaction between the building-foundation and the soil. For the purpose of this and most previous studies the assumption is made that the parking lot instrument is the free-field ground motion.

The geometry of the building, which was designed and constructed in 1925, is shown in Fig. 2. It is a fourteen-story, 149 ft tall structure with a rectangular cross section that measures 217 ft in the longitudinal EW direction and 51 ft in the transverse NS direction. The lateral force resisting system consists of reinforced concrete frames in both directions. The two exterior longitudinal frames and the westward transverse frame are infilled with 8 in thick panels. The vertical load carrying system consists of 8 in thick concrete slabs supported by columns on capitals. In the three longitudinal bays on the west side of the building, one-way slabs on joists are supported by the transverse frames. A partial basement is located 9 ft below the ground level. The foundation consists of reinforced concrete footings on Raymond concrete piles which vary in depth from 12 ft beneath the footings at the end of the building to about 30 ft near the center.

Data about the soil characteristics at the site of the warehouse building are given in Ref. 2. A soil boring to a depth of 300 ft shows that the building is founded on an approximately 100 ft deep layer of soft, sandy clay. The measured P-wave velocity has a nearly constant value of 2400 ft/s within the layer, except in the superficial shallow stratum of clay loam where it is 1090 ft/s. The sandy clay layer is underlaid by approximately 7000 ft of sedimentary formations, which in turn rests on slate.

The location of the accelerometer sensors installed and maintained in the warehouse building by SMIP are shown in Fig. 3. There are twelve channels in the building and three channels in the parking lot instrument.

To demonstrate that soil-structure interaction was of some importance in this structure during the 1 October 1987 Whittier Narrows earthquake, the maximum acceleration response spectra computed from the corrected and processed records from the parking lot instrument and the basement are shown in Fig. 4. In both directions there is a difference in response in the very short period range. The reduction in basement response compared to the parking lot results from kinematic interaction where the foundation tends to average the effect of the the very short period waves. Of more interest is the difference in response near the fundamental vibration period. In the transverse direction, the fundamental vibration period is 1.9 sec. At this period there is almost no difference in the spectra for the parking lot and basement indicating essentially no change in motion from soil-structure interaction. In the longitudinal direction, the fundamental vibration period is 0.62 sec. The response spectrum for the basement is significantly less than the spectrum ordinate for the parking lot indicating a reduction in basement response because of soil-structure interaction.

Methodology for Evaluation

This study addresses the following question: what is the importance of soil-structure interaction in the engineering design of lateral force resisting systems in buildings? The objective of the study is to determine the lateral forces developed in the warehouse building including soil-structure interaction compared to the lateral forces that would develop if the soil is assumed rigid and interaction effects are neglected. The force quantity of interest is the maximum base shear that occurs during an earthquake.

Although the sensors shown in Fig. 3 give the overall translational and torsional response of the building they are insufficient for determining soil-structure interaction effects. The reasons are:

- There are insufficient acceleration data to compute the inertial forces and hence the lateral forces and shear force at the base of the building.
- It is impossible to determine the response of the building if interaction effects did *not* occur during the earthquake response.

Given these limitations in the available data the following methodology for determining the effects of soil-structure interaction in the warehouse building was adopted:

- Develop a three-dimensional mathematical model of the building superstructure to determine the fixed base vibration properties.
- Use the fixed base vibration properties in a complete model of the building, foundation, and soil in each translational direction.

- Select parameters for the model of the building-foundation-soil system to correlate the model response with the response recorded during the earthquake.

- Compute the response of the building-foundation-soil model including and neglecting the effects of interaction.

A linear, elastic model of the building and soil are assumed in this analysis. This is justified because the moderate earthquake did not result in observed damage of the warehouse. Using this methodology the conclusions on the effects of soil-structure interaction are determined from the building-foundation-soil model which is calibrated to the actual response given by the strong motion records.

Mathematical Model

The fixed base vibration properties of the warehouse building were obtained from the three-dimensional mathematical model shown in Fig. 5(a). The vibration modes and periods were verified using forced vibration data for the building and analysis of response from previous earthquakes. Because the available vibration data includes soil-structure interaction effects an iterative procedure was used to determine the vibration periods of the building on fixed base. In the iterative procedure, a shear wave velocity for the soil of 1190 ft/sec was selected based on the soil data and an estimate of the strain level during the earthquake. The fixed base modes are summarized in Table 1.

The model of the building-foundation-soil system is shown in Fig. 5(b). The model includes motion of the building in each translational direction independently. Torsional effects are not included which is justified because of the near symmetry of the warehouse building. The model of the complete system closely follows the soil-structure interaction analysis procedure presented in Ref. 1. The building is represented by the fixed base vibration modes of the structure which were obtained in the previous step. The foundation-soil system is characterized by frequency-dependent impedance functions that represent the stiffness and energy dissipation characteristics of the foundation and soil. The input motion is the free-field ground motion assuming to occur from vertically propagating shear waves in the soil.

The foundation in the model is assumed to be a rigid circular disk on the surface of the soil [6]. The soil is a homogeneous viscoelastic material extending to infinity below the surface. In addition to the flexibility of the soil, the model represents the material damping that occurs in soil through the viscoelastic properties. The semi-infinite extent of the soil represents the energy radiation that occurs due to waves propagating away from the structure.

The vibration periods in the two translational directions used in the response analysis are given in Table 2. Three vibration modes are used in the transverse direction and two modes in the longitudinal direction. Soil-structure interaction always lengthens the vibration periods because of the flexibility of the soil. The amount of period lengthening depends on the relative stiffness of the building compared to the stiffness of the soil. In the warehouse building the effects of interaction are more pronounced in the longitudinal than in the transverse direction. This difference occurs because

the soil is relatively stiff and the flexible transverse frames do not develop large enough base shear and overturning moment to produce significant deformation of the soil. In the longitudinal direction, however, the much stiffer frame and panels develop sufficient base forces to deform the soil.

INTERPRETATION OF RESPONSE RESULTS

After evaluating the vibration properties of the building and soil system, two important parameters of the system must be determined: the damping ratios for the vibration modes in the building and the material damping ratio for the soil. The material damping factor for the soil was assumed to be 0.20 based on an estimate of the strain level and guidelines for sandy clay soils.

The viscous damping ratios for the vibration modes of the building were determined by comparing the frequency response of the system during the 1987 Whittier Narrows earthquake (as given by the processed data from SMIP) and the frequency response of the building-foundation-soil model. The frequency response used in the comparison is the transfer (or transmissibility) function from the free-field and basement to the floors of the building with response records. The transfer function is for total acceleration. Matching the peaks of the transfer functions from the recorded response and the model response gives a viscous damping ratio in the transverse modes of 3.5% and in the longitudinal modes 8.0%.

Figure 6 shows the comparison of the recorded and model transfer function between the free-field and several story levels in the transverse direction. The comparison is excellent. Figure 7 shows the comparison of the recorded and model transfer functions between the basement and several story levels in the longitudinal direction. The comparison is very good indicating that the vibration properties in the transverse direction are well represented.

The comparison of the transfer function between the free-field and several stories in the longitudinal direction is shown in Fig. 8. Here the comparison is not as good. The difficulty in capturing the response of the complete system in the longitudinal direction arises from two sources. The first is that there is some rigid-body torsional motion of the building and foundation that appears as an amplified peak in the transfer function. This cannot be represented in the translational model used in the study. The second major source of the discrepancy is that the parking lot motion is probably not really the free-field ground motion. There appears to be significant coupling between the parking lot and basement instruments because of their proximity compared to the foundation dimensions of the building.

Accepting the comparison, however, as an approximate model of the building-foundation-soil system the maximum base shear of the model is determined by a frequency-domain response analysis using the parking lot records from the 1987 Whittier Narrows earthquake as the free-field ground motion. The maximum base shear obtained from the model is shown in Table 3. In the transverse direction there is little soil-structure interaction, so as expected there is little effect on the base base shear. In the longitudinal direction, the interaction effects are more significant. For this building, soil-structure interaction reduces the maximum base shear by 17%.

CONCLUSIONS

Although there are limitation in the modeling of the system, the response data recorded in the 14 story warehouse building during the 1987 Whittier Narrows earthquake clearly shows that soil-structure interaction reduced the base shear by a significant amount in the longitudinal direction. The concept of base shear reduction is codified in the NEHRP recommendations for soil-structure interaction [3] and in accordance with soil-structure interaction principles [6]. Using the proposed procedure, a 3% reduction in base shear would be allowed in the transverse direction and a 9% reduction in the longitudinal direction.

ACKNOWLEDGEMENTS

The Strong Motion Instrumentation Program (SMIP), External Data Utilization Program, of the California Department of Conservation with Tony Shakal as the Program Manager provided the support for this investigation. Their assistance is greatly appreciated. Graduate research assistant Giorgio Serino offered substantial contributions to the research and this report.

REFERENCES

1. Chopra, A.K., and J.A. Gutierrez, "Earthquake Analysis of Multistory Buildings Including Foundation Interaction," Report No. UCB/EERC-73/13, Earthquake Engineering Research Center, University of California, Berkeley, CA, June, 1973.
2. Duke, C.M., and D.J. Leeds, "Site Characteristics of Southern California Strong-Motion Earthquake Stations," Report No. 62-55, Department of Civil Engineering, University of California, Los Angeles, CA, November, 1962.
3. National Earthquake Hazards Reduction Program, "Recommended Provisions for the Development of Seismic Regulations for New Buildings," Part 1 and 2, FEMA/95, Federal Emergency Management Agency, February, 1986.
4. Shakal, A.F., M.J. Huang, C.E. Ventura, D.L. Parke, T.Q. Cao, R.W. Sherburne, and R. Blazquez, "CSMIP Strong-Motion Records from Whittier, California Earthquake of 1 October 1987," Report No.OSMS 87-05, Office of Strong-Motion Studies, California Strong Motion Instrumentation Program, California Department of Conservation, Sacramento, CA, October, 1987.
5. Veletsos, A.S., "Dynamics of Structure-Foundation Systems," in Structural and Geotechnical Mechanics, edited by W. J. Hall, Prentice Hall, Englewood Cliffs, NJ, 1976, pp. 333-361.
6. Veletsos, A.S., and Y.T. Wei, "Lateral Rocking and Vibration of Footings," Journal of the Soil Mechanics and Foundation Division, ASCE, Vol. 97, September, 1971, pp. 1227-1248.

TABLE 1. Fixed Base Vibration Modes and Periods of 14-Story Warehouse Building

No.	Mode	Period (sec)
1	translational-transverse	1.80
2	torsional	0.88
3	translational-longitudinal	0.58
4	translation-transverse	0.55
8	translational-longitudinal	0.18

TABLE 2. Vibration Periods (in sec) of 14-Story Warehouse Building Neglecting and Including Soil-Structure Interaction

	Transverse Direction		Longitudinal Direction	
	Neglecting	Including	Neglecting	Including
No.	SSI	SSI	SSI	SSI
1	1.80	1.90	0.58	0.62
2	0.55	0.56	0.18	0.19
3	0.29	0.30	—	—

TABLE 3. Maximum Base Shear (in kip) of 14-Story Warehouse Building Neglecting and Including Soil-Structure Interaction

Direction	Neglecting SSI	Including SSI	Change
Transverse	927	924	-0.3%
Longitudinal	4750	3960	-17%

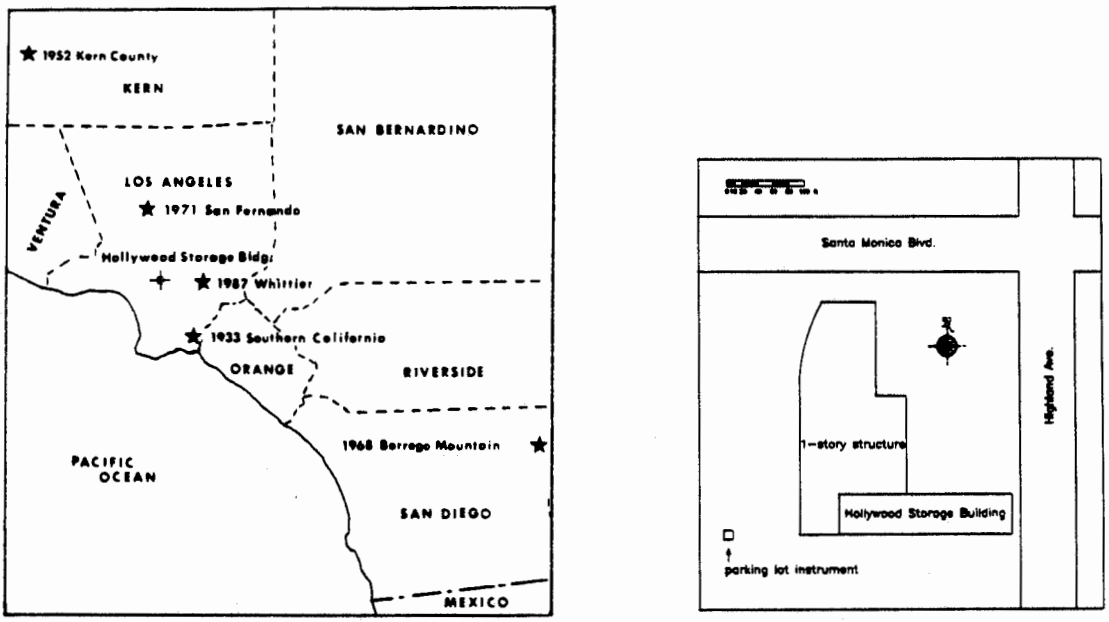

FIGURE 1. Location of 14-Story Warehouse Building. (a) Epicenters of Previous Earthquakes, (b) Location of Sensors in Parking Lot.

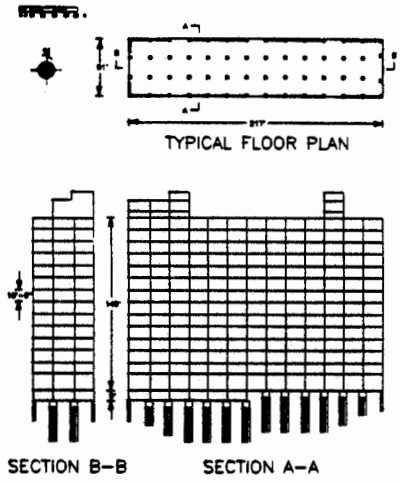

FIGURE 2. Structural System of 14-Story Warehouse Building.

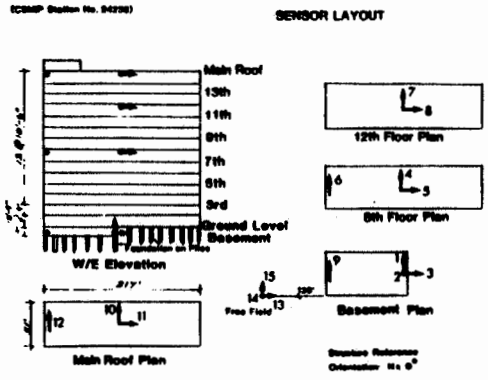

FIGURE 3. Locations of SMIP Accelerometer Sensors [4].

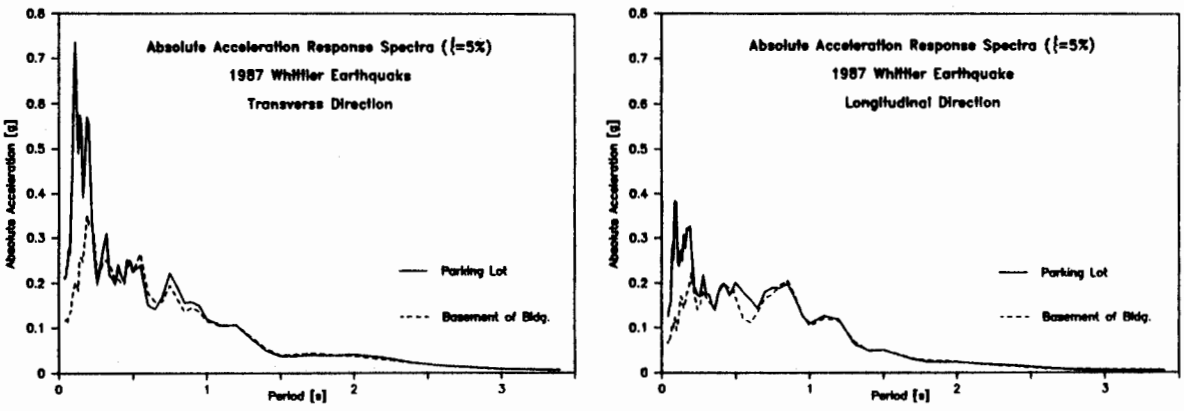

FIGURE 4. Absolute Acceleration Response Spectra for Parking Lot and Basement Records From the 1987 Whittier Narrows Earthquake.

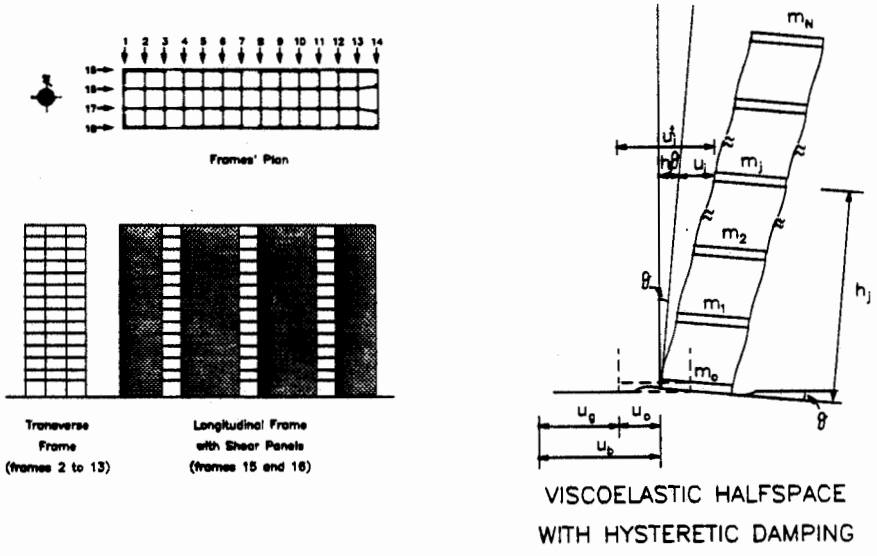

FIGURE 5. Mathematical Model of 14-Story Warehouse Building. (a) Building Superstructure, (b) Building-Foundation-Soil System.

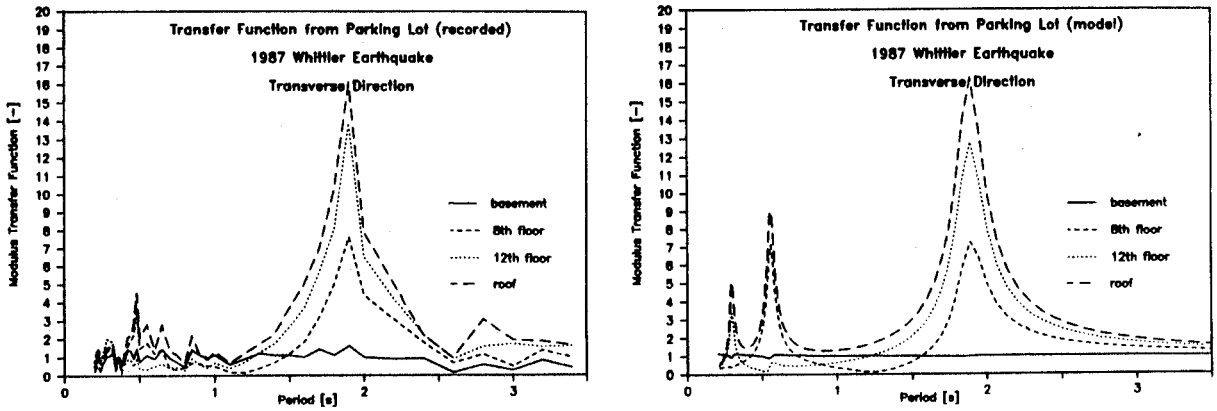

FIGURE 6. Transfer Function Between Free-Field and Story Levels in the Transverse Direction.

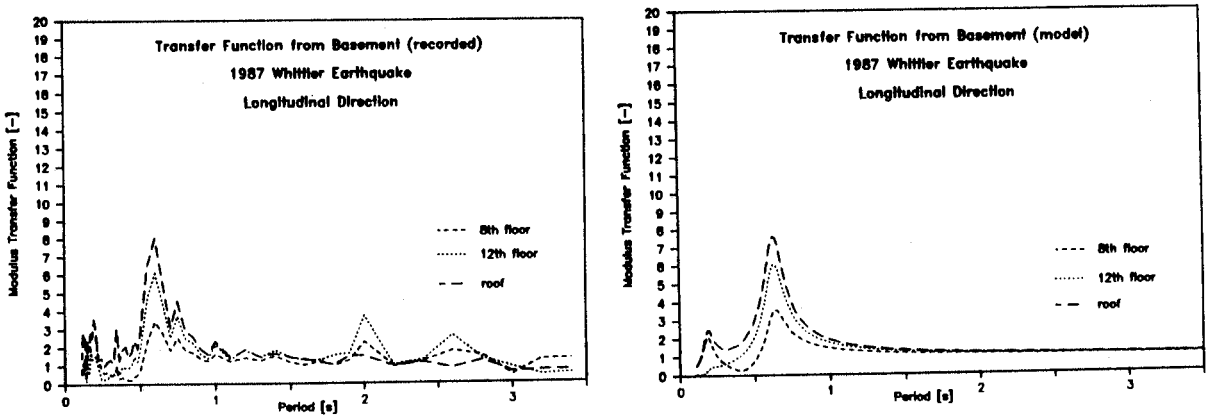

FIGURE 7. Transfer Function Between Basement and Story Levels in the Longitudinal Direction.

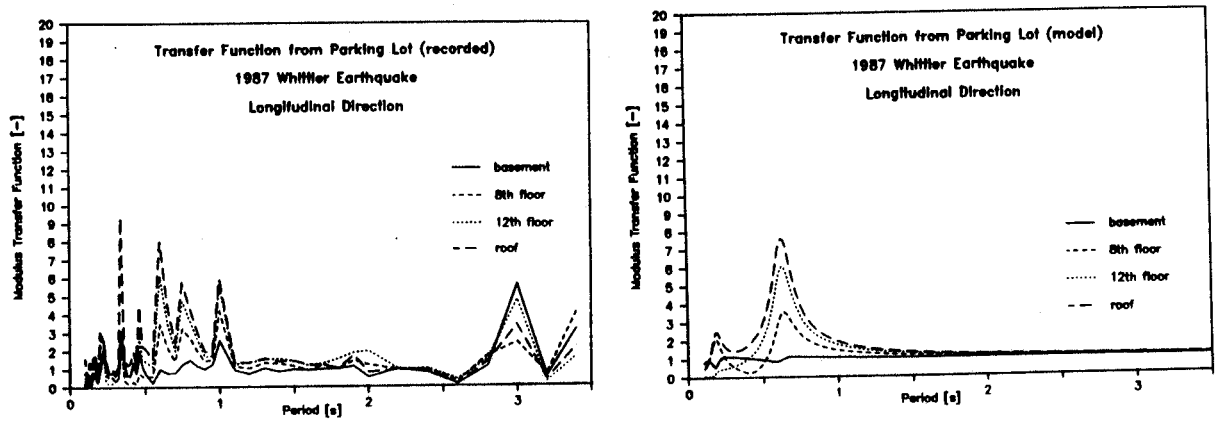

FIGURE 8. Transfer Function Between Free-Field and Story Levels in the Longitudinal Direction.

ENGINEERING INTERPRETATION OF THE RESPONSES OF THREE INSTRUMENTED BUILDINGS IN SAN JOSE

Stephen A. Mahin, Ruben Boroschek and Cristos Zeris
Department of Civil Engineering
University of California, Berkeley

ABSTRACT

The response records obtained in three buildings located in San Jose, California are examined and interpreted in this paper to identify their basic behavioral characteristics and engineering design parameters such as period, damping, and mode shapes. The buildings range in height from 10 to 13 stories. Observations related to the seismic response of different types of structural systems are extracted from this data.

INTRODUCTION

Instrumentation of structures to obtain records of actual seismic response is a essential aspect of improving our understanding of the nature of seismic behavior and increasing the reliability of our design and analysis methods. Ideally, structural response records would be used as part of a integrated investigation in which interpreted records are used along with analytical results and, if damage is observed, experimental data to assess and improve current engineering practices. However, the recorded responses can by themselves provide much valuable information.

In this study, the responses of three buildings subjected to the Morgan Hill earthquake of 24 April, 1984 and the Mt. Lewis earthquake of March 31, 1986 are evaluated based on measured accelerograph records obtained by the Strong Motion Instrumentation Program (SMIP) of the Division of Mines and Geology of the California Department of Conservation. These buildings are located near one another in San Jose, California, about 20 km (12 miles) from the epicenter. These buildings are described in Table 1 and Fig. 1. Additional information on the buildings and the records can be obtained in Refs. 1-3.

No structural analyses were performed as part of this investigation and none of the buildings studied suffered structural damages. None-the-less, important information regarding the basic behavioral characteristics of the structures are developed from the records and information regarding the differences in seismic responses as affected by structural system and earthquake ground motion characteristics is obtained.

BUILDING 1

This ten story residential building (SMIP Station No. 57356) was designed and constructed between 1971 and 1972. The vertical load carrying system consists of a one-way post-tensioned, lightweight concrete, flat slab on reinforced concrete bearing walls. The lateral load resisting system consists of reinforced concrete shear walls. In the transverse (EW) direction these are spaced at regular intervals, while in the longitudinal (NS) direction one of the major walls is terminated at the sixth floor and additional irregularities occur at the ground level. A pile foundation provides support for the building.

TABLE 1 -- BUILDING DATA

Name	Structural System	No. of Stories	Height (ft)	Peak Horiz. Accel. (g) Ground	Building	Max.Amp. Ratio
Building 1	RC Shear Wall	10	96	0.06(0.03)	0.22(0.12)	4.0 (4.1)
Building 2	RC Shear Wall RC Moment Frame	10	124	0.06(0.04)	0.22(0.08)	3.6 (2.7)
Building 3	Steel Moment Frame	13	187	0.04(0.04)	0.17(0.32)	4.9 (7.1)

Note: Numbers in (..) correspond to the Mt. Lewis earthquake

Thirteen analog instruments were installed in the building. These were located to estimate such response features as torsional motions, wall rocking, and in-plane diaphragm deformations. The records used to study this building (as well as all the other buildings considered herein) were reprocessed by SMIP to obtain a signal to noise ratio of approximately 10 to 1. This gives an reliability of about 1.5 cm/sec/sec (0.0015g) and 0.1 cm (0.04 inches) for absolute displacements (and about twice this amount for relative drifts).

Acceleration Response. -- The maximum ground acceleration (Table 1) was 0.06g and the maximum structural acceleration at the roof was 0.22g. The amplification ratios for the various locations in the structure were computed. They were found to be (Table 1) similar for both earthquakes studied, but from 22% to 100% larger in the NS direction than in the EW direction. Some of the processed records obtained during the Morgan Hill earthquake are shown in Fig. 2. These show that the ground motion is characterized by relatively high frequency motions during the first 17 seconds of motion and by much longer period motions during the latter portions of the motion. The acceleration response records indicate that the building is more flexible in the NS direction and suffers higher accelerations in that direction.

Drifts. -- Drifts obtained by subtracting horizontal displacement records from corresponding ground level displacements are quite small, on the same order as the accuracy of the measurements. In general, the drifts in the EW direction are of higher frequency and smaller in amplitude than for the NS direction. Average drifts between the roof and ground in the EW direction never exceeded 0.03% of the building height (less than 6% of the value permitted by the 1985 UBC) and 0.07% for the NS direction (more than twice as much, but still less than 17% of the code value). Some deflected shapes for the building are shown in Fig. 3. The motion of the roof in two directions is plotted in Fig. 4. The total displacement of the structure is nearly twice the relative displacement. It should be noted that the structure is somewhat stiffer in the EW direction, but it achieves several cycles where the maximum displacements are nearly reached simultaneously in both directions.

Inspection of the records indicates that there was little torsion or bowing of the floor slabs. Measured values were near or below the confidence level for the records. Rocking of the walls was estimated using the derived vertical displacement records at the base of the walls. Unfortunately, these values were below the confidence level of the records. Analysis of transfer functions obtained from Fourier amplitude spectra of the corresponding vertical acceleration records indicates that the rocking of the walls contributes

to the response in the transverse direction.

Periods and Mode Shape. -- Due to the low level of response, only the first mode could be identified for each principal direction of the building. Based on visual observation of the records as well as inspection of Fourier amplitude spectra and transfer functions, the estimated periods are summarized in Table 2. No significant differences were detected for the two earthquakes. Uniform Building Code estimates for the building are also shown in the table. These indicate that the 1985 UBC equation incorrectly identifies the NS direction as being stiffer. The equations in the 1988 UBC result in a value lying between the measured values for the two directions when the average period coefficient C_t is taken as 0.02 and conservatively under-estimates both periods by about 30% when the coefficient is computed according to the code.

TABLE 2 -- PERIODS (IN SECONDS) FOR BUILDING 1

Direction	Measured Values	1985 UBC	1988 UBC C_t = 0.02	1988 UBC C_t computed
EW	0.4-0.5	0.59	0.61	0.33
NS	0.6-0.7	0.32	0.61	0.50

Based on the records, the first mode shape for both directions is estimated to be 1.0, 0.4 and 0.0 for the roof, sixth floor and ground. There does appear to be some higher mode influence especially for the NS direction. However, the response is too small to correctly identify this without using system identification procedures.

Damping. -- Equivalent viscous damping coefficients were estimated. Values obtained for the first mode are about 5% for the NS direction and 11 to 14 % for the EW direction. This latter value is considered unreliable due to the low level of response in this direction and soil-structure interaction effects.

Seismic Demands. -- During the Morgan Hill earthquake the building developed a base shear coefficient of 0.096 in the EW direction and 0.1 in the NS direction. Corresponding values for the Mt. Lewis earthquake were 0.05 and 0.04, respectively. The working stress design base shear coefficient was 0.08 and 0.097 for the EW and NS directions, respectively. Thus, the Morgan Hill earthquake corresponded roughly to working stress level event for the design code. The 1985 UBC, however, requires design base shears nearly 2.6 times larger than the original design values. Thus, for a similar building designed according to modern codes, this earthquake corresponds to a very minor earthquake. The shear capacity of the building can be estimated easily using the 1988 UBC. This capacity corresponds to a base shear coefficient in the EW direction of 1.04 and 0.14 for the NS direction. The capacity of the walls in the NS direction are relatively small in comparison with the values for the EW direction, but appear consistent with code requirements. Dynamic analyses of the building would be desirable to better characterize soil structure interaction effects, the effects of discontinuities of the walls in the NS direction and to better estimate the capacity of the building.

BUILDING 2

This commercial/office building (SMIP Station No. 57355) is ten stories

tall with one basement level. It was designed in 1964 and constructed in 1967. The vertical load carrying system consists of light weight reinforced concrete joist floors supported on normal weight concrete frames. The lateral force resisting system consists of reinforced concrete shear walls at the ends of the building in the transverse (EW) direction and moment frames in the longitudinal (NS) direction. The building is supported on a 5 ft. (1.5 m) thick mat foundation. The building was instrumented similar to Building 1.

Acceleration Response. -- As with Building 1 the maximum ground acceleration during the Morgan Hill earthquake was 0.06g and the maximum structural acceleration was 0.22g. The EW direction develops slightly greater accelerations and larger amplification ratios than in the more flexible NS direction. More significant is the fact that the duration of intense motion in the NS direction is substantially longer. Also, it is important to note that the accelerations at the center of the fifth floor diaphragm are about 20% larger than those at the ends for the Morgan Hill earthquake and 100% larger for the Mt. Lewis earthquake, indicating that the diaphragm undergoes important in-plane deformations.

Drifts. -- EW drifts are characterized by low, but nearly constant amplitude, cycles of drift with several cycles between 17 and 20 sec. having more than double the amplitude of the other portions of the record (Fig 5). Drift indices in the EW direction do not exceed 0.06%, approximately one-tenth the value permitted by the code at working stress levels. Analyses of the corrected vertical acceleration and displacement records under the shear wall indicate that nearly 35% of the lateral displacement in the EW direction is associated with rigid body rocking about the base of the wall. In the more flexible NS direction, the response is largest during the latter portions of the record. The deformations correspond to average interstory drift index of only around 0.1%. The structure displaces more in the NS direction, but as with Building 1 there are several major cycles where it develops its maximum displacement in both directions simultaneously (Fig. 4). No significant torsion was detected in the records for this regular symmetric building.

Periods and Mode Shapes. -- The periods estimated for the building are summarized in Table 3. It is interesting to note that the periods for the EW direction roughly obey the rule of thumb for cantilever structures that the higher mode periods vary as 1/6, 1/18, etc. of the fundamental period, while the periods in the NS direction obey the relationships for a shear (frame) building (i.e., 1/3, 1/5, etc. of the fundamental period). Values obtained using the 1985 and 1988 UBC code give values similar to the measured values. However, it is very significant to note that the more refined computation of C_t results overly conservative prediction, in comparison with Building 1.

TABLE 3 -- PERIODS (IN SECONDS) FOR BUILDING 2

Direction	Mode	Measured Values	Quick Guess	1985 UBC	1988 UBC C_t=0.02	1988 UBC Calc. C_t	Computed Ref. 4
EW	1	0.6-0.65	0.63	0.69	0.73	0.36	0.44
	2	0.2-0.25	0.28	--	--	--	0.12
NS	1	0.91-0.96	0.94	1.0	1.1	--	0.74
	2	0.25-0.28	0.31	--	--	--	0.24
	3	0.14-0.18	0.19	--	--	--	0.13
Torsion	1	0.33-0.40	--	--	--	--	--

In the EW direction, the first and second mode shape have the following relative amplitudes at the roof, fifth and basement levels: (1.0, 0.45, 0.0) and (1.0, -1.0, 0.0), respectively. In the NS direction the first, second and third mode shapes have the following ratios for the roof, fifth, second and basement levels: (1.0, 0.5, 0.1, 0.0), (1.0, -1.0, -0.36, 0.0) and (1.0, 0.6, 0.6, 0.0), respectively.

Damping. -- Viscous damping was estimated to be between 3 and 5% in the NS direction and very approximately between 5 and 10% in the EW direction.

Seismic Demands. -- The building developed in the EW direction a base shear coefficient of 0.14 during the Morgan Hill earthquake and 0.05 during the Mt. Lewis earthquake. In the NS direction, it developed base shear coefficients of 0.11 and 0.04, respectively, for the two earthquakes. The values for the Morgan Hill earthquake are 88% larger than the non-factored values used in the original design in the EW direction and 27% larger in the NS direction. The 1988 UBC requires design forces 18% larger than used in the original design for the EW direction, and in the NS direction the base shear coefficient could be lowered by 32%, if a ductile frame were used. The shear capacity of the two shear walls in the EW direction is estimated to be 4700 kips, 34% more than the demanded base shear and 153% more than required in the original design. Additional analyses are desired to assess the influence of soil-structure interaction, bidirectional motion and damping on the response and to better estimate the frame capacity.

BUILDING 3

This building (SMIP Station No. 57357) is a thirteen story office building located approximately 1.5 miles (2 km) north of the other two buildings. It was designed in 1972 and construction was completed in 1976. The vertical load carrying system consists of a concrete slab on metal deck, supported by steel frames. Lateral load resistance is provided by moment resisting frames. Due to special framing around the elevators and nonuniform placement of cladding, the structure is not symmetric and torsional response is expected. A mat foundation is used to support the building.

Twenty two analog instruments were installed and connected to two centralized recording units. Four accelerometers were located horizontally at four floors and three vertical and three horizontal accelerometers were located at the ground level. A free field instrument had been installed, but was removed shortly prior to the Morgan Hill event.

Acceleration Response. -- The input motion to this building was less severe than for the other buildings, but the amplification ratio was higher so the recorded motions were similar or higher than those measured in the other structures. The amplification for the Morgan Hill earthquake was in excess of 5 and that for the Mt. Lewis event was greater than 7. Even more significantly, one can see from Fig. 6 that the structure and ground records have an unusually long duration, more than 80 seconds. This is also true for the Mt. Lewis earthquake. The first thirty seconds of the response exhibits growing response and relatively higher frequencies than in the later portions which are characterized relatively narrow band periodic motion with strong amplitude modulation. This amplitude modulation is similar to mechanical beating of dynamic systems with closely spaced natural frequencies. It is significant to note that the maximum accelerations in the upper levels of the structure are

developed long after the strong motion portion of the ground shaking has ended.

Drifts. -- Maximum drift indices for the building for the Morgan Hill earthquake are on the order of 0.33% and 0.65% for the Mt. Lewis event. The 1985 UBC limited drifts under working stresses to 0.5% and the 1988 UBC uses a limit of 0.4% or, if an R_w factor of 12 were used, of 0.25%. Thus, the drifts experienced by the building were larger than accepted by current design practices for nonfactored design loads. Damages to nonsupported book shelves occurred in the upper levels and some nonstructural damages to partitions were observed in the lower levels. Figure 4 shows that the roof displacements are bidirectional, and that most of the total response is due to the structure, and not the ground as with the other two buildings.

The motion of the building shows the three dimensional interaction of more than three modes. This involves coupled translational and torsional motions. It is complicated by the fact that the modal frequencies are similar leading to a beating or modal interference phenomenon. This is clearly shown for the Mt. Lewis event in Fig. 7 where there is a clear transfer of energy from the NS and EW directions. Simple trigonometric time series can be used to examine this behavior. Summing three series will result in a equivalent natural period and two beating periods. Inspection of the records indicates beating periods of about 100 and 16 seconds and an equivalent period of 2.2 seconds. This results in a system with periods about 2.2, 2.1 and 1.7 seconds. The long duration of the response and the high amplitude of the motion may in significant part be associated with the energy in the system transferring slowly back and forth between the first three modes, and the modes constructively reinforcing one another during portions of the motion. The response also appears to be amplified due to resonance of the building to the dynamic characteristics of the site. The contribution of these factors to the severe motion of the building requires more detailed analysis. Foundation rocking is not important.

The flexibility of the floor diaphragms was investigated by using three of the records obtained at a level to predict the fourth, assuming rigid diaphragm action. Errors between 12% and 24% were detected indicating significant diaphragm flexibility. However, the imprecise location of some of the instruments, noise effects, and the different time bases used for some of the recordings at the same level contribute to this error as well.

Periods and Mode Shapes. -- Period values shown in Table 4 have been estimated. The periods are substantially longer than estimated by either the 1985 or 1988 UBC.

TABLE 4 -- PERIODS (IN SECONDS) FOR BUILDING 3

Direction	Mode	Measured Values	1985 UBC	1988 UBC	Damping %
EW	1	2.15-2.2	1.3	1.77	2-3
NS	2	2.05-2.1	1.3	1.77	3-4
Torsion	3	1.70	--	--	--
EW	4	0.65-0.75	--	--	--
NS	5	0.60-0.70	--	--	--

Damping. -- Due to the interaction of the closely spaced modes, a clear

identification of viscous damping was not possible. An approximate value was obtained by observing the free amplitude decay near the end of response records not significantly influenced by torsion. Estimated values are shown in Table 4.

Comments. -- In view of the complex nature of the three dimensional response, influenced by beating of closely spaced coupled modes, possible soil-structure interaction effects, site amplification, the resistance of cladding and other nonstructural components, it is desirable that a dynamic analysis of this building be carried out. System identification procedures should be utilized to better characterize modal characteristics. A free field instrument should be installed to assist in identifying the relative importance of soil-structure interaction and site effects.

CONCLUSIONS AND RECOMMENDATIONS

The records of the three buildings studied herein have provided significant insight into their dynamic characteristics and the accuracy of various code assumptions. The studies show that the response of buildings is clearly bidirectional and directionally oriented in accordance with their stiffnesses. The behavior of the first two buildings was dominated by the Morgan Hill earthquake while that of the third building was controlled by the less sever Mt. Lewis event. Period calculations using code empirical equations have improved, but additional improvements are desirable. SMIP program data may be indispensable in this effort. The buildings were subjected to levels of excitation consistent with their working stress design basis. No structural damage was thus expected or observed. While much information was obtained in these studies, structural analyses of the buildings are required. Studies are also needed to better assess the confidence that can be place in relative drift and deformation values obtained by manipulation of displacement records derived from processed acceleration records.

ACKNOWLEDGMENTS

Much appreciation is given to the staff of the SMIP, especially for reprocessing the records. Thanks is also given to the SMIP Building Sub-committee and to the Engineers of Record of the buildings studied. The financial support of the Department of Conservation is greatly appreciated. The findings of this study are, however, those of the authors alone.

REFERENCES

1. Boroschek,R., Mahin, S. and Zeris, C., "Engineering Interpretation of Responses of Three Instrumented Buildings in San Jose, California," SMIP Report in preparation.

2. Shakal, A.F. and Huang, M. J., "Torsional Response of Three Instrumented Buildings during the 1984 Morgan Hill Earthquake, 3rd USNCEE, 1986.

3. SMIP, "Processed Data from the Strong motion Records of the Morgan Hill Earthquake," Part II, OSMS-85-05, 1985.

4. ATC, "An Evaluation of a Response Spectrum Approach to Seismic Design of Buildings," 1974.

Building 3

CSMIP Station No. 57357

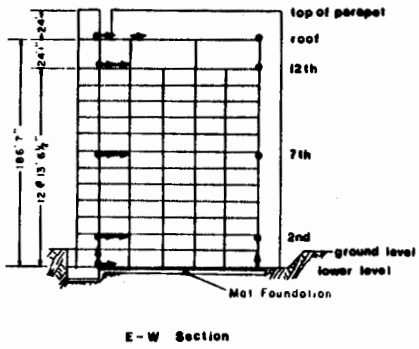

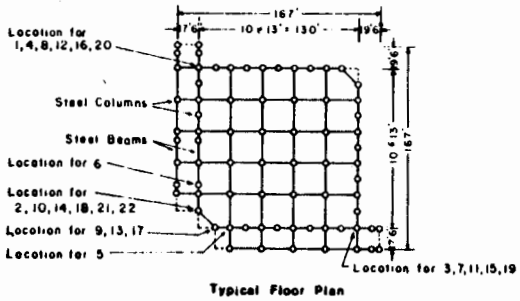

Building 1

CSMIP Station No. 57356

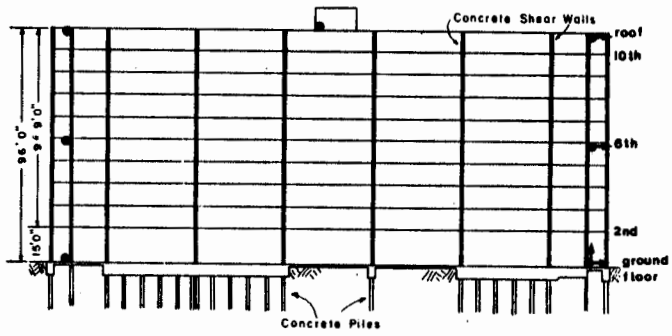

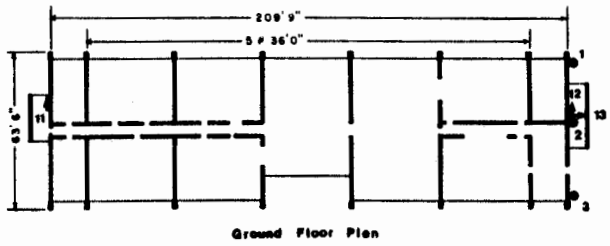

Building 2

CSMIP Station No. 57355

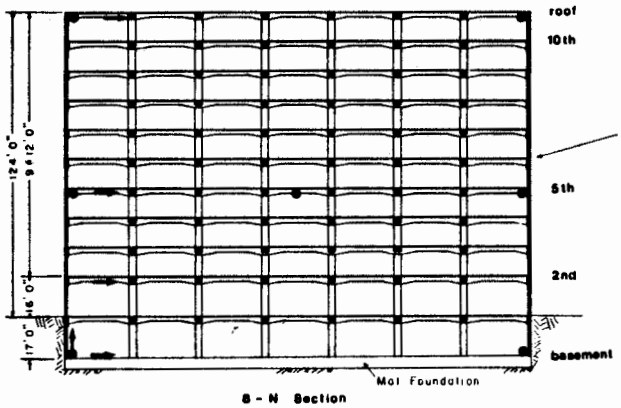

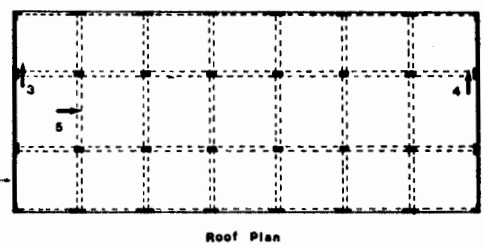

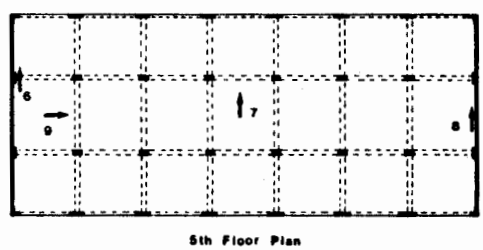

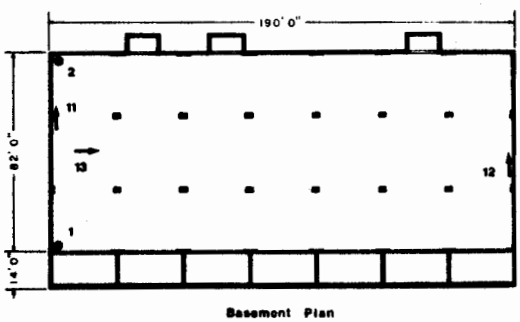

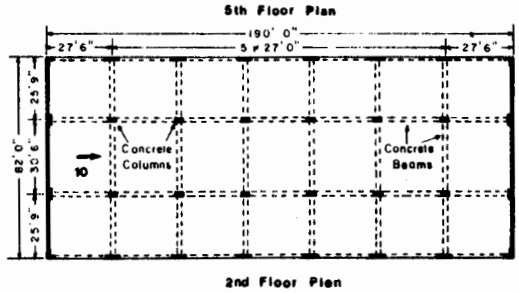

Figure 1- Buildings Studied.

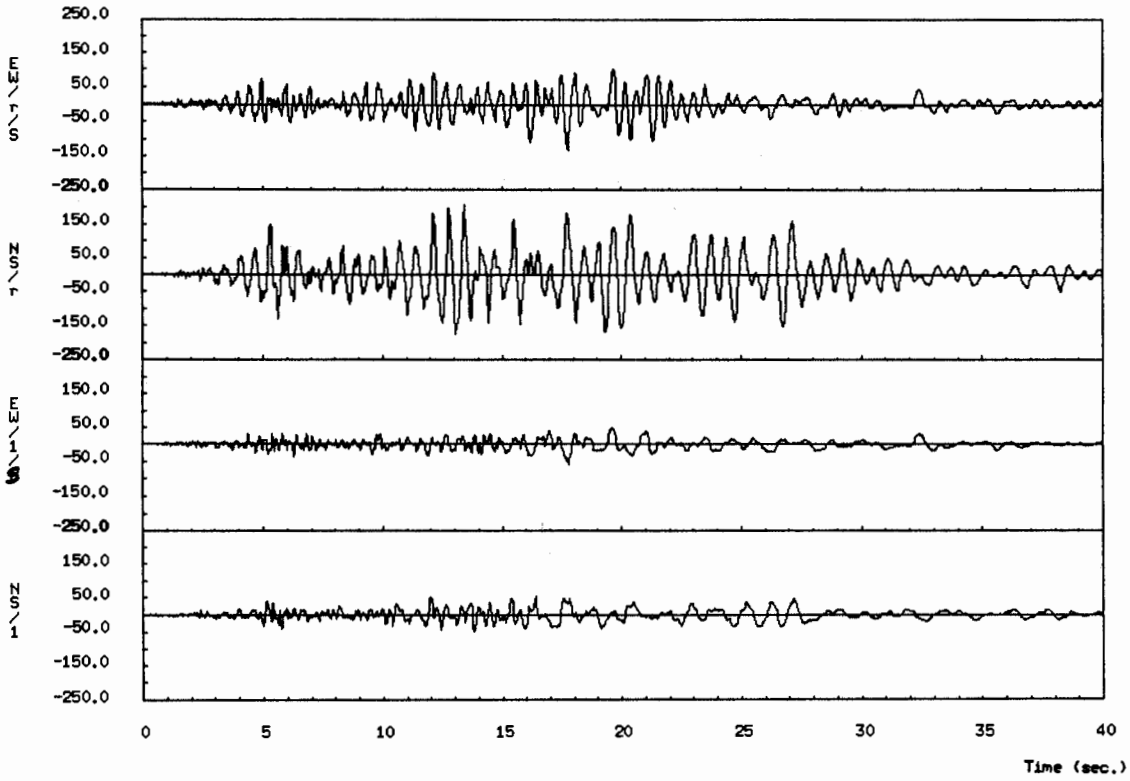

Figure 2 - Acceleration Records for Building 1. Morgan Hill Earthquake.

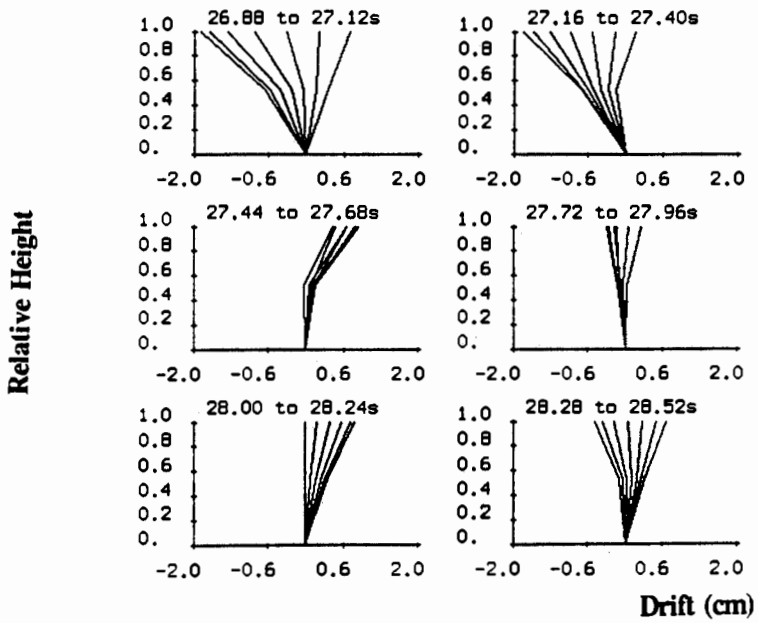

Figure 3 - Relative NS drift. Morgan Hill Earthquake.

Building 1

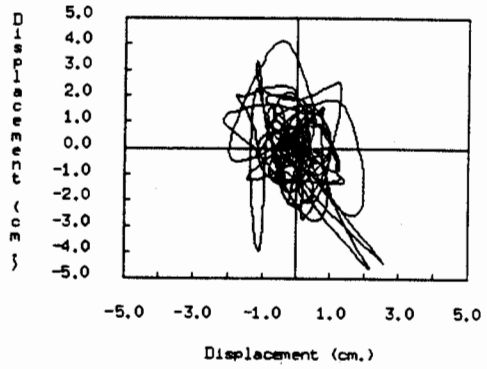

(a)

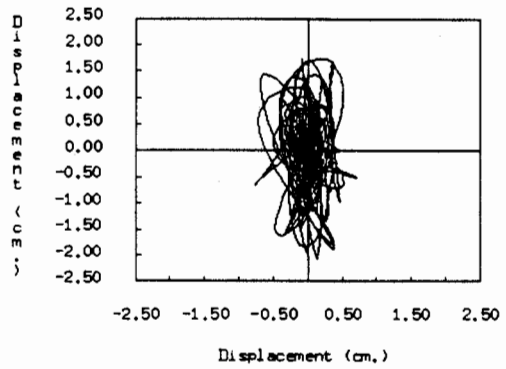

(d)

Building 2

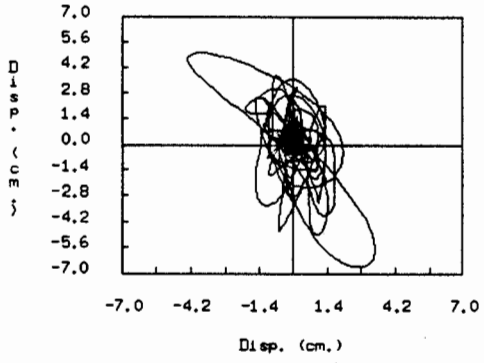

(b)

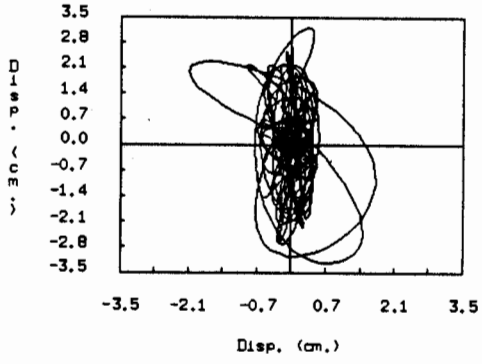

(e)

Building 3

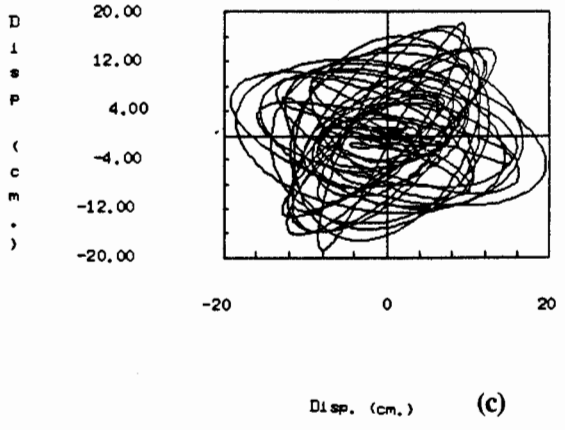

(c)

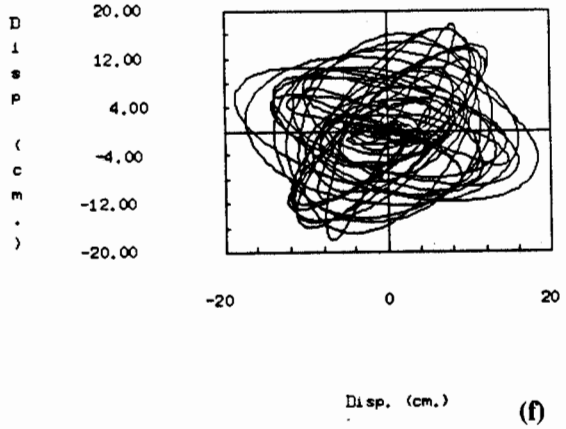

(f)

Figure 4 - Roof Orbital Displacement Histories: Total Displacement a, b, c; Relative Displacement d, e, f.

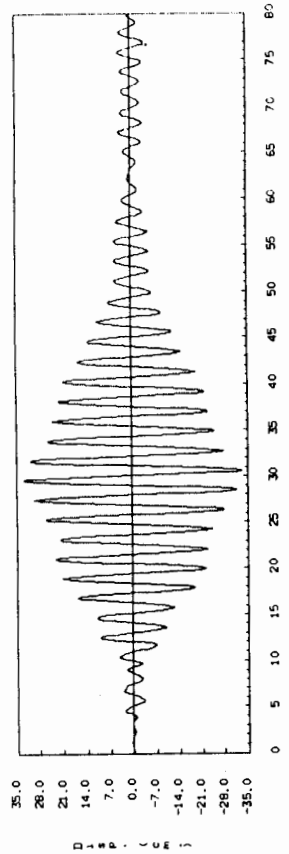

Figure 5 - Drifts for Building 2. a) EW direction; b) NS Direction.

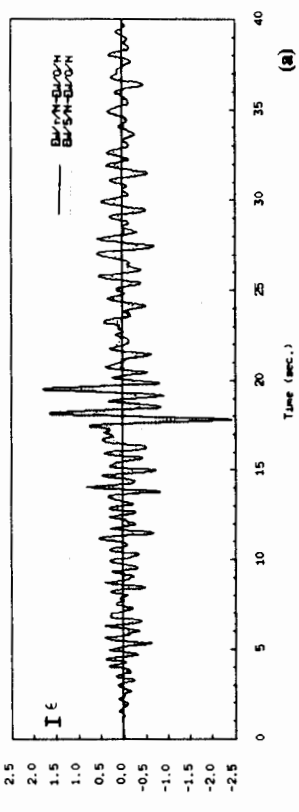

Figure 6 - Displacement Record Building 3. Roof and Base

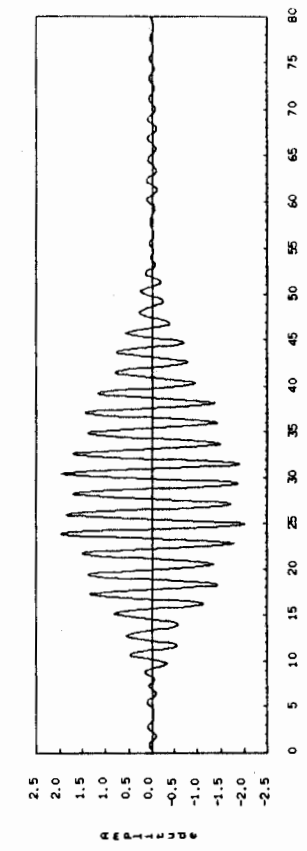

Figure 7 - Beating Behavior Building 3, Mt. Lewis Earthquake. a) Roof displacement NS direction. b) Roof displacement EW direction. c) Simple trigonometric series.